8
Resonant Perturbations

The heavens themselves, the planets, and this centre
Observe degree, priority, and place,
Insisture, course, proportion, season, form,
Office, and custom, in all line of order.

William Shakespeare, *Troilus and Cressida, I, iii*

8.1 Introduction

We saw in Chapter 6 how resonant effects arise in the small divisor problem when we considered the motion of an asteroid whose orbital period was a simple fraction of Jupiter's period. The naïve theory predicted that, as the ratio of mean motions approached the exact resonant value, the small divisor approached zero and large-amplitude variations in the elements would result. In this chapter we examine the theory of resonance in more detail. Starting from simple geometrical and physical approaches, we go on to show how the simple model breaks down. In order to understand the basic dynamics of resonance we start by using the pendulum approach valid for resonant phenomena in the asteroid belt. We then give a complete and detailed model of resonance using a Hamiltonian approach. Throughout this chapter we develop a variety of approaches to handle the problem of orbit–orbit resonance in the solar system and beyond.

Although there is an extensive range of literature on celestial mechanics, there is little devoted specifically to the theory of resonance. Useful reviews of the subject, particularly in the context of orbital evolution through resonance, have been given by Greenberg (1977), Peale (1986), and Malhotra (1988).

8.2 The Geometry of Resonance

We consider the geometrical importance of resonant mechanisms. Consider an asteroid in a 2:1 resonance with Jupiter. For simplicity we assume that Jupiter is

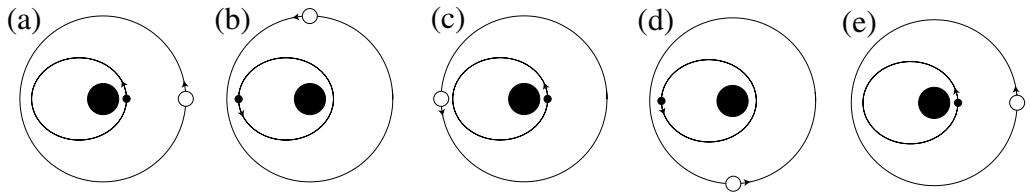

Fig. 8.1. The relative positions of Jupiter (white circle) and an asteroid (small filled circle) for the stable configuration when their orbital periods are in a ratio of 2:1. If $T_{\rm J}$ is the period of Jupiter's orbit then the diagrams illustrate the configurations at times (a) $t = 0$, (b) $t = \frac{1}{4}T_{\rm J}$, (c) $t = \frac{1}{2}T_{\rm J}$, (d) $t = \frac{3}{4}T_{\rm J}$, and (e) $t = T_{\rm J}$.

in a circular orbit and that all motion takes place in the plane of Jupiter's orbit. In this situation we are ignoring any perturbations between the two objects as we are only interested in how resonant relationships lead to repeated encounters of "good" and "bad" kinds.

Figure 8.1 illustrates the relative configurations of the asteroid and Jupiter such that, at some time $t = 0$, Jupiter and the asteroid are at conjunction and the asteroid is at the perihelion of its orbit. This is illustrated in Fig. 8.1a. Since the objects are in a 2:1 resonance, the asteroid will complete two periods for every one period of Jupiter. We consider time steps of one quarter Jupiter periods. Neglecting any actual perturbations between the objects, the asteroid and Jupiter will have moved to relative positions shown in Fig. 8.1b at time $t = \frac{1}{4}T_{\rm J}$. The asteroid is now at the aphelion of its orbit, and Jupiter has completed $1/4$ of an orbit. Although the closest approach between the two orbits is at the asteroid's aphelion, Jupiter is not nearby when the asteroid is at this position. Similarly, when Jupiter reaches this position at time $t = \frac{1}{2}T_{\rm J}$, the asteroid is back at perihelion (Fig. 8.1c). At time $t = \frac{3}{4}T_{\rm J}$ the asteroid returns to the danger point but Jupiter is not nearby (Fig. 8.1d), while at time $t = T_J$ (Fig. 8.1e) the original configuration shown in Fig. 8.1a is repeated. Thus, although there appears to be the potential for close approaches and large perturbations from Jupiter at the asteroid's aphelion, such approaches are avoided by the resonant mechanism. This would be an example of a stable equilibrium configuration between Jupiter and the asteroid.

Conversely, if we start Jupiter and the asteroid at conjunction at the asteroid's aphelion (Fig. 8.2), we would have an unstable equilibrium configuration, where the damaging close approaches would be repeated every Jupiter period.

We can examine the geometry of resonance for a more general case by first considering two satellites moving around a central planet in circular, coplanar orbits. Let us assume that

$$\frac{n'}{n} = \frac{p}{p+q}, \tag{8.1}$$

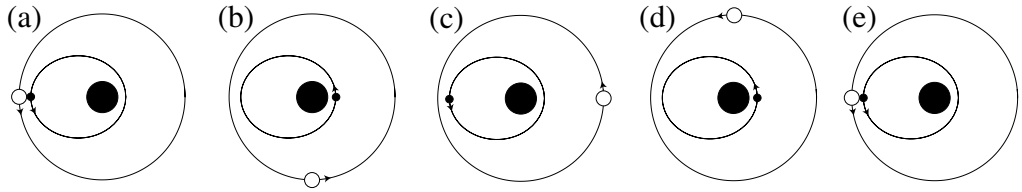

Fig. 8.2. The relative positions of Jupiter (white circle) and an asteroid (small filled circle) for the unstable configuration when their orbital periods are in a ratio of 2:1. If $T_{\rm J}$ is the period of Jupiter's orbit then the diagrams illustrate the configurations at times (a) $t = 0$, (b) $t = \frac{1}{4}T_{\rm J}$, (c) $t = \frac{1}{2}T_{\rm J}$, (d) $t = \frac{3}{4}T_{\rm J}$, and (e) $t = T_{\rm J}$.

where n and n' are the mean motions of the inner and outer satellites respectively and p and q are integers. If the two satellites are in conjunction at time $t = 0$ then the next conjunction will occur when

$$nt - n't = 2\pi \tag{8.2}$$

and the period, $T_{\rm con}$, between successive conjunctions is given by

$$T_{\rm con} = \frac{2\pi}{n - n'}. \tag{8.3}$$

But $p(n - n') = qn'$ and therefore

$$T_{\rm con} = \frac{p}{q}\frac{2\pi}{n'} = \frac{p}{q}T' = \frac{p+q}{q}T, \tag{8.4}$$

where T and T' are the orbital periods of the two satellites. Hence

$$qT_{\rm con} = pT' = (p+q)T. \tag{8.5}$$

If $q = 1$, then each satellite completes a whole number of orbits between successive conjunctions and every conjunction occurs at the same longitude in inertial space. If $q = 2$, then only every second conjunction occurs at the same longitude, etc.

Now consider the case when $e = 0$, $e' \neq 0$, and $\dot{\varpi}' \neq 0$, where e denotes the eccentricity and ϖ the longitude of pericentre. If the resonant relation

$$(p+q)n' - pn - q\dot{\varpi}' = 0 \tag{8.6}$$

is satisfied, then we can rewrite this as

$$\frac{n' - \dot{\varpi}'}{n - \dot{\varpi}'} = \frac{p}{p+q}, \tag{8.7}$$

where $n' - \dot{\varpi}'$ and $n - \dot{\varpi}'$ are relative motions; these can be considered as the mean motions in a reference frame corotating with the pericentre of the outer satellite. From the viewpoint of this reference frame the *orbit* of the outer satellite is fixed or stationary.

Now if $q = 1$, then every conjunction takes place at the same point in the orbit of the outer satellite, but not at the same longitude in inertial space. If $q = 2$, then every second conjunction takes place at the same point in the orbit, etc.

If the resonant relation given in Eq. (8.6) holds, the corresponding resonant argument is

$$\varphi = (p+q)\lambda' - p\lambda - q\varpi'. \tag{8.8}$$

At a conjunction of the two satellites, $\lambda = \lambda'$ and we have

$$\varphi = q(\varpi' - \lambda') = q(\varpi' - \lambda). \tag{8.9}$$

Thus φ is a measure of the displacement of the longitude of conjunction from pericentre of the outer satellite. For example, observations of the saturnian satellites Titan and Hyperion show that the resonant angle $\varphi = 4\lambda' - 3\lambda - \varpi'$ oscillates or librates about the apocentre of Hyperion's orbit with an amplitude of 14.0° and a period of 18.75 y.

At this stage we reintroduce the concept of the rotating reference frame used throughout Chapter 3 and mentioned in the context of spin–orbit coupling in Chapter 5. Consider the orbits of an asteroid and Jupiter where there exists a 2:1 commensurate relationship between the orbital periods and Jupiter is assumed to move in a circular orbit (Fig. 8.3). Again we are ignoring the actual perturbations between these objects since we are only interested in the relative geometry of their orbits.

The path in the rotating frame (Fig. 8.3b) approximates that of a centred ellipse for low eccentricities of the keplerian orbit. As the orbital periods are related by

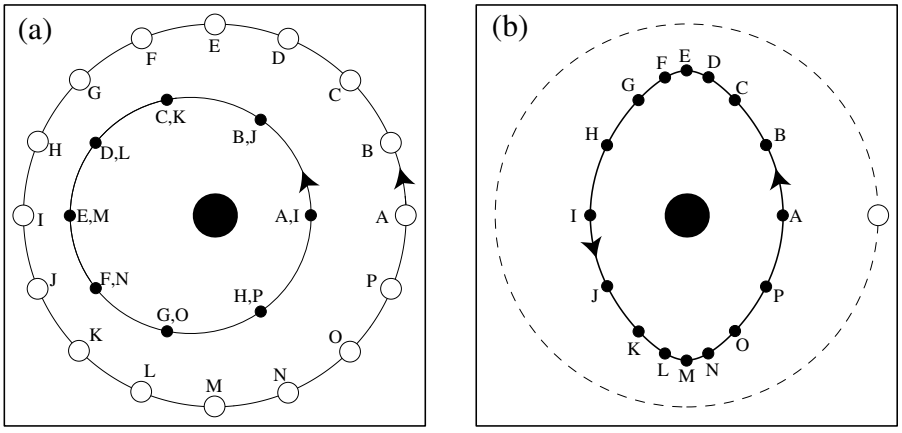

Fig. 8.3. (a) Points along the orbit of an asteroid (small black circles) and Jupiter (white circles) at fixed time intervals of 1/16 Jupiter period in a nonrotating reference frame for the 2:1 resonance. The letters at each point on one orbit match up with an equivalent point on the other orbit. (b) The path of the asteroid in a rotating frame moving with the mean motion of Jupiter. The letters denote the same points as shown in Fig. 8.3a. The eccentricity of the asteroid's orbit is 0.2.

the 2:1 commensurability, the asteroid will orbit twice for every single orbit of Jupiter. At each of its two aphelion passages (points E and M) Jupiter is $\pm 90^\circ$ away in longitude. At aphelion the angular velocity of the asteroid is a minimum and close to that of Jupiter. Therefore the points become closer together as seen in the rotating frame. For sufficiently large values of the eccentricity the angular velocity of the asteroid at aphelion is smaller than the fixed angular velocity of Jupiter and so in the rotating frame the asteroid will appear to be moving backwards.

We can illustrate the behaviour shown in Fig. 8.3 for a variety of eccentricities and resonances. Figure 8.4 shows the paths in the rotating frame for particles at a variety of first-order interior, second-order interior, first-order exterior, and second-order exterior resonances respectively. In each case there are no mutual perturbations.

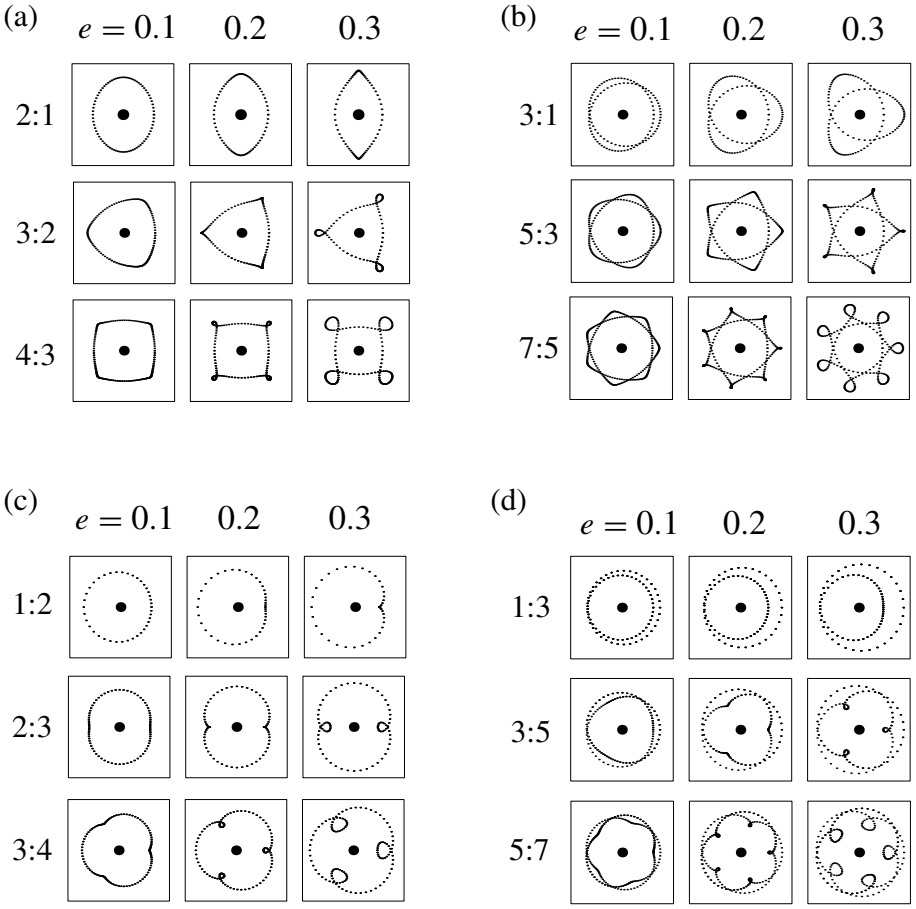

Fig. 8.4. Paths in the rotating frame for a test particle at (a) the 2:1, 3:2, and 4:3 first-order, interior resonances, (b) the 3:1, 5:3, and 7:5 second-order, interior resonances, (c) the 1:2, 2:3, and 3:4 first-order, exterior resonances, and (d) the 1:3, 3:5, and 5:7 second-order, exterior resonances for values of the eccentricity $e = 0.1$, 0.2, and 0.3. The positions of the particle along each path are drawn at equal time intervals.

The particle paths in the rotating frame illustrate the relationship between the resonance and the frequency of conjunctions with the internal or external object. In the case where the particle is in a $p+q : p$ interior resonance with the external object the configuration repeats itself every $p+q$ orbits of the particle. However, when the particle is in a $p : p+q$ exterior resonance with the internal object there is a repeated configuration every p orbits of the particle.

One obvious feature of the plots shown in Fig. 8.4 is the formation of "loops" in the rotating frame trajectories. When they occur it is always at the apocentre of internal particle orbits and the pericentre of external particle orbits. Because it takes $p+q$ and p orbits for particle's configuration to repeat itself in the $p+q : p$ interior and $p : p+q$ exterior resonances respectively, we would expect the respective number of loops to be $p+q$ and p in each case. At a unique, critical value of the particle's eccentricity the angular velocity of the particle on its orbit matches the (constant) angular velocity of the perturber; in this case a "cusp" occurs on the trajectory. For larger eccentricities the particle appears to loop backwards for part of its orbit in the rotating frame. It is easy to show that for internal and external orbits the cusp occurs at the value of e and e' respectively that satisfy the cubic equations

$$(1+e)^3 = [(p+q)/p]^2(1-e), \tag{8.10}$$

$$(1-e')^3 = [p/(p+q)]^2(1+e'). \tag{8.11}$$

For example, solution of Eq. (8.10) gives predicted values of the critical e for the internal 2:1, 3:2, and 4:3 resonances of 0.365, 0.211, and 0.148 respectively. These values are consistent with the behaviour shown in Fig. 8.4a.

8.3 The Physics of Resonance

In order to understand the physical mechanism of resonance, we follow the example of Peale (1976), Greenberg (1977), and Peale (1986). Let us consider the case of two objects orbiting a central mass and let us examine the net effect of their repeated conjunctions. In our case we assume that the object on the interior orbit has negligible mass and that the exterior object is moving on a circular orbit in the same plane. The objects are in a mean motion resonance such that conjunctions always occur at the same longitude.

If the conjunctions always occur exactly at either pericentre or apocentre, then the tangential force experienced by the particle immediately before conjunction is equal and opposite to the tangential force experienced immediately after conjunction. Thus, there is no net tangential force. From the formulae derived in Sect. 2.9, we know that the angular momentum can change only under the effects of a tangential force (see Eq. (2.149)). Similarly, if conjunctions occur at pericentre or apocentre (i.e., $f = 0$ or $f = 180^\circ$ respectively in Eq. (2.145)) then

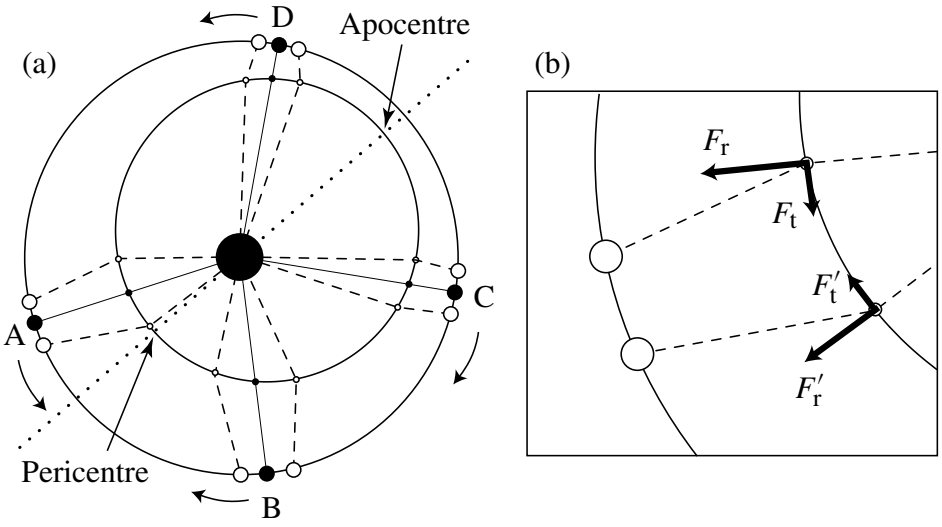

Fig. 8.5. Schematic diagrams illustrating resonant encounters between an object of negligible mass on an internal, elliptical orbit and a massive object on an external, circular orbit. (a) The geometry of encounters at four different points of conjunction, labelled A, B, C, and D. The dotted line denotes the major axis of the internal object. The arrows denote the directions towards which each conjunction should be moving; the stable conjunction is at the pericentre of the orbit. (b) A close-up of conjunction A showing the radial (subscript r) and tangential (subscript t) forces acting on the internal object immediately before (unprimed quantities) and after (primed quantities) the conjunction.

we also require a tangential force to change the semi-major axis. This symmetry is destroyed if conjunctions occur at any other point on the orbit.

We can examine the effects of other types of encounters by considering conjunctions at the points labelled A, B, C, and D in Fig. 8.5a. Here we are assuming that the longitude of pericentre of the interior object is fixed and that the resonance relationship implies that conjunctions will occur at the same point if there is no gravitational interaction between the objects.

If conjunction occurs at point A, close to the pericentre of the interior object, then the objects on their orbits are in the process of diverging from one another (see Fig. 8.5b). Therefore the tangential force, F_t, experienced by the interior object immediately prior to conjunction is larger than the tangential force, F_t', it experiences immediately after conjunction. Furthermore, the angular velocity of the inner object is closer to the (constant) angular velocity of the outer object just before conjunction than just after. Therefore the larger tangential force in the direction of motion acts for a longer time than the smaller tangential force, which acts in the opposite after conjunction has occurred. Hence the net result of the encounter is an increase in angular momentum of the inner object and a decrease in its mean angular velocity; this means that subsequent conjunctions will occur closer to pericentre.

If conjunctions occur after pericentre, say at point B in Fig. 8.5a, the net result would be a loss of angular momentum and a gain in mean angular velocity, again resulting in movement of the conjunction closer to pericentre. For conjunctions at points C and D, which are closer to the apocentre of the orbit of the inner body, there would again be a tendency to drive the point of conjunction closer to pericentre. Thus there is a net tendency at all asymmetric encounter points to drive conjunctions towards the pericentre of the orbit. This can be considered as the stable equilibrium configuration of the system, while conjunction at apocentre is the unstable configuration. In Sect. 8.6 we show the same result using a pendulum model for resonance.

Now consider the case where conjunction always occur at pericentre. Because the radial force exerted by the external object at conjunction is always in the opposite direction to the central mass, there will be an acceleration of the interior mass away from the central mass and therefore it will move on an orbit that is slightly larger than it would have done if it had not received the perturbation (cf. Eq. (2.145)). This means that it will have reached its pericentre slightly later than it would have done and hence its longitude of pericentre has moved in the prograde sense (cf. Eq. (2.165)). Given that natural satellite orbits usually undergo rapid precession due to the oblateness of the planet, this implies that the effect would be enhanced for those satellites trapped in a resonance with an exterior satellite.

In the case where the object of negligible mass is on an external, eccentric orbit (this is the case examined by Peale (1976, 1986) and Greenberg (1977)), it can easily be shown that conjunctions at apocentre give the stable configuration. Furthermore, the resonance mechanism in these cases results in a regression of the pericentre of the small mass on the exterior orbit; in the case of satellite orbits, especially those that are far from the central planet, the pericentre regression effect can dominate over the pericentre precession introduced by the J_2 of the planet. For example, the saturnian satellite Hyperion is in a 3:4 external resonance with Titan; this is sufficient to introduce a net regression of $19^\circ\ \mathrm{y}^{-1}$ in Hyperion's orbit. The dynamics of this resonance will be discussed later in this chapter.

8.4 Variation of Orbital Elements

In Chapter 6 we derived Lagrange's equations, which determine the variation of the orbital elements for a given perturbing potential. If we consider only the lowest order terms in e and I then the approximate form of Eqs. (6.145)–(6.150) is given by

$$\dot{n} = -\frac{3}{a^2}\frac{\partial \mathcal{R}}{\partial \lambda}, \tag{8.12}$$

$$\dot{e} = -\frac{1}{na^2 e}\frac{\partial \mathcal{R}}{\partial \varpi}, \tag{8.13}$$

$$\dot{I} = -\frac{1}{na^2 \sin I}\frac{\partial \mathcal{R}}{\partial \Omega}, \tag{8.14}$$

$$\dot{\varpi} = \frac{1}{na^2 e}\frac{\partial \mathcal{R}}{\partial e} + \frac{\sin \frac{1}{2}I}{na^2}\frac{\partial \mathcal{R}}{\partial I}, \tag{8.15}$$

$$\dot{\Omega} = \frac{1}{na^2 \sin I}\frac{\partial \mathcal{R}}{\partial I}, \tag{8.16}$$

$$\dot{\epsilon} = \frac{e}{2na^2}\frac{\partial \mathcal{R}}{\partial e}, \tag{8.17}$$

where we have chosen to write the equation for $\dot{n}$ rather than $\dot{a}$ (using $\dot{n} = -\frac{3}{2}n\dot{a}/a$), and we have used the usual procedure of replacing partial derivatives involving the mean longitude of epoch by those involving the mean longitude λ (see Sect. 6.7). Note that in the case of $\dot{\epsilon}$ we have ignored terms involving partial derivatives with respect to a; this is equivalent to assuming that the terms involving Laplace coefficients are constant.

From Eq. (6.139) the general form of an appropriate argument in the expansion of the disturbing function is

$$\varphi = j_1\lambda' + j_2\lambda + j_3\varpi' + j_4\varpi + j_5\Omega' + j_6\Omega \tag{8.18}$$

and to lowest order the general term in the averaged expansion is

$$\langle \mathcal{R} \rangle = \frac{\mathcal{G}m'}{a'}\left[\mathcal{R}_{\mathrm{D}}^{(\mathrm{sec})} + e^{|j_4|}e'^{|j_3|}s^{|j_6|}s'^{|j_5|}\left[f_{\mathrm{d}}(\alpha) + f_{\mathrm{e}}(\alpha)\right]\cos\varphi\right], \tag{8.19}$$

$$\langle \mathcal{R}' \rangle = \frac{\mathcal{G}m}{a}\left[\alpha\mathcal{R}_{\mathrm{D}}^{(\mathrm{sec})} + e^{|j_4|}e'^{|j_3|}s^{|j_6|}s'^{|j_5|}\left[\alpha f_{\mathrm{d}}(\alpha) + f_{\mathrm{i}}(\alpha)\right]\cos\varphi\right] \tag{8.20}$$

for internal and external resonances respectively where $s = \sin\frac{1}{2}I$, $s' = \sin\frac{1}{2}I'$, and we have included the secular contribution given by

$$\begin{aligned}\mathcal{R}_{\mathrm{D}}^{(\mathrm{sec})} = {} & (e^2 + e'^2)f_{\mathrm{s},1}(\alpha) + ee'f_{\mathrm{s},2}(\alpha)\cos(\varpi' - \varpi) \\ & + (s^2 + s'^2)f_{\mathrm{s},3}(\alpha) + ss'f_{\mathrm{s},4}(\alpha)\cos(\Omega' - \Omega)\end{aligned} \tag{8.21}$$

(cf. Eq. (7.1)). We can use Appendix B to obtain expressions for $f_{\mathrm{d}}(\alpha)$, $f_{\mathrm{e}}(\alpha)$, $f_{\mathrm{i}}(\alpha)$, and $f_{\mathrm{s,i}}(\alpha)$ $(i = 1, 2, 3, 4)$. For convenience these are given explicitly in Tables 8.1–8.4.

Note that the secular terms given in Eq. (8.21) will make no contribution if we restrict our expansions to terms of the first order in the eccentricities and inclinations. Furthermore, in these cases there will be no contribution from the inclination terms, because s and s' only occur when terms of order two or higher are considered.

Table 8.1. Direct terms in the expansion of the disturbing function.

j_1	j_2	j_3	j_4	j_5	j_6	$f_{\rm d}(\alpha)$
j	$1-j$	0	-1	0	0	$\frac{1}{2}\left[-2j-\alpha D\right] b_{1/2}^{(j)}$
j	$1-j$	-1	0	0	0	$\frac{1}{2}\left[-1+2j+\alpha D\right] b_{1/2}^{(j-1)}$
j	$2-j$	0	-2	0	0	$\frac{1}{8}\left[-5j+4j^2-2\alpha D +4j\alpha D+\alpha^2 D^2\right] b_{1/2}^{(j)}$
j	$2-j$	-1	-1	0	0	$\frac{1}{4}\left[-2+6j-4j^2+2\alpha D -4j\alpha D-\alpha^2 D^2\right] b_{1/2}^{(j-1)}$
j	$2-j$	-2	0	0	0	$\frac{1}{8}\left[2-7j+4j^2-2\alpha D +4j\alpha D+\alpha^2 D^2\right] b_{1/2}^{(j-2)}$
j	$2-j$	0	0	0	-2	$\frac{1}{2}\alpha b_{3/2}^{(j-1)}$
j	$2-j$	0	0	-1	-1	$-\alpha b_{3/2}^{(j-1)}$
j	$2-j$	0	0	-2	0	$\frac{1}{2}\alpha b_{3/2}^{(j-1)}$

Table 8.2. Indirect terms in the expansion of the disturbing function for an external perturber.

j_1	j_2	j_3	j_4	j_5	j_6	$f_{\rm e}(\alpha)$
2	-1	-1	0	0	0	-2α
3	-1	-2	0	0	0	$-\frac{27}{8}\alpha$

Table 8.3. Indirect terms in the expansion of the disturbing function for an internal perturber.

j_1	j_2	j_3	j_4	j_5	j_6	$f_{\rm i}(\alpha)$
2	-1	-1	0	0	0	$-\frac{1}{2}/\alpha$
3	-1	-2	0	0	0	$-\frac{3}{8}/\alpha$

Table 8.4. Secular terms in the expansion of the disturbing function.

i	$f_{\mathrm{s,i}}(\alpha)$
1	$\frac{1}{8}\left[2\alpha D + \alpha^2 D^2\right] b_{1/2}^{(0)}$
2	$\frac{1}{4}\left[2 - 2\alpha D - \alpha^2 D^2\right] b_{1/2}^{(1)}$
3	$-\frac{1}{2}\alpha b_{3/2}^{(1)}$
4	$\alpha b_{3/2}^{(1)}$

The equations for the time variation of the orbital elements are required when we have to calculate the time derivative of the general angle φ given in Eq. (8.18). This is given by

$$\dot{\varphi} = j_1(n' + \dot{\epsilon}') + j_2(n + \dot{\epsilon}) + j_3\dot{\varpi}' + j_4\dot{\varpi} + j_5\dot{\Omega}' + j_6\dot{\Omega} = 0. \tag{8.22}$$

We say that the perturbed body is in *exact resonance* when the time variation of a particular resonant argument, $\dot{\varphi}$, is exactly zero. This implies that in this case there exists a particular linear combination of mean motions and precession rates (i.e., a particular set of values of the $j_1, j_2, \ldots, j_6$) such that $\dot{\varphi} = 0$.

It is clear from Eq. (8.23) that if we neglect the contributions from all the variations of the longitudes then "exact" resonance occurs when

$$j_1 n' + j_2 n \approx 0\,. \tag{8.23}$$

Let $j_1 = p + q$ and $j_2 = -p$, where p and q are positive integers and q is the *order of the resonance*. We define the *nominal resonance location,* a_{n}, of the $p + q : p$ resonance to be the semi-major axis of the inner body that satisfies the relation

$$a_{\mathrm{n}} = \left(\frac{p}{p+q}\right)^{2/3} a', \tag{8.24}$$

with a similar definition for external resonances. However, this relationship provides only an approximate location for the resonance. In cases where there are significant contributions to the precession rates the locations in semi-major axis of the different exact resonances associated with a $p + q : p$ commensurability are separate and distinct. For example, in Sect. 6.10.1 we noted that to second order there are six possible resonant arguments associated with the basic 3:1 commensurability. If we ignore the variations in mean longitude of epoch the six time derivatives of the resonant angles are given by

$$\begin{aligned}
&\dot{\varphi}_1 = 3n' - n - 2\dot{\varpi}, \quad \dot{\varphi}_2 = 3n' - n - \dot{\varpi} - \dot{\varpi}', \quad \dot{\varphi}_3 = 3n' - n - 2\dot{\varpi}', \\
&\dot{\varphi}_4 = 3n' - n - 2\dot{\Omega}, \quad \dot{\varphi}_5 = 3n' - n - \dot{\Omega} - \dot{\Omega}', \quad \dot{\varphi}_6 = 3n' - n - 2\dot{\Omega}'\,.
\end{aligned} \tag{8.25}$$

If the bodies involved in these resonances are orbiting an oblate planet then the values of $\dot{\varpi}$, $\dot{\varpi}'$, $\dot{\Omega}$, and $\dot{\Omega}'$ would be principally determined by the value of J_2 and the distance of the relevant body from the planet. Therefore, it is likely that $|\dot{\varpi}| > |\dot{\varpi}'|$ and $|\dot{\Omega}| > |\dot{\Omega}'|$. Furthermore, the nodal rates are usually opposite in sign to the pericentre precession rates. This combination leads to a "splitting" of the basic 3:1 resonance over a range of semi-major axes. The relative extent of this splitting at each planet is thought to provide an explanation for the abundance of mean motion commensurabilities in the jovian and saturnian systems and a lack of such phenomena in the uranian system. This is discussed further in the Sect. 8.15.

8.5 Resonance in the Circular Restricted Three-Body Problem

Although we can proceed to investigate the properties of resonant behaviour in a variety of circumstances it proves instructive to concentrate on perhaps the simplest case of interest. This is the planar, circular, restricted problem where a body on an external orbit perturbs an inner body of negligible mass, with both objects moving in the reference plane. The general term in the averaged expansion reduces to

$$\langle \mathcal{R} \rangle = \frac{\mathcal{G}m'}{a'} \left[f_{\mathrm{s},1}(\alpha) e^2 + f_{\mathrm{d}}(\alpha) e^{|j_4|} \cos \varphi \right], \tag{8.26}$$

where

$$\varphi = j_1 \lambda' + j_2 \lambda + j_4 \varpi \tag{8.27}$$

and the corresponding equations of motion become

$$\dot{n} = 3 j_2 \mathcal{C}_{\mathrm{r}} n e^{|j_4|} \sin \varphi, \tag{8.28}$$

$$\dot{e} = j_4 \mathcal{C}_{\mathrm{r}} e^{|j_4|-1} \sin \varphi, \tag{8.29}$$

$$\dot{\varpi} = 2\mathcal{C}_{\mathrm{s}} + |j_4| \mathcal{C}_{\mathrm{r}} e^{|j_4|-2} \cos \varphi, \tag{8.30}$$

$$\dot{\epsilon} = \mathcal{C}_{\mathrm{s}} e^2 + \frac{1}{2} |j_4| \mathcal{C}_{\mathrm{r}} e^{|j_4|} \cos \varphi. \tag{8.31}$$

Here the constants arising from the resonant and secular parts of the disturbing function are given by

$$\mathcal{C}_{\mathrm{r}} = \frac{\mathcal{G}m'}{na^2 a'} f_{\mathrm{d}}(\alpha) = \left(\frac{m'}{m_{\mathrm{c}}} \right) n \alpha f_{\mathrm{d}}(\alpha) \tag{8.32}$$

and

$$\mathcal{C}_{\mathrm{s}} = \frac{\mathcal{G}m'}{na^2 a'} f_{\mathrm{s},1}(\alpha) = \left(\frac{m'}{m_{\mathrm{c}}} \right) n \alpha f_{\mathrm{s},1}(\alpha) \tag{8.33}$$

respectively, where m_{c} is the mass of the central body and we have used Kepler's third law to write $\mathcal{G} = n^2 a^3 / m_{\mathrm{c}}$. Note that f_{d} comes from either the first or third entry in Table 8.1 and $f_{\mathrm{s},1}$ is given in Table 8.4

Examining Eqs. (8.28)–(8.31) allows us to deduce some basic properties of the variation of the orbital elements. Given that $|j_4| \geq 1$, the mean motion and semi-major axis are almost constant, because of the $e^{|j_4|}$ term on the right-hand side of Eq. (8.28). The variation of e is proportional to one smaller power of e (see Eq. (8.29)) and so the eccentricity will undergo larger variations. The equation for $\dot{\varpi}$ shows that a near-circular orbit will undergo rapid changes in the longitude of pericentre as the second (resonant) term on the right-hand side of Eq. (8.30) dominates over the first (secular) term. Similarly the variation of ϵ will be dominated by the resonant contribution for first-order resonances, but the secular term will be comparable to the resonant term for second-order resonances. Since $\dot{n} = -(3/2)(n/a)\dot{a}$ we have that

$$\dot{a} = -2 j_2 \mathcal{C}_{\mathrm{r}} a e^{|j_4|} \sin\varphi \tag{8.34}$$

and hence

$$\frac{\mathrm{d}a}{\mathrm{d}e} = -2(j_2/j_4)ae\,. \tag{8.35}$$

This implies that the variations of a and e are always correlated. If j_2 and j_4 have the same sign (the case for an interior resonance), $\mathrm{d}a/\mathrm{d}e < 0$ and a maximum of a corresponds to a minimum of e and vice versa. For opposite signs of j_2 and j_4 (the case for an exterior resonance) $\mathrm{d}a/\mathrm{d}e > 0$ and a and e are at maximum or minimum together.

It is interesting to compare Eq. (8.35) with a similar expression derived from the Tisserand relation. In Sect. 3.4 we showed that

$$\frac{1}{2a} + \sqrt{a(1-e^2)}\cos I = \text{constant} \tag{8.36}$$

for the restricted three-body problem, provided a, e, and I are calculated far from the perturber. Recall that in this expression a is the semi-major axis of the perturber. Setting $I = 0$ in Eq. (8.36) and differentiating with respect to e gives

$$\frac{\mathrm{d}a}{\mathrm{d}e} = \frac{2a^{\frac{5}{2}}e}{a^{\frac{3}{2}} - 1} \tag{8.37}$$

to lowest order in e. Therefore, for orbits interior to that of the perturber (i.e., $a < 1$ in these units), $\mathrm{d}a/\mathrm{d}e < 0$ whereas for exterior orbits $\mathrm{d}a/\mathrm{d}e > 0$. This gives the same result regarding maxima and minima as stated above for the resonance case. In Sect. 8.8 we use a Hamiltonian approach to show that the Tisserand relation is a constant of the motion.

To complete the resonant equations of motions we have to derive an equation for the variation of the resonant angle φ. Recalling that the orbit of the external body is fixed we have

$$\dot{\varphi} = j_1 n' + j_2(n + \dot{\epsilon}) + j_4 \dot{\varpi}. \tag{8.38}$$

Table 8.5. The numerical values of α and the coefficients $\alpha f_{\mathrm{s},1}(\alpha)$ and $\alpha f_{\mathrm{d}}(\alpha)$ for a selection of first- and second-order internal resonances of the form $p+q:p$. The value of α is the nominal value for each resonance.

$p+q:p$	α	$\alpha f_{\mathrm{s},1}(\alpha)$	$\alpha f_{\mathrm{d}}(\alpha)$
2 : 1	0.629961	0.244190	−0.749964
3 : 2	0.763143	0.879751	−1.54553
4 : 3	0.825482	1.88147	−2.34472
5 : 4	0.861774	3.24494	−3.14515
6 : 5	0.885549	4.96857	−3.94613
3 : 1	0.480750	0.0683812	0.287852
5 : 3	0.711379	0.515657	2.32892
7 : 5	0.799064	1.33523	6.28903
9 : 7	0.845740	2.51812	12.1673
11 : 9	0.874782	4.06179	19.9639

Table 8.5 gives the values of $\alpha = a/a'$, $\alpha f_{\mathrm{s},1}(\alpha)$, and $\alpha f_{\mathrm{d}}(\alpha)$ for a number of first- and second-order internal resonances of the form $p+q:p$ using the nominal value of α in each case. The quantities have been derived from the definitions given in Tables 8.1 and 8.4. Note that the magnitude of the $\alpha f_{\mathrm{s},1}(\alpha)$ and $\alpha f_{\mathrm{d}}(\alpha)$ terms increases as α increases.

The set of formulae given in Eqs. (8.28)–(8.31) and (8.38) describe the variation of the orbital elements in the vicinity of a resonance in the planar, circular restricted problem. These can easily be extended to cover the variation of orbital elements for other cases. For example, if we consider motion in circular inclined orbits there is a parallel between the behaviour of the inclination and node and that of the eccentricity and pericentre seen above.

8.6 The Pendulum Model

We now examine the parallels between the simple resonance model outlined above and the motion of a pendulum. Consider the second time derivative of the argument φ given in Eq. (8.27). Given that we are assuming $\dot{n}' = 0$, the time derivative of Eq. (8.38) gives

$$\ddot{\varphi} = j_2\dot{n} + j_2\ddot{\epsilon} + j_4\ddot{\varpi} \,. \tag{8.39}$$

If we write

$$\dot{\epsilon} = \mathcal{C}_{\mathrm{s}}e^2 + |j_4|\mathcal{C}_{\mathrm{r}}F(e)\cos\varphi, \tag{8.40}$$

$$\dot{\varpi} = 2\mathcal{C}_{\mathrm{s}} + |j_4|\mathcal{C}_{\mathrm{r}}G(e)\cos\varphi, \tag{8.41}$$

where

$$F(e) = \frac{1}{2}e^{|j_4|} \qquad \text{and} \qquad G(e) = e^{|j_4|-2}, \tag{8.42}$$

then the second time derivatives of ϵ and ϖ are given by

$$\ddot{\epsilon} = 2\mathcal{C}_{\rm s} e\dot{e} + |j_4|\mathcal{C}_{\rm r}\left(\frac{{\rm d}F(e)}{{\rm d}e}\dot{e}\cos\varphi - F(e)\dot{\varphi}\sin\varphi\right), \tag{8.43}$$

$$\ddot{\varpi} = |j_4|\mathcal{C}_{\rm r}\left(\frac{{\rm d}G(e)}{{\rm d}e}\dot{e}\cos\varphi - G(e)\dot{\varphi}\sin\varphi\right). \tag{8.44}$$

Recalling that the constants $\mathcal{C}_{\rm r}$ and $\mathcal{C}_{\rm s}$ already contain a factor of $m'/m_{\rm c}$, which is usually a small quantity, the presence of $\dot{e}$ and $\dot{\varphi}$ in Eqs. (8.43) and (8.44) introduces another factor of $m'/m_{\rm c}$ and so the contribution of $\ddot{\epsilon}$ and $\ddot{\varpi}$ to $\ddot{\varphi}$ can be neglected in most circumstances. However, an inspection of Eq. (8.44) shows that in the case of first-order resonances (in our model those for which $|j_4| = 1$) there can be a significant contribution to the precession of ϖ because $G(e) = 1/e$ and e is a small quantity. In these circumstances the $\ddot{\varpi}$ term can contribute to $\ddot{\varphi}$. Note that in either case there is no longer a contribution from the secular part of the disturbing function.

If we neglect the contributions from $\ddot{\epsilon}$ and $\ddot{\varpi}$, and make use of the expression for $\dot{n}$ in Eq. (8.28), then the equation for $\ddot{\varphi}$ becomes

$$\ddot{\varphi} = 3j_2^2\mathcal{C}_{\rm r} n e^{|j_4|}\sin\varphi\,. \tag{8.45}$$

An inspection of the last column of Table 8.5 suggests that the constant $\mathcal{C}_{\rm r}$ is negative when q, the order of the resonance, is odd and positive when q is even. If we restrict ourselves to odd-order resonances then the equation for $\ddot{\varphi}$ has the form

$$\ddot{\varphi} = -\omega_0^2\sin\varphi, \tag{8.46}$$

where we take

$$\omega_0^2 = -3j_2^2\mathcal{C}_{\rm r} n e^{|j_4|} \tag{8.47}$$

and we assume that n, e, and hence ω_0 are approximately constant. Note that ω_0^2 is always a positive quantity. Therefore in the case of odd-order resonances the equation for $\ddot{\varphi}$ is identical to that of a simple pendulum with stable motion about $\varphi = 0$.

In the case of even-order resonances the motion is still similar to that described by a simple pendulum equation but in this case the stable point is about $\varphi = \pi$ rather than $\varphi = 0$. This can easily be seen by making the substitution $\varphi' = \varphi + \pi$ in Eq. (8.46), giving $\ddot{\varphi}' = -\omega_0^2\sin\varphi'$. In further discussions of librational motion for all resonances we will refer to Eq. (8.46) as the equation of a simple pendulum, even though technically there are minor differences in the case of even-order resonances. Note that when φ is small the differential equation can be written as $\ddot{\varphi} = -\omega_0^2\varphi$, the solution of which describes simple harmonic motion with a period independent of amplitude.

The differential equation given in Eq. (8.46) has some well-known properties. The solution can be described either as a circulation or a libration of the argument

φ, with the type of motion depending on the energy of the system, and hence on the starting conditions. The total energy E of the system is the sum of the kinetic energy per unit mass ($T = \frac{1}{2}\dot{\varphi}^2$) and potential energy per unit mass ($U = 2\omega_0^2 \sin^2 \frac{1}{2}\varphi$). Hence

$$E = \frac{1}{2}\dot{\varphi}^2 + 2\omega_0^2 \sin^2 \frac{1}{2}\varphi \,. \tag{8.48}$$

We can now classify the various types of motion by considering different values of the energy E. This is illustrated in Fig. 8.6a where we have plotted the potential energy and three possible values of the total energy, each corresponding to a different behaviour of the angle φ.

1) If $E > E_3$ (as in the case $E = E_1$) then the motion of φ is *unbounded* and this corresponds to *circulation* of the angle φ. In the case of a pendulum this implies a 360° motion of the bob about the point of suspension.
2) If $E < E_3$ (as in the case $E = E_2$) then the motion of φ is *bounded* and this corresponds to *oscillation* or *libration* of the angle φ. For a pendulum this implies a backwards and forwards motion about the point of suspension.
3) In the special case when $E = E_3$ motion occurs on the *separatrix*, which divides the circulation regime from the libration regime. This corresponds to the suspension of the pendulum bob in the vertical upward position.

The different possible trajectories are shown in Fig. 8.6b. For $E = E_1$ there is variation of $\dot{\varphi}$ with φ but $\dot{\varphi}$ is never zero. However, for $E = E_2$, $\dot{\varphi}$ does take zero values, each of which corresponds to an extreme of the motion of the angle φ. In the special case where $E = E_3$, the energy associated with the separatrix, we have a peculiar type of motion where the period is infinite.

Note from Fig. 8.6b that there are two singular points at $\dot{\varphi} = 0$. The first is at the origin, which corresponds to an *elliptic* fixed point, which is *stable* to small displacements. The second is at $\varphi = \pm\pi$, which corresponds to a *hyperbolic*

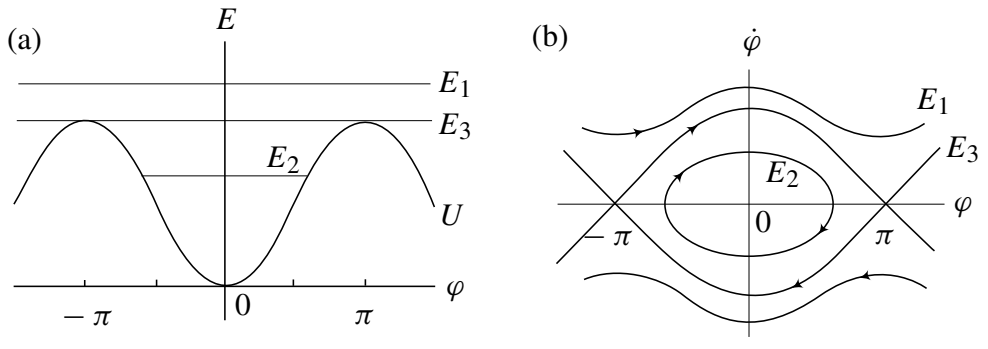

Fig. 8.6. (a) The potential energy U as a function of φ compared with three possible values E_1, E_2 and E_3 of the total energy E. (b) Three trajectories of the pendulum in $(\varphi, \dot{\varphi})$ space corresponding to each of the total energies shown in (a).

fixed point, which is *unstable* to small displacements. Thus we have provided the mathematical reasoning behind the physical arguments given in Sect. 8.3 for stable and unstable resonant configurations.

The time taken for φ to move from an angle $\varphi = 0$ to an angle $\varphi = \varphi_0$ is given by

$$t = \int_0^{\varphi_0} \frac{\mathrm{d}\varphi}{\dot{\varphi}}. \tag{8.49}$$

If $\dot{\varphi} = 0$ when $\varphi = \varphi_0$ the expression for the librational period of the motion is

$$T_{\mathrm{lib}} = 4 \int_0^{\varphi_0} \frac{\mathrm{d}\varphi}{\dot{\varphi}}. \tag{8.50}$$

Hence, because $E = 2\omega_0^2 \sin^2 \varphi_0/2$,

$$T_{\mathrm{lib}} = \frac{1}{\omega_0} \int_0^{2\pi} \frac{\mathrm{d}\theta}{\left(1 - \left(E/2\omega_0^2\right) \sin^2 \theta\right)^{1/2}} = \frac{4}{\omega_0} K\left(\frac{E}{2\omega_0^2}\right), \tag{8.51}$$

where we have set $\sin(\varphi/2) = \sin(\varphi_0/2) \sin\theta$. Here $K(x)$ is the complete elliptical integral of the first kind. This has the property that $K(0) = \pi/2$. Therefore, when E is small corresponding to small amplitude librations about the equilibrium point, we have

$$\lim_{\varphi_0 \to 0} T_{\mathrm{lib}} = \frac{2\pi}{\omega_0}. \tag{8.52}$$

This approximation is equivalent to assuming that $\sin\varphi \approx \varphi$. In this case the pendulum equation reduces to that for simple harmonic motion, $\ddot{\varphi} = -\omega_0^2 \varphi$ where the period of the libration is independent of the amplitude. In the more general case the period *is* a function of the amplitude and, in fact, the nature of the function $K(x)$ is such that $T_{\mathrm{lib}} \to \infty$ as the separatrix is approached.

8.7 Libration Width

The principal advantage of deriving an analytical model of resonance is that we can provide estimates of the variation in orbital parameters caused by individual resonances. In the context of solar system dynamics the most important such estimate is the extent of the libration in semi-major axis (or mean motion) for an object in resonance. This is because we can then try to relate the known libration width with an observed phenomenon such as a ring feature or a gap in the asteroid distribution. We can accomplish this by using our simple pendulum model and making modifications incorporating additional terms that arise in the case of low eccentricity orbits near first-order resonances.

Consider the relationship between the kinetic and potential energies given by Eq. (8.48) where we assume that we are dealing with the equation of a simple

pendulum. It is clear from Fig. 8.6 that the energy associated with maximum libration occurs when $\dot{\varphi} = 0$ at $\varphi = \pm\pi$. This implies

$$E_{\max} = -6j_2^2 \mathcal{C}_{\rm r} n e^{|j_4|}. \tag{8.53}$$

We now set the value of E equal to $E_{\max}$ and consider the variation of φ given by

$$\dot{\varphi} = \pm j_2 \left(12|\mathcal{C}_{\rm r}| n e^{|j_4|}\right)^{1/2} \cos\frac{1}{2}\varphi\,. \tag{8.54}$$

We can relate the variation of φ to the variation in n by means of Eq. (8.28). This gives

$$\begin{aligned} {\rm d}n &= 3j_2 \mathcal{C}_{\rm r} n e^{|j_4|} \frac{\sin\varphi}{\dot{\varphi}}\,{\rm d}\varphi \\ &= \pm\left(3|\mathcal{C}_{\rm r}| n e^{|j_4|}\right)^{1/2} \sin\frac{1}{2}\varphi\,{\rm d}\varphi \end{aligned} \tag{8.55}$$

making use of Eq. (8.54). Integration gives

$$n = n_0 \pm \left(12|\mathcal{C}_{\rm r}| n e^{|j_4|}\right)^{1/2} \cos\frac{1}{2}\varphi, \tag{8.56}$$

and so the maximum change in the mean motion is

$$\delta n_{\max} = \pm\left(12|\mathcal{C}_{\rm r}| n e^{|j_4|}\right)^{1/2}, \tag{8.57}$$

which occurs when $\varphi = 0$. The equivalent maximum change in semi-major axis can be easily derived from Kepler's third law. It is

$$\delta a_{\max} = \pm\left(\frac{16}{3}\frac{|\mathcal{C}_{\rm r}|}{n} e^{|j_4|}\right)^{1/2} a. \tag{8.58}$$

In the derivation of the pendulum-type equation in Sect. 8.6 we noted that in the case of first-order resonances ($|j_4| = 1$) we cannot neglect the contribution to $\ddot{\varphi}$ from significant terms in $\ddot{\varpi}$. Now we consider this in more detail and determine the modifications to the maximum libration width. Using $j_4 = -1$ we take the general argument of a first-order resonance to be

$$\varphi = j_1\lambda' + j_2\lambda - \varpi \tag{8.59}$$

with

$$\dot{\varphi} = j_1 n' + j_2 n - \dot{\varpi}, \tag{8.60}$$

$$\ddot{\varphi} = j_2\dot{n} - \ddot{\varpi}, \tag{8.61}$$

where, from Eqs. (8.29) and (8.44),

$$\ddot{\varpi} = \frac{\mathcal{C}_{\rm r}^2}{e^2}\sin 2\varphi - \frac{\mathcal{C}_{\rm r}}{e}\left(j_1 n' + j_2 n\right)\sin\varphi\,. \tag{8.62}$$

This gives

$$\ddot{\varphi} = \left[3j_2^2 \mathcal{C}_{\rm r} ne + \frac{\mathcal{C}_{\rm r}}{e}\left(j_1 n' + j_2 n\right)\right] \sin\varphi - \frac{\mathcal{C}_{\rm r}^2}{e^2} \sin 2\varphi\,. \tag{8.63}$$

We can construct a solution to this modified form of the pendulum equation by assuming a form similar to the previous solution given in Eq. (8.56). We write

$$n = n_0 + k \cos\frac{1}{2}\varphi, \tag{8.64}$$

where n_0 is the mean motion associated with the nominal value of the resonance and k is a constant that has yet to be determined. Note that $j_1 n' + j_2 n_0$ is also a constant. Ignoring the smaller, secular term in Eq. (8.31), we can now rewrite Eq. (8.60) as

$$j_1 n' + j_2 n_0 + j_2 k \cos\frac{1}{2}\varphi = \dot{\varphi} + \frac{\mathcal{C}_{\rm r}}{e}\cos\varphi. \tag{8.65}$$

Taking $\dot{\varphi} = 0$ at $\varphi = \pi$ gives

$$j_1 n' + j_2 n_0 = -\frac{\mathcal{C}_{\rm r}}{e}\,. \tag{8.66}$$

Hence

$$j_1 n' + j_2 n = -\frac{\mathcal{C}_{\rm r}}{e} + j_2 k \cos\frac{1}{2}\varphi, \tag{8.67}$$

and the equation for $\ddot{\varphi}$ becomes

$$\ddot{\varphi} = \left[3j_2^2 \mathcal{C}_{\rm r} ne - \frac{\mathcal{C}_{\rm r}^2}{e^2}\right] \sin\varphi + j_2 k \frac{\mathcal{C}_{\rm r}}{e} \cos\frac{1}{2}\varphi \sin\varphi - \frac{\mathcal{C}_{\rm r}^2}{e^2} \sin 2\varphi, \tag{8.68}$$

with the energy integral

$$\frac{1}{2}\dot{\varphi}^2 = 2\left[3j_2^2 \mathcal{C}_{\rm r} ne - \frac{\mathcal{C}_{\rm r}^2}{e^2}\right] \sin^2\frac{1}{2}\varphi - \frac{4}{3} j_2 k \frac{\mathcal{C}_{\rm r}}{e} \cos^3\frac{1}{2}\varphi - \frac{\mathcal{C}_{\rm r}^2}{e^2} \sin^2\varphi + E. \tag{8.69}$$

As before we find $E_{\max}$ by setting $\dot{\varphi} = 0$ and $\varphi = \pi$. With $E = E_{\max}$ we can find an equation for $\dot{\phi}$ when $\varphi = 0$. This procedure yields

$$\dot{\varphi}^2\Big|_{\varphi=0} = -12 j_2^2 \mathcal{C}_{\rm r} ne + 4\frac{\mathcal{C}_{\rm r}}{e^2} - \frac{8}{3} j_2 k \frac{\mathcal{C}_{\rm r}}{e}. \tag{8.70}$$

Taking $\varphi = 0$ in Eqs. (8.65) and (8.67) and squaring the resulting expression for $\dot{\varphi}$ gives

$$\dot{\varphi}^2\Big|_{\varphi=0} = 4\frac{\mathcal{C}_{\rm r}}{e^2} + j_2^2 k^2 - 4 j_2 k \frac{\mathcal{C}_{\rm r}}{e}\,. \tag{8.71}$$

Equating this expression with Eq. (8.70) gives the following quadratic in the unknown constant k:

$$k^2 - \frac{4}{3}\frac{1}{j_2}\frac{\mathcal{C}_{\rm r}}{e} k + 12 \mathcal{C}_{\rm r} ne = 0, \tag{8.72}$$

with the solution

$$k = \frac{2}{3}\frac{1}{j_2}\frac{\mathcal{C}_\mathrm{r}}{e} \pm \left(12|\mathcal{C}_\mathrm{r}|ne\right)^{1/2}\left(1 + \frac{1}{27j_2^2e^3}\frac{|\mathcal{C}_\mathrm{r}|}{n}\right)^{1/2}, \tag{8.73}$$

where we have made use of the fact that $\mathcal{C}_\mathrm{r} < 0$ for first-order resonances. Substituting $\varphi = 0$ in Eq. (8.64) and making use of Eq. (8.66) gives

$$\delta n_\mathrm{max} = k + \frac{|\mathcal{C}_\mathrm{r}|}{j_2 e} \tag{8.74}$$

and hence, using our solution for k, we have

$$\delta n_\mathrm{max} = \pm\left(12|\mathcal{C}_\mathrm{r}|ne\right)^{1/2}\left(1 + \frac{1}{27j_2^2e^3}\frac{|\mathcal{C}_\mathrm{r}|}{n}\right)^{1/2} + \frac{|\mathcal{C}_\mathrm{r}|}{3j_2e}. \tag{8.75}$$

Note that for moderate values of e this is consistent with the approximate expression given in Eq. (8.57) with $j_4 = -1$. These expressions are equivalent to those given by Dermott & Murray (1983). In terms of semi-major axis we can write

$$\frac{\delta a_\mathrm{max}}{a} = \pm\left(\frac{16}{3}\frac{|\mathcal{C}_\mathrm{r}|}{n}e\right)^{1/2}\left(1 + \frac{1}{27j_2^2e^3}\frac{|\mathcal{C}_\mathrm{r}|}{n}\right)^{1/2} - \frac{2}{9j_2e}\frac{|\mathcal{C}_\mathrm{r}|}{n}. \tag{8.76}$$

In Sect. 8.8.1 we use a Hamiltonian approach to derive a similar expression for the case of a first-order resonance.

These results imply that in the case of first-order resonances the maximum libration width in terms of mean motion or semi-major axis decreases as the eccentricity decreases until, for a low enough values of e, the width starts to increase again. We illustrate this behaviour in Fig. 8.7 where we have plotted the maximum libration width for the 3:1, 2:1, 5:3, 3:2, and 4:3 jovian internal resonances. The plots were produced by taking $m'/m_\mathrm{c} = 9.54 \times 10^{-4}$ and $a' = 5.2033$ with values of $|\mathcal{C}_\mathrm{r}|/n = (m'/m_\mathrm{c})\alpha f_\mathrm{d}(\alpha)$ taken from Table 8.5.

The plots shown in Fig. 8.7 have to be treated with some caution. It has to be remembered that the expansion of the disturbing function on which they are based has been truncated to lowest order in the eccentricity. Therefore the libration widths will not be accurate at large eccentricity. Furthermore, an object with an eccentricity of 0.25 at the 4:3 resonance would have an orbit that intersected the orbit of Jupiter and so some of the convergence conditions of the series expansion of the disturbing function would not hold. However, the plots illustrate the difference between first- and second-order resonances at low eccentricity. As $e \to 0$ there is an enhanced precessional effect for first-order

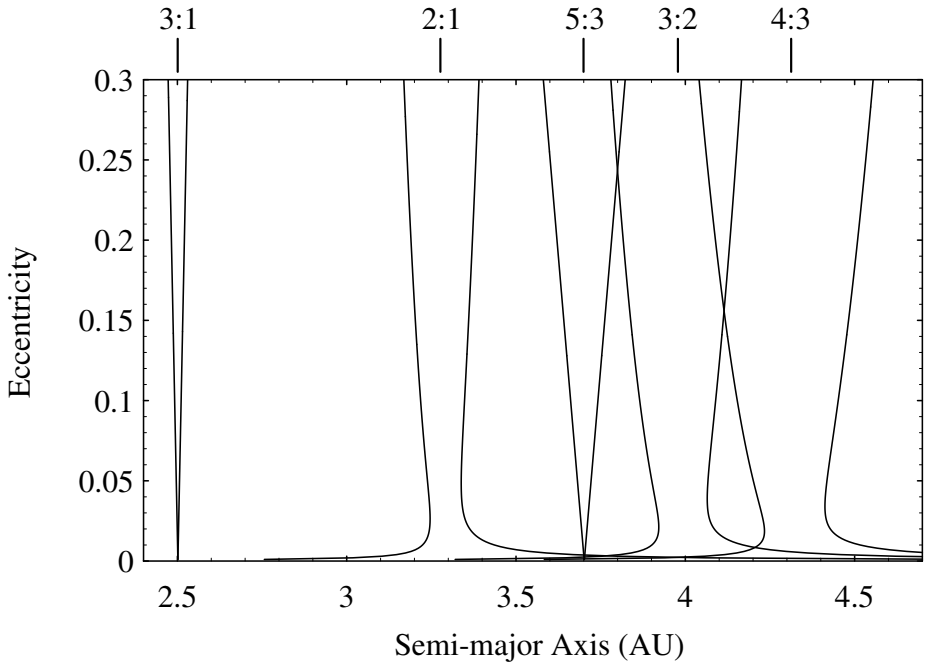

Fig. 8.7. Maximum libration zones as a function of semi-major axis and eccentricity for a selection of internal jovian resonances using an analytical model based on the circular restricted three-body problem. The nominal resonance locations are indicated above the plot.

resonances that increases the libration width, although this has to be treated with some caution (see Sect. 8.9 for a discussion of this phenomenon).

8.8 The Hamiltonian Approach

Given the similarity between the equations of motion of an object in resonance and those of a simple pendulum, it is not surprising that many celestial mechanicians have used a generalisation of the Hamiltonian for a pendulum as their fundamental model of resonance. This formulation was introduced by Poincaré (1902, 1905) and used by Message (1966), Yoder (1973), Peale (1976), Wisdom (1980), and Henrard & Lemaître (1983) and resulted in a powerful new Hamiltonian method for studying resonance. Their approach proves particularly useful when considering dissipative systems (such as tidally evolving satellites) and allows a new understanding of resonance capture and the effects of resonance passage.

The approach given below follows that of Peale (1986). From the definitions of the Poincaré variables (see Sect. 2.10) we note that $e^2 \approx 2\Gamma/\Lambda$ for moderate eccentricities. Hence we can derive the Hamiltonian for our system by making use of our expression for the disturbing function (the perturbing potential per unit mass) given in Eq. (8.26). To begin with we consider the effect of the e^k term (where $k = 1, 2, 3, \ldots$) associated with a single, kth order resonant argument. In

terms of the Poincaré variables we have

$$\begin{aligned}\mathcal{H} = &-\frac{\mathcal{G}^2 m_c^2 m^3}{2\Lambda^2} - \frac{\mathcal{G}^2 m_c^2 m'^3}{2\Lambda'^2} \\ &- \frac{\mathcal{G}^2 m_c m m'^3}{\Lambda'^2} f_d \left(\frac{2\Gamma}{\Lambda}\right)^{\frac{k}{2}} \cos[j\lambda' + (k-j)\lambda + k\gamma] \\ &- \Gamma\dot{\varpi}_{sec} - Z\dot{\Omega}_{sec} + \Lambda\dot{\lambda}_{sec} - \Gamma'\dot{\varpi}'_{sec} - Z'\dot{\Omega}'_{sec} + \Lambda'\dot{\lambda}'_{sec}, \end{aligned} \tag{8.77}$$

where the first two terms are the individual two-body parts of the Hamiltonian (cf. Eq. (2.182)); the third term is the resonant contribution from the e^k resonant argument; and the remaining terms allow for all secular contributions (to the second order in eccentricity and inclination) to the pericentres, nodes, and mean longitudes of each object. Note that we are considering a resonance of the form $j : (j-k)$ and hence $k > 0$ is the order of the resonance. This is in keeping with the notation used to list the disturbing function terms in Appendix B.

The six degrees of freedom of the Hamiltonian can be reduced to four by noting that $z = -\Omega$ and $z' = -\Omega'$ do not appear in $\mathcal{H}$. Hence Z and Z' are constants of the motion, a consequence of considering resonant perturbations dominated by a planar term. We can now introduce a new set of four variables, θ_i, defined by

$$\theta_1 = j\lambda' + (k-j)\lambda + k\gamma, \tag{8.78}$$

$$\theta_2 = j\lambda' + (k-j)\lambda + k\gamma', \tag{8.79}$$

$$\theta_3 = \lambda, \tag{8.80}$$

$$\theta_4 = \lambda'. \tag{8.81}$$

The relationships between the corresponding momenta, Θ_i, and the original momenta can be obtained by solving the simple system of equations

$$\sum_{i=1}^{4} \Theta_i \, \mathrm{d}\theta_i = \Lambda \, \mathrm{d}\lambda + \Lambda' \, \mathrm{d}\lambda' + \Gamma \, \mathrm{d}\gamma + \Gamma' \, \mathrm{d}\gamma' \tag{8.82}$$

to give

$$(k-j)(\Theta_1 + \Theta_2) + \Theta_3 = \Lambda, \tag{8.83}$$

$$j(\Theta_1 + \Theta_2) + \Theta_4 = \Lambda', \tag{8.84}$$

$$k\Theta_1 = \Gamma, \tag{8.85}$$

$$k\Theta_2 = \Gamma', \tag{8.86}$$

where Θ_2, Θ_3, and Θ_4 are all constants since θ_2, θ_3, and θ_4 no longer appear in $\mathcal{H}$. At this stage the problem has been reduced to a one degree of freedom system in the variables θ_1 and Θ_1. Before proceeding it is worthwhile examining these constants in more detail.

From Eqs. (8.83)–(8.86) we have

$$\Theta_4 = \Lambda' - j(\Theta_1 + \Theta_2) \approx m' \sqrt{\mathcal{G}(m_c + m')a'} \tag{8.87}$$

to lowest order. Therefore Θ_4 is related to a', a constant in the absence of a perturbation from the mass m. From the definitions we have

$$\Theta_2 = \frac{\Gamma'}{k} = \frac{m'}{k}\sqrt{\mathcal{G}(m_c + m)a'}\left(1 - \sqrt{1 - e'^2}\right) \approx \frac{m'}{2k}\sqrt{\mathcal{G}(m_c + m)a'}\, e'^2. \quad (8.88)$$

Therefore Θ_2 is related to the eccentricity of the external body. Because there is no perturbation from the inner body included in $\mathcal{H}$, the quantities a' and e' are fixed and hence Θ_2 must be a constant.

The third constant, Θ_3, is another form of the Tisserand relation, itself derived from the Jacobi constant (see Sect. 3.4). We can demonstrate this by using Eq. (8.83) to write

$$\Theta_3 = \Gamma - (k - j)(\Theta_1 + \Theta_2) = \text{constant}. \quad (8.89)$$

Because Θ_2 is also a constant we have

$$\Lambda - (k - j)\frac{\Gamma}{k} = \text{constant} \quad (8.90)$$

and hence

$$\dot{\Lambda} = \frac{k - j}{k}\dot{\Gamma}. \quad (8.91)$$

Expressed in terms of a and e the previous relation can be rewritten as

$$\frac{\dot{a}}{\dot{e}} = 2\frac{k - j}{k}ae, \quad (8.92)$$

which is equivalent to the previous result given in Eq. (8.35).

Returning to our expression for $\dot{\Lambda}$ in Eq. (8.91) we can find another expression for $(k - j)/k$ by making use of the fact that at the $j : (j - k)$ resonance location we have the approximate relation $jn' - (j - k)n \approx 0$ and hence

$$j + (k - j)m^3\Lambda^{-3} \approx 0, \quad (8.93)$$

with a suitable choice of units such that $n' = 1$. Therefore

$$\frac{k}{k - j} = 1 - m^3\Lambda^{-3} \quad (8.94)$$

and we can write

$$\dot{\Lambda}\left(1 - \frac{m^3}{\Lambda^3}\right) = \dot{\Gamma}, \quad (8.95)$$

which integrates to give

$$\Lambda + \frac{m^3}{2\Lambda^2} = \Gamma + \text{constant}. \quad (8.96)$$

In our choice of units this can be rewritten as

$$\frac{1}{2a} + \sqrt{a(1 - e^2)} = \text{constant} \quad (8.97)$$

(cf. Eq. (3.46) with $I = 0$).

In terms of the new coordinates and momenta the Hamiltonian given in Eq. (8.77) can be written as

$$\begin{aligned}\mathcal{H} = &-\frac{\mathcal{G}^2 m_c^2 m^3}{2[\Theta_3 + (k-j)\Theta_1]^2} - \frac{\mathcal{G}^2 m_c^2 m'^3}{2(\Theta_4 + j\Theta_1)^2} \\ &- \frac{\mathcal{G}^2 m_c m m'^3}{(\Theta_4 + j\Theta_1)^2} \frac{(2k\Theta_1)^{k/2}}{[\Theta_3 + (k-j)\Theta_1]^{k/2}} f_d \cos\theta_1 \\ &- k\Theta_1 \dot{\varpi}_{sec} + [\Theta_3 + (k-j)\Theta_1]\dot{\lambda}_{sec} - k\Theta_2 \dot{\varpi}'_{sec} + (j\Theta_1 + \Theta_4)\dot{\lambda}'_{sec}, \end{aligned} \tag{8.98}$$

where Θ_2 has been set to zero or incorporated with Θ_3 and Θ_4 where it occurs in Λ and Λ'; this has little effect on the dynamics of the resonance. The Hamiltonian in Eq. (8.98) can be used to study the dynamics for arbitrarily large eccentricities (see Wisdom 1980). Except for these cases, we can legitimately carry out the expansions given below. From the definitions we see that $|\Theta_1| \ll \Theta_3$ and $|\Theta_1| \ll \Theta_4$, so that we can make use of the approximations

$$[\Theta_3 + (k-j)\Theta_1]^{-2} \approx \frac{1}{\Theta_3^2} - 2(k-j)\frac{\Theta_1}{\Theta_3^3} + 3(k-j)^2 \frac{\Theta_1^2}{\Theta_3^4}, \tag{8.99}$$

$$[\Theta_4 + j\Theta_1]^{-2} \approx \frac{1}{\Theta_4^2} - 2j\frac{\Theta_1}{\Theta_4^3} + 3j^2 \frac{\Theta_1^2}{\Theta_4^4}, \tag{8.100}$$

where the first term on the right-hand side of each equation is a constant and will therefore be ignored when we substitute back in $\mathcal{H}$. Similarly we can ignore the Θ_1 and Θ_2 contributions to the divisors in the third term in $\mathcal{H}$ given in Eq. (8.98) since there is already a small factor in the numerator. Taking $\Theta_3 \approx \Lambda$ and $\Theta_4 \approx \Lambda'$, and substituting our definitions of Θ_1, Θ_2, Λ, and Λ', we can now write the approximate Hamiltonian as

$$\begin{aligned}\mathcal{H} = &\left[j(n' + \dot{\lambda}'_{sec}) + (k-j)(n + \dot{\lambda}_{sec}) - k\dot{\varpi}_{sec}\right]\left(\frac{\Gamma}{k}\right) \\ &- \frac{3}{2}\left[\frac{j^2}{m'a'^2} + \frac{(k-j)^2}{ma^2}\right]\left(\frac{\Gamma}{k}\right)^2 \\ &- (n^2)^{1-k/4} f_d \frac{a^{3-k}}{a'} \frac{m'}{m_c} m^{1-k/2} \left(2\Gamma\right)^{k/2} \cos\theta_1, \end{aligned} \tag{8.101}$$

where again we have ignored constant terms in the Hamiltonian and made use of the relationships $n^2 \approx \mathcal{G}m_c/a^3$ and $n'^2 \approx \mathcal{G}m_c/a'^3$ (i.e., we have assumed that m and m' are much smaller than m_c).

Now we make a small change to the resonant variable, θ_1, by defining $\theta'_1 = \theta_1/k$ and dropping the prime. The reasons for this step are outlined by Peale (1986) and involve the need to maintain a proper choice of canonical variables when $k > 1$. At the same time we change the sign of the Hamiltonian by setting $\mathcal{H}^\dagger = -\mathcal{H}$. This gives rise to a Hamiltonian of the form

$$\mathcal{H}^\dagger = \bar{\alpha}\Gamma + \bar{\beta}\Gamma^2 + \bar{\epsilon}(2\Gamma)^{k/2}\cos k\theta_1, \tag{8.102}$$

where

$$\bar{\alpha} = [(j-k)n^* - jn'^* + k\dot{\varpi}_{\rm sec}]/k, \tag{8.103}$$

$$\bar{\beta} = \frac{3}{2k^2}\left[\frac{(j-k)^2}{ma^2} + \frac{j^2}{m'a'^2}\right], \tag{8.104}$$

$$\bar{\epsilon} = (n^2)^{1-\frac{k}{4}}\, f_{\rm d}\, \frac{a^{3-k}}{a'}\frac{m'}{m_{\rm c}}\, m^{1-k/2}, \tag{8.105}$$

with $n^* = n + \dot{\lambda}_{\rm sec}$ and $n'^* = n' + \dot{\lambda}'_{\rm sec}$. Note that the quantity $\bar{\alpha}$ is a measure of the proximity to the resonance, with $\bar{\alpha} = 0$ denoting the location of exact resonance (i.e., the place where the time derivative of the resonant argument is zero).

So far in the analysis we have only considered a single dominant resonant term, which corresponds to that of an internal, kth-order resonance in the restricted problem. However, it is relatively easy to extend this to an external resonance. In this case the Hamiltonian becomes

$$\begin{aligned}\mathcal{H}' = &-\frac{\mathcal{G}^2 m_{\rm c}^2 m^3}{2\Lambda^2} - \frac{\mathcal{G}^2 m_{\rm c}^2 m'^3}{2\Lambda'^2} \\ &- \frac{\mathcal{G}^2 m_{\rm c} m m'^3}{\Lambda'^2} f_{\rm d}\left(\frac{2\Gamma'}{\Lambda'}\right)^{k/2} \cos[j\lambda' + (k-j)\lambda + k\gamma'] \\ &- \Gamma\dot{\varpi}_{\rm sec} - Z\dot{\Omega}_{\rm sec} + \Lambda\dot{\lambda}_{\rm sec} - \Gamma'\dot{\varpi}'_{\rm sec} - Z'\dot{\Omega}'_{\rm sec} + \Lambda'\dot{\lambda}'_{\rm sec},\end{aligned} \tag{8.106}$$

which differs from the original $\mathcal{H}$ in only one term, and $f_{\rm d}$ now incorporates any relevant indirect terms. The transformed Hamiltonian is

$$\mathcal{H}'^{\dagger} = \bar{\alpha}'\Gamma' + \bar{\beta}'\Gamma'^2 + \bar{\epsilon}'(2\Gamma')^{k/2}\cos k\theta_2, \tag{8.107}$$

where

$$\bar{\alpha}' = [(j-k)n^* - jn'^* + \dot{\varpi}'_{\rm sec}]/k, \tag{8.108}$$

$$\bar{\beta}' = \frac{3}{2k^2}\left[\frac{(j-k)^2}{ma^2} + \frac{j^2}{m'a'^2}\right] = \bar{\beta}, \tag{8.109}$$

$$\bar{\epsilon}' = (n'^2)^{1-\frac{k}{4}}\, f_{\rm d}\, a'^{2-k}\frac{m}{m_{\rm c}} m'^{1-k/2}. \tag{8.110}$$

Note that $\mathcal{H}'^{\dagger}$ has a form that is identical to that of $\mathcal{H}^{\dagger}$ and so we can proceed with an analysis of the internal resonance case knowing that it also applies to the external case with slight modifications to the constants.

We have made the implicit assumption that $f_{\rm d}$ is treated as a constant throughout, even though in reality it is a function of $\alpha = a/a'$. However, it can easily be shown that the size of the cosine term in Eq. (8.107) is dominated by the variation in eccentricity rather than semi-major axis. Similarly the effects of the variation of a on the parameter $\bar{\beta}$ are negligible in most circumstances (Peale 1976). Under this assumption it is possible further to simplify the Hamiltonian

in Eq. (8.107) by a scale transformation designed to introduce a single free parameter related to $\bar{\alpha}$, the measure of the proximity to resonance. If we scale the momentum such that

$$\Phi = \frac{\Gamma}{\eta}, \tag{8.111}$$

where $\eta > 0$ is a constant, the Hamiltonian becomes

$$\mathcal{H} = \bar{\alpha}\eta\Phi + \bar{\beta}\eta^2\Phi^2 + \bar{\epsilon}\eta^{k/2}(2\Phi)^{k/2}\cos k\phi, \tag{8.112}$$

where the coordinate conjugate to Φ is given by

$$\phi = \begin{cases} \theta_1 + \pi, & \text{if } \bar{\epsilon} > 0, \\ \theta_1, & \text{if } \bar{\epsilon} < 0. \end{cases} \tag{8.113}$$

Note that the definition of ϕ depends on the sign of $\bar{\epsilon}$, which in turn depends on the sign of $f_{\rm d}$, the constant involving Laplace coefficients. It can be shown that this is positive or negative depending on whether the resonance has an even or odd order, respectively (see, for example, Table 8.5).

The requirement that the coefficients of the last two terms in $\mathcal{H}$ are equal implies that

$$\bar{\epsilon}\eta^{k/2} = (-1)^k 2\bar{\beta}\eta^2, \tag{8.114}$$

and hence the scaling parameter is given by

$$\eta = \left[\frac{(-1)^k 2\bar{\beta}}{\bar{\epsilon}}\right]^{\frac{2}{k-4}}, \tag{8.115}$$

where the factor $(-1)^k$ is needed to take account of both possible signs of $\bar{\epsilon}$. Scaling $\mathcal{H}$ by the factor $\bar{\beta}\eta^2$ gives

$$\mathcal{H} = \bar{\delta}\Phi + \Phi^2 + 2(-1)^k(2\Phi)^{k/2}\cos k\phi, \tag{8.116}$$

where the Hamiltonian is now parameterised by

$$\bar{\delta} = \frac{\bar{\alpha}}{\bar{\beta}\eta} = \bar{\alpha}\left[\frac{4}{\bar{\epsilon}^2\bar{\beta}^{2-k}}\right]^{\frac{1}{4-k}}. \tag{8.117}$$

Note that if $\bar{\alpha} = 0$ in Eq. (8.117) then $\bar{\delta} = 0$ and the perturbed object is at exact resonance.

Now we can investigate some properties of the equilibrium points of the new Hamiltonian. Because the time derivatives of ϕ and Φ are derived from the partial derivatives of $\mathcal{H}$ with respect to Φ and ϕ, the equilibrium points are simply the solutions of $\partial\mathcal{H}/\partial\phi = \partial\mathcal{H}/\partial\Phi = 0$. The resulting simultaneous equations are

$$\bar{\delta} + 2\Phi + 2(-1)^k k(2\Phi)^{\frac{k-2}{2}}\cos k\phi = 0, \tag{8.118}$$

$$2(-1)^{k+1}k(2\Phi)^{k/2}\sin k\phi = 0. \tag{8.119}$$

For $k \geq 2$ there is always an equilibrium point at $\Phi = 0$. For nonzero Φ the second equation can only be satisfied when $k\phi = i\pi$, where i is an integer. The first equation then gives the value of Φ at the equilibrium points as the solution of

$$\bar{\delta} + 2\Phi + 2(-1)^{k+i} k (2\Phi)^{\frac{k-2}{2}} = 0. \tag{8.120}$$

We can rewrite this in terms of a new variable, $R = \sqrt{2\Phi}$, where R is the radial location of the equilibrium point and is always positive. We there by obtain

$$\bar{\delta} + R^2 = (-1)^{k+i+1} 2k R^{k-2}. \tag{8.121}$$

We can illustrate the solutions by defining two functions,

$$f(\bar{\delta}, R) = \bar{\delta} + R^2 \qquad \text{and} \qquad g(k, R) = (-1)^{k+i+1} 2k R^{k-2}. \tag{8.122}$$

The first function always describes a parabola with a minimum at $(0, \bar{\delta})$. The nature of $g(k, R)$ depends on the value of k. For example, for $k = 1$ the resulting curves are two hyperbolas, for $k = 2$ they are two straight lines parallel to the R axis and for $k = 3$ they are two straight lines through the origin with equal and opposite gradients. The values of R at the points of intersection of $f(\bar{\delta}, R)$ and $g(k, R)$ give the location of the equilibrium points for a particular value of $\bar{\delta}$. Families of such curves and their intersection points for the cases $k = 1$, 2, and 3 are shown in Fig. 8.8.

It is clear from Fig. 8.8 that a double root of Eq. (8.121) (and hence a bifurcation point) will occur where the two functions meet tangentially. This occurs where $f'(\bar{\delta}, R) = g'(k, R)$, where the prime denotes partial differentiation with respect

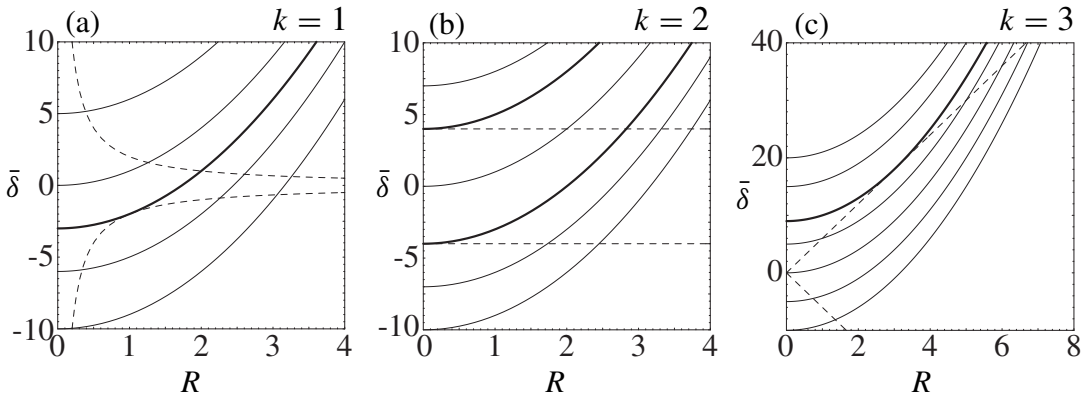

Fig. 8.8. Plots of the parabolas $f(\bar{\delta}, R)$ for various values of $\bar{\delta}$ (solid curves) and $g(k, R)$ (dashed curves and lines) for $k = 1$, 2, and 3. In each case the parabola defined by $f(\bar{\delta}_\mathrm{b}, R)$ is shown as a thicker curve. (a) The curves for $k = 1$ and $\bar{\delta} = -10, -7, 0, 5$ and the bifurcation value of $\bar{\delta}_\mathrm{b} = -3$. (b) The curves for $k = 2$ and $\bar{\delta} = -10, -7, 0, 7$ and the two bifurcation values of $\bar{\delta}_\mathrm{b} = \pm 4$. (c) The curves for $k = 3$ and $\bar{\delta} = -10, -5, 0, 5, 15, 20$ and the bifurcation value of $\bar{\delta}_\mathrm{b} = 9$.

to R. The resulting bifurcation value, $R_{\rm b}$, is given by

$$R_{\rm b} = \left[(-1)^{k+i+1}k(k-2)\right]^{\frac{1}{4-k}}. \tag{8.123}$$

Substituting $R = R_{\rm b}$ in Eq. (8.121) and solving for $\bar{\delta}$ gives the corresponding value of $\bar{\delta}$ at the bifurcation point as

$$\bar{\delta}_{\rm b} = (4-k)\left[(-1)^{k+i+1}k\right]^{\frac{2}{4-k}}(k-2)^{\frac{k-2}{4-k}}. \tag{8.124}$$

With the appropriate signs this equation gives $\bar{\delta}_{\rm b} = -3, \pm 4$, and 9 for $k = 1$, 2, and 3 respectively.

Before proceeding let us examine the scaling that we have introduced. After so many transformations it is easy to lose track of the relationship between the current set of variables and the original orbital elements; this is one of the disadvantages of working with canonical elements. However, from the definitions of $\bar{\beta}$ and $\bar{\epsilon}$, and making use of the approximation $\alpha \approx [(j-1)/j]^{2/3}$ derived from Kepler's third law, the relationship between R and e for the case of an external perturber can be written

$$R = \left\{\frac{3(-1)^k}{k^2 f_{\rm d}}\left[(j-k)^{\frac{4}{3}}j^{\frac{2}{3}}\frac{m_{\rm c}}{m'} + j^{\frac{4}{3}}(j-k)^{\frac{2}{3}}\frac{m}{m'}\frac{m_{\rm c}}{m'}\right]\right\}^{\frac{1}{4-k}} e. \tag{8.125}$$

The equivalent expression for the case of an internal perturber is

$$R = \left\{\frac{3(-1)^k}{k^2 f_{\rm d}}\left[(j-k)^{\frac{4}{3}}j^{\frac{2}{3}}\frac{m'}{m}\frac{m_{\rm c}}{m} + j^2\frac{m_{\rm c}}{m}\right]\right\}^{\frac{1}{4-k}} e'. \tag{8.126}$$

Note that in the case where the perturbing mass is significantly larger than the perturbed mass suitable approximations can be made.

Now that we have developed the general theory for internal and external kth-order resonances we can proceed to consider the nature of the different trajectories associated with each type of resonance.

8.8.1 The e and e′ Resonances

Consider the case of an internal, $j : (j-1)$ first-order resonance. The resonant argument is

$$\theta = j\lambda' + (1-j)\lambda - \varpi \tag{8.127}$$

and the associated $f_{\rm d}$ term is given by the first entry in Table 8.1. We refer to this as the *e resonance* because the associated term in the disturbing function is of $\mathcal{O}(e)$. The relevant values of the single-parameter Hamiltonian and the constants $\bar{\delta}$, $\bar{\alpha}$, $\bar{\beta}$, and $\bar{\epsilon}$ can easily be obtained by substituting $k = 1$ in Eq. (8.116) and Eqs. (8.103)–(8.105). The final Hamiltonian is

$$\mathcal{H}_1 = \bar{\delta}\Phi + \Phi^2 - 2\sqrt{2\Phi}\cos\phi, \tag{8.128}$$

where ϕ is given by Eq. (8.113) with $\theta_1 = \theta$ and

$$\bar{\delta} = \bar{\alpha}\left(\frac{4}{\bar{\epsilon}^2\bar{\beta}}\right)^{\frac{1}{3}}. \tag{8.129}$$

To make it easier to study the types of motion we introduce a mixed canonical transformation (see Sect. 2.10) given by

$$x = \sqrt{2\Phi}\cos\phi \qquad \text{and} \qquad y = \sqrt{2\Phi}\sin\phi, \tag{8.130}$$

where, as above, $\sqrt{2\Phi}$ can be thought of as the radial distance, R, from the origin. The Hamiltonian becomes

$$\mathcal{H}_1(x, y) = \frac{1}{2}\bar{\delta}(x^2 + y^2) + \frac{1}{4}(x^2 + y^2)^2 - 2x. \tag{8.131}$$

From Eq. (8.125) the approximate relationships between R and e is

$$R \approx \left[\frac{-3}{f_{\rm d}}(j-1)^{\frac{4}{3}} j^{\frac{2}{3}} \frac{m_{\rm c}}{m'}\right]^{\frac{1}{3}} e, \tag{8.132}$$

and the radial distance from the origin in (x, y) space is simply a scaled value of the eccentricity of the perturbed object.

Now consider the case of an external, $j : (j-1)$ first-order resonance. The resonant argument is

$$\theta = j\lambda' + (1-j)\lambda - \varpi' \tag{8.133}$$

and the associated $f_{\rm d}$ term is given by the second entry in Table 8.1. We refer to this as the e' *resonance* because the associated term in the disturbing function is of $\mathcal{O}(e')$. In the special case of $j = 2$ we need to include the indirect term $f_{\rm e}$ (the first entry Table 8.3); this is best done by absorbing it in $f_{\rm d}$. We have already noted that the relevant Hamiltonian, $\mathcal{H}'$, has a form identical to $\mathcal{H}$, with suitable, minor modifications to the constants. The resulting approximate relationship between R and e' for the case where $m' \ll m$ is

$$R \approx \left[\frac{-3}{f_{\rm d}} j^2 \frac{m_{\rm c}}{m}\right]^{\frac{1}{3}} e'. \tag{8.134}$$

Therefore the theory developed for the e resonance can also be applied to the e' resonance with a suitable change of resonant angle and scaling.

In the previous section we showed how the radial locations of the equilibrium points of the system can be found for a kth-order resonance. By solving $\partial\mathcal{H}_1/\partial x = 0$ and $\partial\mathcal{H}_1/\partial y = 0$ it is easy to show that the equilibrium points lie along the x axis and are given by the solution of the cubic equation

$$x^3 + \bar{\delta}x - 2 = 0. \tag{8.135}$$

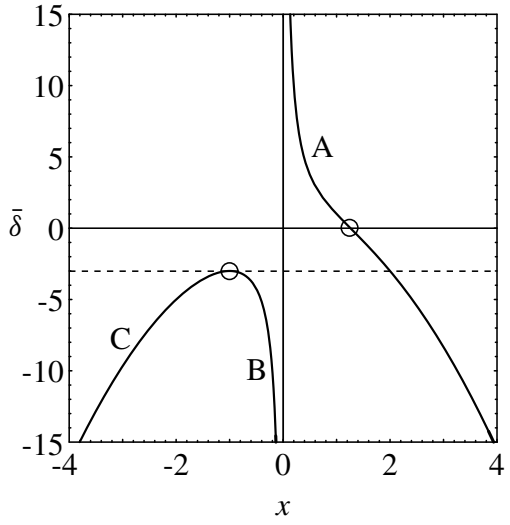

Fig. 8.9. A plot of $\bar{\delta} = (2-x^3)/x$ illustrating the relationship between the value of $\bar{\delta}$ and the position on the x axis of the equilibrium points for e and e' resonances. Branches A and B give rise to stable equilibrium points; branch C gives rise to an unstable equilibrium point. The intersection of the left-hand branch of the curves and the dashed line given by $\bar{\delta} = -3$ denotes the location of the bifurcation point (circled) where the stable and unstable branches meet. The intersection point associated with exact resonance at $\bar{\delta} = 0$ is also circled.

Here, of course, x can be positive or negative whereas before we were interested in the radial distance, R, of the equilibrium points. The roots of this cubic give the x values of equilibrium points of $\mathcal{H}_1$ for a given value of $\bar{\delta}$. Figure 8.9 shows $\bar{\delta}$ as a function of x. Note that for small $|x|$ this equation becomes $\bar{\delta}x - 2 \approx 0$ whereas for large $|x|$ we have $x^2 + \bar{\delta} \approx 0$. The solutions of Eq. (8.135) are

$$x_1 = \frac{-3^{\frac{1}{3}}\bar{\delta} + \Delta^{\frac{2}{3}}}{3^{\frac{2}{3}}\Delta^{\frac{1}{3}}}, \tag{8.136}$$

$$x_{2,3} = \frac{(3^{\frac{1}{3}} \pm 3^{\frac{5}{6}}\,\mathrm{i})\bar{\delta} + (-1 \pm \sqrt{3}\,\mathrm{i})\Delta^{\frac{2}{3}}}{3^{\frac{2}{3}}2\Delta}, \tag{8.137}$$

where $\mathrm{i} = \sqrt{-1}$ and

$$\Delta = 9 + \sqrt{3}\sqrt{27 + \bar{\delta}^3}. \tag{8.138}$$

Substituting $k = 1$ in Eq. (8.124) gives $\bar{\delta}_\mathrm{b} = -3$ for the value of $\bar{\delta}$ at which the bifurcation occurs. This point and the equilibrium point associated with exact resonance are circled in Fig. 8.9. It is clear from its definition that Δ is always real for $\bar{\delta} \geq -3$ and this always gives one real root, x_1. For $\bar{\delta} < -3$ there are always three real roots, even though the quantity Δ becomes complex.

We can illustrate the dependence on $\bar{\delta}$ by plotting the curves of constant Hamiltonian for various values of $\bar{\delta}$. The initial values of the semi-major axis, eccentricity, and ϕ determine the Hamiltonian (a constant of the system) and

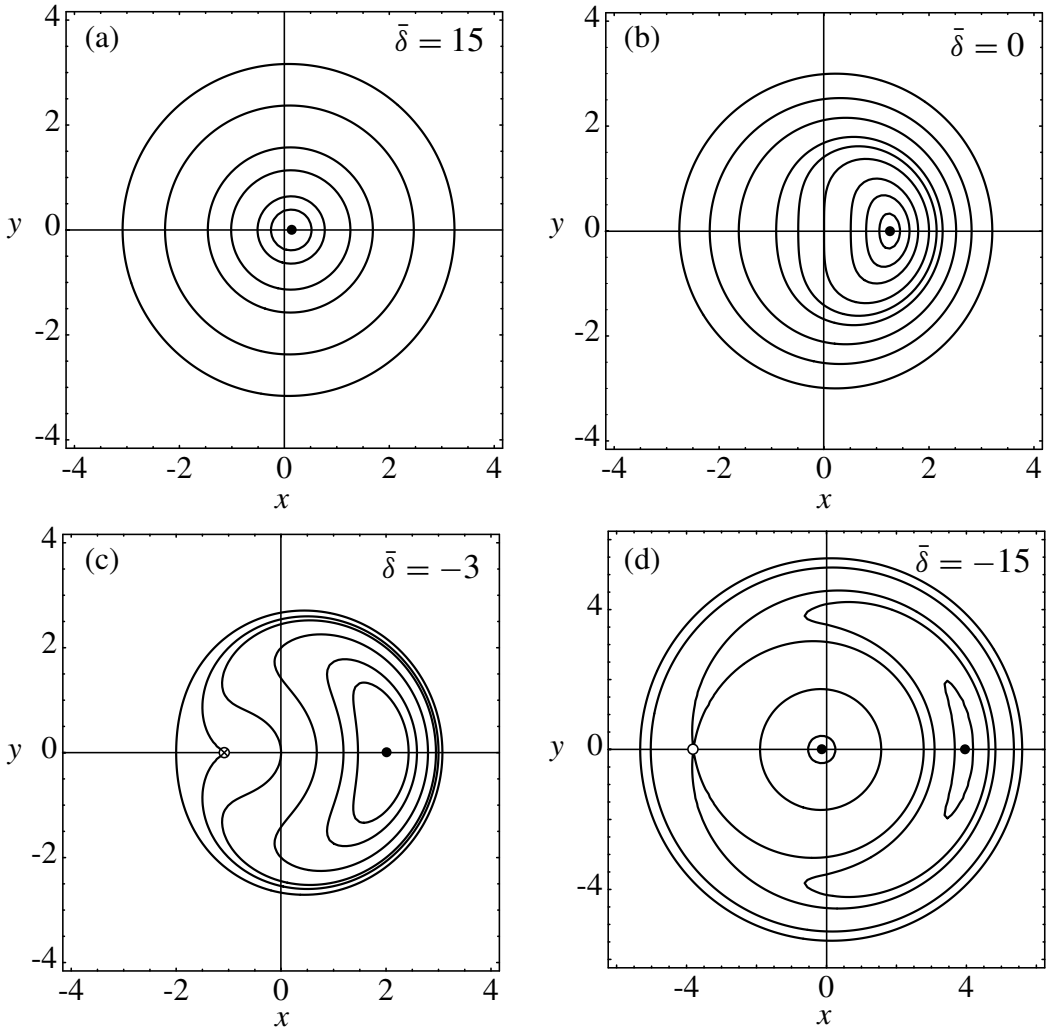

Fig. 8.10. Curves of constant Hamiltonian for the e and e' resonances. (a) $\bar{\delta} = 15$ with $\mathcal{H}_1 = 1$, 3, 10, 20, 50, 100. (b) $\bar{\delta} = 0$ (exact resonance) with $\mathcal{H}_1 = -9/5, -3/2, -1$, 0, 1, 2, 5, 10, 20. (c) $\bar{\delta} = -3$ (the bifurcation value) with $\mathcal{H}_1 = -5, -4, -2, 0, 3/4, 2$. (d) $\bar{\delta} = -15$ with $\mathcal{H}_1 = -63, -55, -48.57189, -20, -1$.

the particular value of $\bar{\delta}$ for an individual orbit. The orbit will then remain on that curve for all time. In Fig. 8.10 the locations of the stable and unstable equilibrium points are marked by small, filled and unfilled circles, respectively. For $\bar{\delta} = 15$ (i.e., large and positive), there is only one equilibrium point situated close to, but just to the right of, the origin in the positive x direction (Fig. 8.10a). In this case there is only one type of motion for most eccentricities (recalling that the radial coordinate in Fig. 8.10 is a scaled eccentricity), although for very small eccentricities it is possible that the angle ϕ, directly related to the resonant angle, is librating about the stable equilibrium point at $\phi = 0$.

The situation at exact resonance ($\bar{\delta} = 0$) is shown in Fig. 8.10b. Here the equilibrium point is well to the right of the origin. Note that although some of

the trajectories in this plot represent libration in resonance (i.e., the curve does not enclose the origin) the larger curves of constant $\mathcal{H}_1$ are circulating rather than librating.

In the special case where $\bar{\delta} = -3$ a cusp forms (see Fig. 8.10c), indicating the presence of a double root at $x = -1$ in addition to the single root with positive x. The small, crossed circle in Fig. 8.10c indicates the location of the bifurcation point where the stable and unstable branching occurs.

As $\bar{\delta}$ is decreased further we see that the existence of three equilibrium points is now obvious (see Fig. 8.10d). The first, corresponding to the C branch of the left-hand curve in Fig. 8.9, is always unstable while the second (which approaches the origin as $\bar{\delta}$ decreases) is always stable. The third point, the one that always exists for any value of $\bar{\delta}$, now moves in the positive x direction and the stable orbits around it describe a characteristic "banana" shape, all with large eccentricity and, for large-amplitude librations, large excursions in eccentricity. It is important to note that although Figs. 8.10a and 8.10d show the trajectories for large $|\bar{\delta}|$ values that are equidistant from exact resonance, they illustrate very different types of resonant phenomena. At this stage it is helpful to recall that the radial distance in Fig. 8.10 is a scaled eccentricity and the radial location of a stable equilibrium point in these diagrams allows us to calculate the value of the forced eccentricity at an equilibrium point. An interesting fact is that the curves of constant Hamiltonian derived directly from the unexpanded Hamiltonian given in Eq. (8.98) are identical in form to those shown in Fig. 8.10. However, a new bifurcation occurs for large negative values of $\bar{\delta}$ resulting in (i) the appearance of an unstable equilibrium point at $\theta = 0$ close to the origin and (ii) the disappearance of the stable equilibrium point at $\theta = \pi$. This was found by Wisdom (1980) and is relevant to the motion of objects with large eccentricity.

This work has direct applications to the study of planetary rings, where eccentricities are typically very small ($e \sim 10^{-6}$). Figure 8.10 shows that the shape of the curves depends on the value of $\bar{\delta}$. Although there are fundamental differences between Figs. 8.10a and 8.10d there are similarities in the vicinity of the origin. For small x and large $|\bar{\delta}|$ in Eq. (8.135) the x^3 term can be neglected. Therefore, for a given $\bar{\delta}$ the x value of the equilibrium point in the vicinity of the origin is given by $x \approx 2/\bar{\delta}$. Figure 8.11 shows additional curves of constant Hamiltonian for $\bar{\delta} = -15$ (Fig. 8.11a) and $\bar{\delta} = +15$ (Fig. 8.11b). Note that both show concentric circles displaced to either side of the origin. The centre of each circle is at $x \approx \mp 2/15$ in these cases. Therefore the traversal of the resonance introduces a shift of 180° in ϕ. Note that the forced eccentricity is a simple function of the distance from resonance. The mechanism illustrated in Fig. 8.11, and the phase shift on either side of exact resonance, are the basis of our understanding of the first-order Lindblad resonances that occur in planetary ring systems (see Sect. 10.3.2).

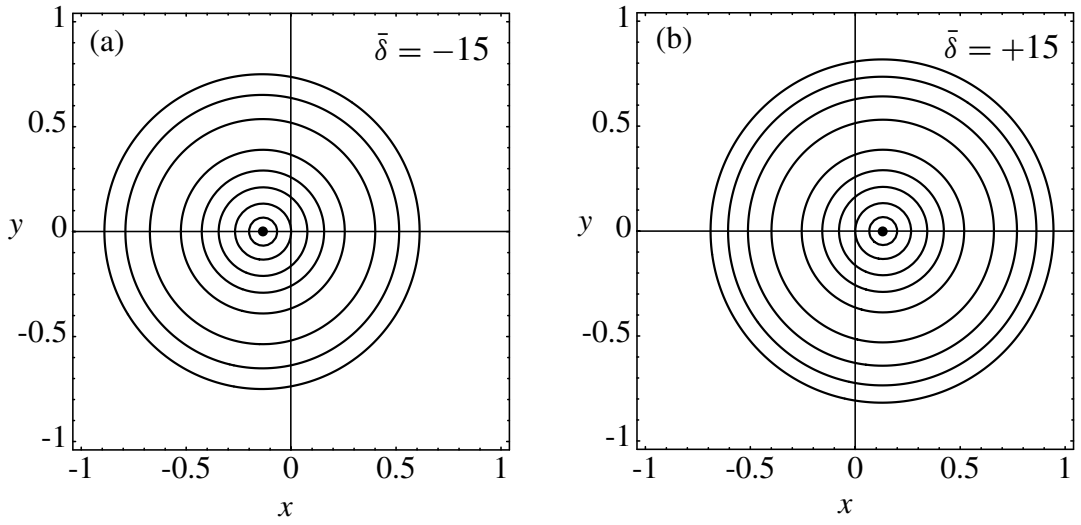

Fig. 8.11. The curves of constant Hamiltonian for the e and e' resonances in the case where the eccentricity is small and the system is not close to exact resonance (i.e., large values of $|\bar{\delta}|$). (a) The curves for $\delta = -15$ with $\mathcal{H}_1 = -4, -3, -2, -1, -0.5, -0.2, 0, 0.1$. (b) The curves for $\bar{\delta} = 15$ with $\mathcal{H}_1 = -0.1, 0, 0.2, 0.5, 1, 2, 3, 4, 5$. Note the difference in scale from Figs. 8.10a and 8.10d.

The same resonant equations, but in a different context, are also applicable to the study of the resonant dynamics of asteroids, where $e \approx 0.1$. In fact, as we show below, the pendulum model provides an adequate representation of the dynamics. We can consider the Hamiltonian for the first-order resonance (Eq. (8.128)) as being composed of two parts. We write

$$\mathcal{H}_1 = \mathcal{H}_0 + \mathcal{H}_{\text{res}}, \tag{8.139}$$

where

$$\mathcal{H}_0 = \bar{\delta}\Phi + \Phi^2 \qquad \text{and} \qquad \mathcal{H}_{\text{res}} = -2\sqrt{2\Phi}\cos\phi. \tag{8.140}$$

Here we are treating the resonant term, $\mathcal{H}_{\text{res}}$, as a perturbation to $\mathcal{H}_0$. The resonant value of the eccentricity given by the $\mathcal{H}_0$ system alone has only small variations. We can find the value of Φ (and hence the eccentricity) at exact resonance by solving for Φ when $\dot{\phi} = 0$. Setting $\partial\mathcal{H}_1/\partial\Phi = 0$ gives

$$\bar{\delta} + 2\Phi_{\text{res}} - \frac{2}{\sqrt{2\Phi_{\text{res}}}}\cos\phi = 0. \tag{8.141}$$

However, we are assuming that e is large and hence we can ignore the $\cos\phi$ term in this equation, obtaining

$$\Phi_{\text{res}} = \frac{1}{2}|\bar{\delta}| \tag{8.142}$$

for the resonant value. Because the resonant term does not vary significantly with respect to Φ in the vicinity of the resonance, we replace Φ in $\mathcal{H}_{\text{res}}$ by its value,

$\Phi_{\rm res}$, at the resonance. This is equivalent to an expansion in the vicinity of $\Phi_{\rm res}$. Note that we are only interested in the Φ values for cases where $\bar{\delta} < \bar{\delta}_{\rm b} = -3$ and so the sign of $\bar{\delta}$ is not important.

Incorporating the equilibrium value of Φ in the cosine part of the Hamiltonian and dropping the constant term $-\bar{\delta}^2/4$ gives

$$\mathcal{H}_1 = \left(\Phi + \frac{1}{2}|\bar{\delta}|\right)^2 - 2\sqrt{|\bar{\delta}|}\cos\phi. \tag{8.143}$$

Dropping the constant term on the left-hand side and scaling the new momentum gives

$$\tilde{\mathcal{H}}_1 = \frac{1}{2}\Psi^2 - 2K\cos\psi, \tag{8.144}$$

where $\Psi = \sqrt{2}(\Phi + \frac{1}{2}|\bar{\delta}|)$, $\psi = \phi$, and $K = \sqrt{|\bar{\delta}|}$. This Hamiltonian has the same form as that of a simple pendulum. Therefore we can use the method shown in Sect. 8.6 to derive an expression for the change in Ψ for the Hamiltonian associated with maximum libration. This gives $\Delta\Psi_{\rm max} = 2\sqrt{2K}$ or, equivalently, $\Delta\Phi_{\rm max} = 2\sqrt{K} = 2\left(|\bar{\delta}|\right)^{\frac{1}{4}}$. But e is related to Φ by

$$S^2e^2 = 2\Phi, \tag{8.145}$$

where

$$S = \left[\frac{-3}{f_{\rm d}}(j-1)^{\frac{4}{3}}j^{\frac{2}{3}}\frac{m_{\rm c}}{m'}\right]^{\frac{1}{3}}. \tag{8.146}$$

Differentiating and setting $\Delta\Phi$ equal to its maximum value gives

$$2e\,\Delta e = (4/S^2)\left(|\bar{\delta}|\right)^{\frac{1}{4}}. \tag{8.147}$$

We can use the same scaling relationship between e and Φ to relate $|\bar{\delta}|$ to $e_{\rm res}$. We have

$$\sqrt{2\Phi_{\rm res}} = S\,e_{\rm res} = \sqrt{|\bar{\delta}|}. \tag{8.148}$$

Substituting for $|\bar{\delta}|$ in Eq. (8.147) yields

$$2e\,\Delta e = 4S^{-\frac{3}{2}}\sqrt{e_{\rm res}}. \tag{8.149}$$

From our discussion of the relationship between Θ_3 and the Jacobi constant we showed that $\dot{a}$ and $\dot{e}$ are related by Eq. (8.92). Taking $k = 1$ in this equation (we are only considering first-order resonances) gives

$$\frac{\delta a}{a} = 2(1-j)e\,\Delta e \tag{8.150}$$

and hence

$$\Delta a_{\rm max} = \pm\left(\frac{16}{3}\frac{|\mathcal{C}_{\rm r}|}{n}e_{\rm res}\right)^{\frac{1}{2}}a, \tag{8.151}$$

where we have used the relations $\mathcal{C}_r = (m'/m_c)n\alpha f_d$ and $\alpha = [(j-1)/j]^{\frac{2}{3}}$. The resulting expression for Δa_{max} is identical to that given in Eq. (8.58) where we first considered the pendulum model.

The pendulum approach can be used to understand the dynamics of asteroids at resonance. In the context of planetary ring dynamics the e' resonance is called a *first-order corotation resonance* (see Sect. 10.3.1), while the e resonance is called a *first-order Lindblad resonance* (see Sect. 10.3.2). Although we have restricted our analysis to first-order resonances, with minor modifications the pendulum model is equally applicable to all subsequent resonances discussed in this chapter.

8.8.2 The e^2, e'^2, I^2, and I'^2 Resonances

Consider the case of an internal, $j : (j-2)$ second-order resonance where the single resonant argument is now

$$\theta = j\lambda' + (2-j)\lambda - 2\varpi \tag{8.152}$$

and the associated f_d term is given by the third term in Table 8.1. We refer to this as the e^2 *resonance* because the associated term in the disturbing function is of $\mathcal{O}(e^2)$. From Eq. (8.116) with $k = 2$ the Hamiltonian of the system is given by

$$\mathcal{H}_2 = \bar{\delta}\Phi + \Phi^2 + 4\Phi\cos 2\phi, \tag{8.153}$$

where ϕ is given by Eq. (8.113) with $\theta_1 = \theta$ and

$$\bar{\delta} = 2\bar{\alpha}/\bar{\epsilon} \tag{8.154}$$

is a measure of the proximity to exact resonance. The definitions of the constants $\bar{\alpha}$ and $\bar{\epsilon}$ are given in Eqs. (8.103) and (8.105). Note that in this case the expression for $\bar{\delta}$ does not involve $\bar{\beta}$. In terms of x and y defined in Eq. (8.130) we have

$$\mathcal{H}_2 = \frac{1}{2}\bar{\delta}\left(x^2+y^2\right) + \frac{1}{4}\left(x^2+y^2\right)^2 + 2\left(x^2-y^2\right). \tag{8.155}$$

Substitution of $k = 2$ in Eq. (8.125) gives the approximate scaling relationship between $R = \sqrt{2\Phi}$ and e as

$$R \approx \left[\frac{3}{4f_d}(j-2)^{\frac{4}{3}} j^{\frac{2}{3}} \frac{m_c}{m'}\right]^{\frac{1}{2}} e. \tag{8.156}$$

As with first-order resonances we can also consider the case of an external, $j : (j-2)$ second-order resonance. Here the single resonant argument is

$$\theta = j\lambda' + (2-j)\lambda - 2\varpi' \tag{8.157}$$

and the corresponding expression for f_d is the fifth entry in Table 8.1. We refer to this as the e'^2 *resonance* because the associated term in the disturbing function

is of $\mathcal{O}(e'^2)$. In the case when $j = 2$ an indirect term given by the second entry in Table 8.3 has to be incorporated in f_d. The scaling relationship is

$$R \approx \left[\frac{3}{4f_\mathrm{d}} j^2 \frac{m_\mathrm{c}}{m}\right]^{\frac{1}{2}} e'. \tag{8.158}$$

Therefore the theory developed for the e^2 resonance can also be applied to the e'^2 resonance with a suitable change of resonant angle and scaling.

Although so far we have only considered resonances involving the eccentricity of either body, we can now extend the work to include inclination resonances. Because inclinations always occur in even powers in the expansion of the disturbing function there is no such thing as a first-order inclination resonance. However, when we consider an expansion to second order we have already noted (see, for example, Sect. 6.10.1) that there are three possible resonant arguments involving ascending nodes. Two of these can be investigated using the Hamiltonian theory for the e^2 and e'^2 resonances.

Consider the case of an internal, $j : (j-2)$ second-order resonance where the single resonant argument is now

$$\theta = j\lambda' + (2-j)\lambda - 2\Omega \tag{8.159}$$

and the expression for f_d is given by the sixth term in Table 8.1. We refer to this as the I^2 *resonance*. From the definitions of the Poincaré variables in Eq. (2.176) we have

$$Z = m\sqrt{\mathcal{G}m_\mathrm{c}a(1-e^2)}(1-\cos I) \approx m\sqrt{\mathcal{G}m_\mathrm{c}a}\,2s^2, \tag{8.160}$$

where $s = \sin\frac{1}{2}I$. Hence

$$I^2 \approx \frac{2Z}{\Lambda}, \tag{8.161}$$

and so the Hamiltonian has the same form as the general one given in Eq. (8.153), which was derived for the purely eccentric resonances. Consequently, the scaling developed for second-order eccentricity resonances based on that Hamiltonian is equally applicable to the I^2 resonance provided we replace e by I in Eq. (8.156) and it is understood that the constant f_d now refers to the sixth term in Table 8.1.

The other inclination resonance that can be handled by the same method has the argument

$$\theta = j\lambda' + (2-j)\lambda - 2\Omega', \tag{8.162}$$

and the expression for f_d is given by the eighth term in Table 8.1. We refer to this as the I'^2 *resonance*. The scaling law is that given in Eq. (8.158) with e' replaced by I' and f_d now referring to its I'^2 value in Table 8.1.

We are now in a position to examine the dynamics of the e^2, e'^2, I^2, and I'^2 resonances. From Eq. (8.121) with $k = 2$ we know that the radial distances of

the equilibrium points (apart from the origin itself) are given by the real, positive values of

$$R = \sqrt{\pm 4 - \bar{\delta}} \tag{8.163}$$

and that the bifurcation points occur when $\bar{\delta} = \pm 4$. A selection of curves of constant Hamiltonian for six different values of $\bar{\delta}$ are shown in Fig. 8.12. As with Fig. 8.10 the locations of the stable and unstable equilibrium points are marked by small, filled and unfilled circles, respectively. Bifurcation points are marked with a crossed circle.

For $\bar{\delta} > 4$ (see Fig. 8.12a) there is a single stable equilibrium point at the origin. As $\bar{\delta}$ decreases the curves narrow until at $\bar{\delta} = 4$ the first bifurcation point is reached (see Fig. 8.12b). The bifurcation leads to the formation of an unstable point at the origin and two stable equilibrium points equidistant from the origin along the y axis. This is illustrated in Fig. 8.12c for the case of exact resonance. A further bifurcation occurs when $\bar{\delta} = -4$ (see Fig. 8.12d). At this stage the origin becomes a stable point and two unstable points are created along the x axis. This is illustrated in Fig. 8.12e for $\bar{\delta} = -7$. There are no more bifurcations

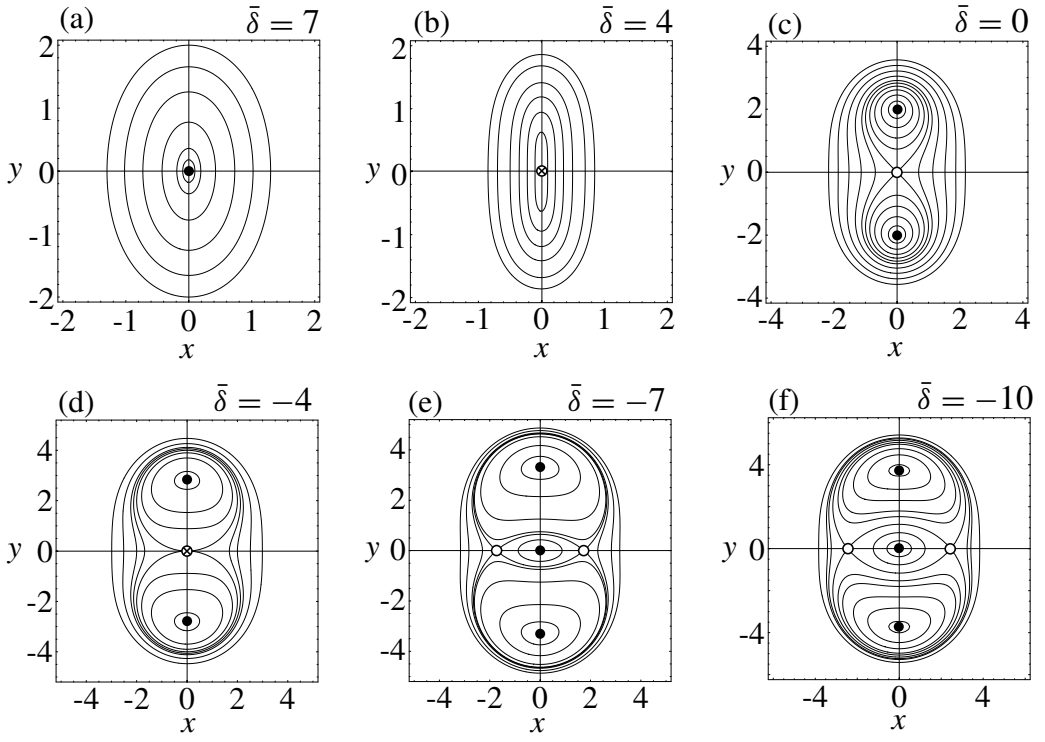

Fig. 8.12. The curves of constant Hamiltonian for the e^2, e'^2, I^2, and I'^2, resonances. (a) $\bar{\delta} = 7$ with $\mathcal{H}_2 = 0.05$, 0.2, 1, 3, 6, 10. (b) $\bar{\delta} = 4$ (a bifurcation value) with $\mathcal{H}_2 = 0.04$, 0.2, 0.5, 1, 2, 3. (c) $\bar{\delta} = 0$ (exact resonance) with $\mathcal{H}_2 = -3.7$, -3, -2, -1, 0, 1, 3, 6, 10, 15. (d) $\bar{\delta} = -4$ (a bifurcation value) with $\mathcal{H}_2 = -15$, -8, -3, 0, 2, 4, 10, 20. (e) $\bar{\delta} = -7$ with $\mathcal{H}_2 = -28$, -20, -8, -3, $-9/4$, -1, 4, 10. (f) $\bar{\delta} = -10$ with $\mathcal{H}_2 = -48$, -40, -30, -20, -15, -9, -4, -1, 10.

and so further reductions in $\bar{\delta}$ do not change the fundamental character of the system (see Fig. 8.12f).

8.8.3 The e^3 and e'^3 Resonances

It is relatively easy to extend our analysis to selected third-order resonant terms. Here we outline the method involved for two third-order arguments. For the case of the e^3 *and* e'^3 *resonances* the resonant arguments are

$$\theta = j\lambda' + (3-j)\lambda - 3\varpi \quad \text{and} \quad \theta = j\lambda' + (3-j)\lambda - 3\varpi' \tag{8.164}$$

respectively. These can be identified as the arguments 4D3.1 and 4D3.4 in Appendix B, and the relevant $f_{\rm d}$ terms can be calculated using the definitions of f_{82} and f_{85} in Table B.12. The Hamiltonian of the system is given by

$$\mathcal{H}_3 = \bar{\delta}\Phi + \Phi^2 - 2(2\Phi)^{\frac{3}{2}}\cos 3\phi, \tag{8.165}$$

where

$$\bar{\delta} = 4\bar{\alpha}\bar{\beta}/\bar{\epsilon}^2. \tag{8.166}$$

In terms of $x = \sqrt{2\Phi}\cos\phi$ and $y = \sqrt{2\Phi}\sin\phi$ the Hamiltonian is

$$\mathcal{H}_3 = \frac{1}{2}\bar{\delta}\left(x^2+y^2\right) + \frac{1}{4}\left(x^2+y^2\right)^2 - 2x\left(x^2-3y^2\right). \tag{8.167}$$

The approximate scaling relationships between $R = \sqrt{2\Phi}$ and e and e' are

$$R \approx \left[\frac{-1}{3f_{\rm d}}(j-3)^{\frac{4}{3}} j^{\frac{2}{3}} \frac{m_{\rm c}}{m'}\right] e \qquad \text{and} \qquad R \approx \left[\frac{-1}{3f_{\rm d}} j^2 \frac{m_{\rm c}}{m}\right] e'. \tag{8.168}$$

The radial distances of the equilibrium points (apart from the origin itself) are given by the real, positive values of

$$R = \pm 3 \pm \sqrt{9-\bar{\delta}}, \tag{8.169}$$

and the bifurcation points occur when $\bar{\delta} = 0$ and 9. A selection of curves of constant Hamiltonian for six different values of $\bar{\delta}$ are shown in Fig. 8.13. As with Fig. 8.10 the locations of the stable and unstable equilibrium points are marked by small, filled and unfilled circles, respectively. Bifurcation points are marked with a crossed circle.

For $\bar{\delta} > 9$ (see Fig. 8.13a) there is a single stable equilibrium point at the origin with the curves following a triangular pattern around it. As $\bar{\delta}$ decreases the sides of the triangle narrow until at $\bar{\delta} = 9$ three bifurcation points occur (see Fig. 8.13b). The bifurcation leads to the formation of three pairs of stable and unstable equilibrium points at two distances from the origin, each pair 120° from the next. As $\bar{\delta}$ decreases the unstable points move towards the origin, reaching it at $\bar{\delta} = 0$. For this value of $\bar{\delta}$ (exact resonance; see Fig. 8.13c) a further bifurcation occurs. The origin remains a stable point and three unstable points are created

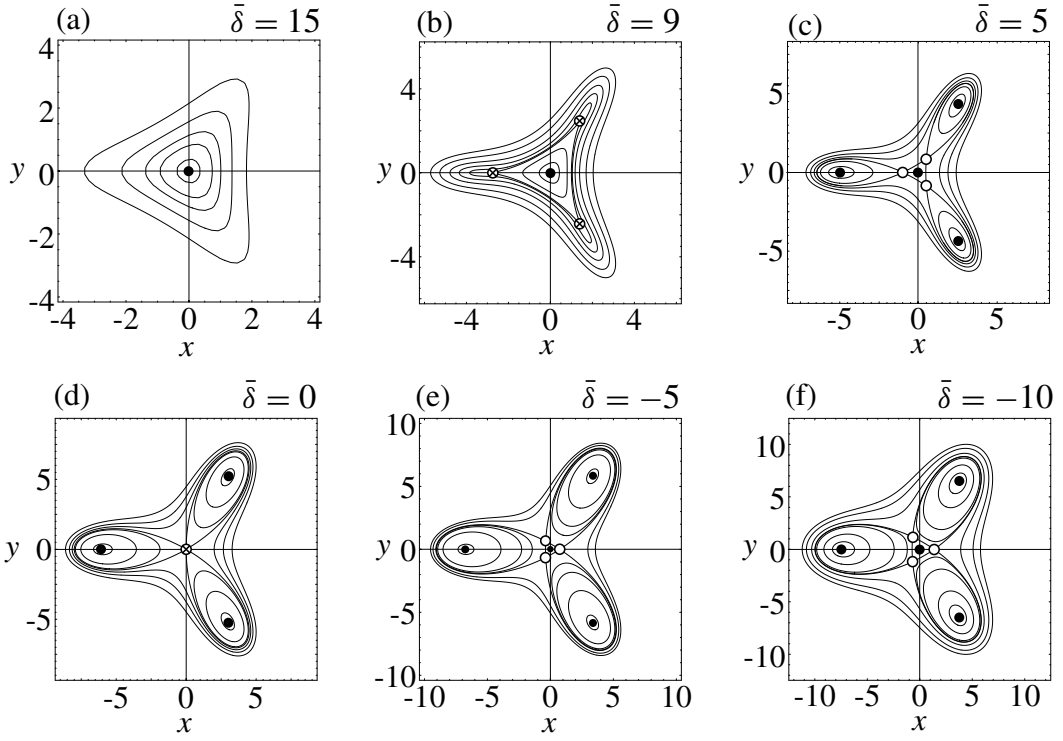

Fig. 8.13. The curves of constant Hamiltonian for the e^3 and e'^3 resonances. (a) $\bar{\delta} = 15$ with $\mathcal{H}_3 = 1, 5, 10, 20, 40$. (b) $\bar{\delta} = 9$ (a bifurcation value) with $\mathcal{H}_3 = 1, 4, 27/4, 15/2, 10, 15, 25, 40$. (c) $\bar{\delta} = 5$ with $\mathcal{H}_3 = -25, -10, 3/4, 10, 25, 50$. (d) $\bar{\delta} = 0$ (exact resonance and a bifurcation value) with $\mathcal{H}_3 = -100, -50, -10, 0, 20, 50, 100$. (e) $\bar{\delta} = -5$ with $\mathcal{H}_3 = -200, -100, -30, -10, \sqrt{14} - 3, 50, 100$. (f) $\bar{\delta} = -10$ with $\mathcal{H}_3 = -300, -200, -50, -10, \sqrt{19} - 3, 100, 300, 500$.

at intervals of 120°. This is illustrated in Fig. 8.13e for $\bar{\delta} = -7$. Note that the small "triangles" near the origin are convex for $\bar{\delta} > 0$ and concave for $\bar{\delta} < 0$, with the unstable point moving from negative to positive values of x. There are no more bifurcations and so further reductions in $\bar{\delta}$ do not change the fundamental character of the system (see Fig. 8.13f).

8.8.4 The ee' and II' Resonances

So far we have avoided any resonances that have an argument involving the pericentres or nodes of both masses. We refer to these as *mixed resonances.* If we restrict ourselves to second-order resonances then there are two mixed resonant arguments to consider. The first of these is the ee' *resonance* with argument

$$\theta = j\lambda' + (2 - j)\lambda - \varpi' - \varpi, \tag{8.170}$$

where the associated $f_{\rm d}$ term is given by the fourth entry in Table 8.1. The argument of the II' *resonance* is

$$\theta = j\lambda' + (2-j)\lambda - \Omega' - \Omega, \tag{8.171}$$

where the associated $f_{\rm d}$ term is given by the seventh entry in Table 8.1. Here we outline the basic steps in an analytical theory to describe motion in these resonances and show that they can be treated as a simple extension of the theory for the first-order e and e' resonances discussed above. In fact, as we show below, it is trivial to extend the theory to deal with the higher-order ee'^k, $e^k e'$, II'^k, and $I^k I'$ resonances. In the terminology of ring dynamics the ee'^k resonance is referred to as a Lindblad resonance of order k, and the II'^k resonance is a vertical resonance of order k. This is discussed further in Chapter 10.

Consider the case of the II' resonance. The Hamiltonian has the form

$$\begin{aligned}\mathcal{H} = &-\frac{\mathcal{G}^2 m_{\rm c}^2 m^3}{2\Lambda^2} - \frac{\mathcal{G}^2 m_{\rm c}^2 m'^3}{2\Lambda'^2} \\ &- \frac{\mathcal{G}^2 m_{\rm c} m m'^3}{\Lambda'^2} f_{\rm d} \left(\frac{2Z}{\Lambda}\right)^{1/2} \left(\frac{2Z'}{\Lambda'}\right)^{1/2} \cos[j\lambda' + (2-j)\lambda + z + z'] \\ &- \Gamma \dot{\varpi}_{\rm sec} - Z\dot{\Omega}_{\rm sec} + \Lambda\dot{\lambda}_{\rm sec} - \Gamma'\dot{\varpi}'_{\rm sec} - Z'\dot{\Omega}'_{\rm sec} + \Lambda'\dot{\lambda}'_{\rm sec}\end{aligned} \tag{8.172}$$

(cf. Eq. (8.77)), where $z = -\Omega$ and $z' = -\Omega'$. In this case Γ and Γ' do not appear in $\mathcal{H}$ and so they (and hence e and e') are constants of the motion. The new set of four variables is given by

$$\theta_1 = j\lambda' + (2-j)\lambda + z' + z, \tag{8.173}$$

$$\theta_2 = j\lambda' + (2-j)\lambda + 2z', \tag{8.174}$$

$$\theta_3 = \lambda, \tag{8.175}$$

$$\theta_4 = \lambda'. \tag{8.176}$$

The conjugate momenta, Θ_i, can be found by equating coefficients in

$$\sum_{i=1}^{4} \Theta_i \, {\rm d}\theta_i = \Lambda \, {\rm d}\lambda + \Lambda' \, {\rm d}\lambda' + Z \, {\rm d}z + Z' \, {\rm d}z'. \tag{8.177}$$

This gives

$$(2-j)(\Theta_1 + \Theta_2) + \Theta_3 = \Lambda, \tag{8.178}$$

$$j(\Theta_1 + \Theta_2) + \Theta_4 = \Lambda', \tag{8.179}$$

$$\Theta_1 = Z, \tag{8.180}$$

$$\Theta_1 + 2\Theta_2 = Z', \tag{8.181}$$

where Θ_2, Θ_3, and Θ_4 are all constants since θ_2, θ_3, and θ_4 no longer appear in $\mathcal{H}$. The constant of interest is

$$\Theta_2 = \frac{1}{2}\left(Z' - Z\right). \tag{8.182}$$

Because $I^2 \approx 2Z/\Lambda$, the existence of Θ_2 implies that the scaled *difference* in the inclinations is a constant of the motion. It is easy to show that the approximate Hamiltonian can now be written as

$$\begin{aligned}\mathcal{H} = &\left[j(n' + \dot{\lambda}'_{\rm sec}) + (2-j)(n + \dot{\lambda}_{\rm sec}) - 2\dot{\Omega}_{\rm sec}\right] Z \\ &- \frac{3}{2}\left[\frac{j^2}{m'a'^2} + \frac{(2-j)^2}{ma^2}\right] Z^2 \\ &- n\, f_{\rm d}\, \alpha \frac{m'}{m_{\rm c}} \left(2Z\right)^{1/2} \left(2Z + C\right)^{1/2} \cos\theta_1, \end{aligned} \tag{8.183}$$

where $C = 4\Theta_2$ is a constant. By carrying out a simple scale transformation with $\bar{\alpha} \to 2\bar{\alpha}$ and $\bar{\beta} \to 4\bar{\beta}$ we obtain

$$\mathcal{H} = \bar{\delta}\Phi + \Phi^2 + 2\sqrt{2\Phi}\sqrt{2\Phi + c}\,\cos\phi, \tag{8.184}$$

where $c = C/\eta$ and $\phi = \theta_1$.

Comparing this Hamiltonian with that given in Eq. (8.116) we see that it has characteristics of second-order resonances (the powers of Φ in the resonant term) as well as first-order resonances (the resonant angle occurs in the form ϕ and not 2ϕ). Furthermore, our new Hamiltonian is a function of two parameters: $\bar{\delta}$ is a measure of the distance to exact resonance and c is related to the constant difference in inclination.

The preceding analysis can equally be applied to the ee' resonance if we replace Z, Z', z, and z' by Γ, Γ', γ, and γ', respectively. In this case it is the difference in eccentricities that is a constant. Note too that we can easily modify the analysis to deal with the case where I or e rather than I' or e' is fixed.

The remaining analysis of the Hamiltonian (locating the equilibrium and bifurcation points) is similar to that carried out for the first-order resonances. Taking $R = \sqrt{2\Phi}$ the equilibrium points are located at the intersection of the two functions

$$f(\bar{\delta}, R) = \bar{\delta} + R^2 \quad \text{and} \quad g(R, c) = 2(-1)^{i+1}\left[\frac{\sqrt{R^2 + c}}{R} + \frac{R}{\sqrt{R^2 + c}}\right], \tag{8.185}$$

where $i = 0, 1, 2, \ldots$. Similarly, the bifurcation points occur where $f'(\bar{\delta}, R) = g'(R, c)$. If we make the substitutions $x = \sqrt{2\Phi}\cos\phi$ and $y = \sqrt{2\Phi}\sin\phi$ the Hamiltonian can be written as

$$\mathcal{H} = \frac{1}{2}\left(x^2 + y^2\right)\bar{\delta} + \frac{1}{4}\left(x^2 + y^2\right)^2 + 2x\left(x^2 + y^2 + c\right)^{1/2}, \tag{8.186}$$

with equilibrium points along the x axis. Because the location of the equilibrium points depends on c as well as $\bar{\delta}$, we have to consider plots of

$$\bar{\delta} = \frac{1}{x}\left(-x^3 - 2(x^2 + c)^{\frac{1}{2}} - 2x^2(x^2 + c)^{-1/2}\right) \tag{8.187}$$

and the curves of constant Hamiltonian for each individual value of c. In Fig. 8.14 we show plots of (i) $f(\bar{\delta}, R)$ and $g(R, c)$, (ii) $\bar{\delta}$ as a function of the x value of the

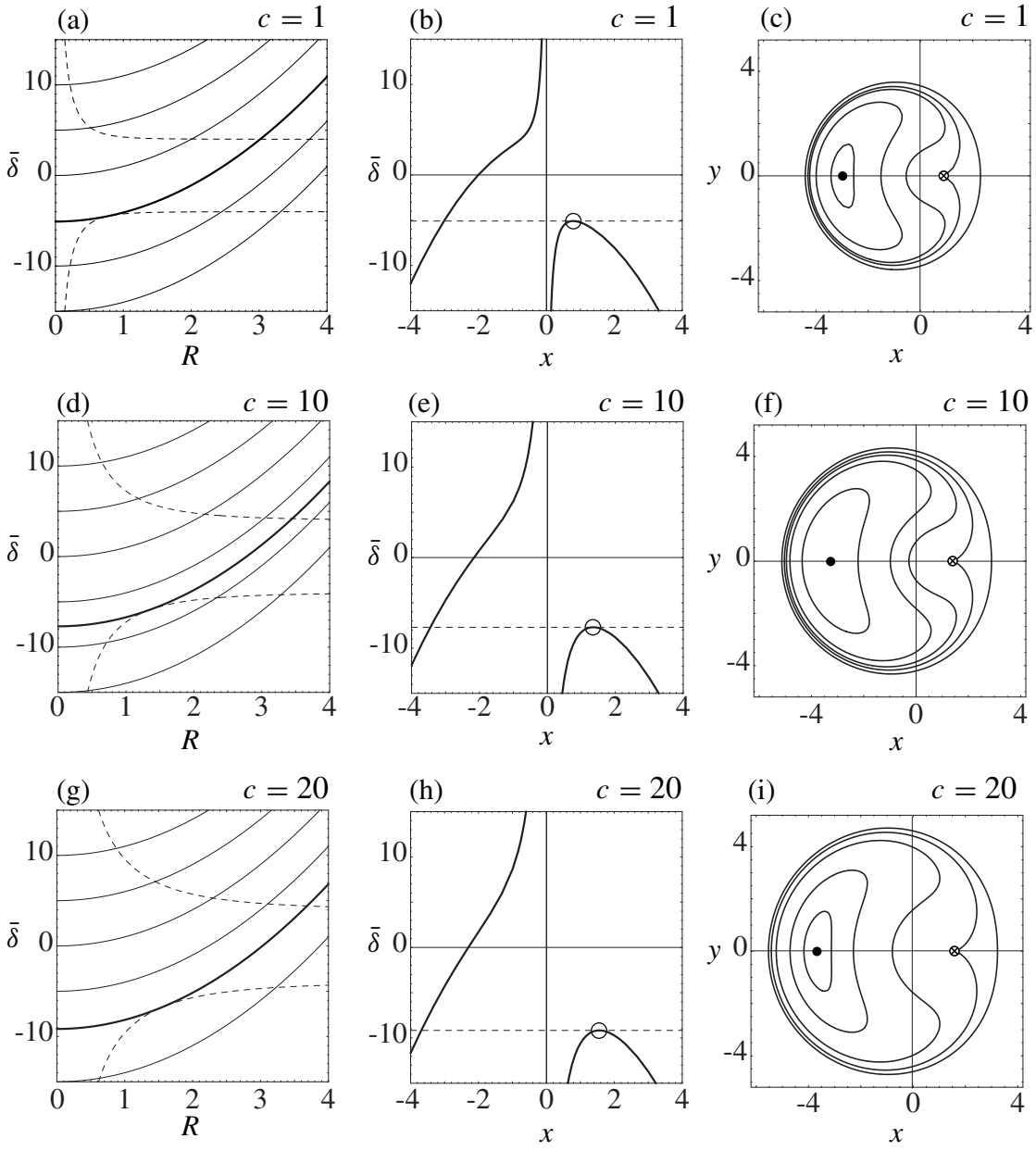

Fig. 8.14. The dynamics of the mixed resonance as a function of the value of c. The conventions used in Figs. 8.8, 8.9, and 8.10 apply. (a) Plots of $f(\bar{\delta}, R)$ (parabolas) and $g(R, c)$ (dashed curves) for $c = 1$. The thicker parabola denotes f for the bifurcation value $\bar{\delta} = -5.09017$. (b) The relationship between $\bar{\delta}$ and the value of x associated with the equilibrium points for $c = 1$. (c) Curves of constant Hamiltonian in the x–y plane for $\bar{\delta} = -5.09017$ and $c = 1$. (d) Plots of $f(\bar{\delta}, R)$ and $g(R, c)$ for $c = 10$. The thicker parabola denotes f for the bifurcation value $\bar{\delta} = -7.70166$. (e) The relationship between $\bar{\delta}$ and the value of x associated with the equilibrium points for $c = 10$. (f) Curves of constant Hamiltonian for $\bar{\delta} = -7.70166$ and $c = 10$. (g) Plots of $f(\bar{\delta}, R)$ and $g(R, c)$ for $c = 20$. The thicker parabola denotes f for the bifurcation value $\bar{\delta} = -9.1646$. (h) The relationship between $\bar{\delta}$ and the value of x associated with the equilibrium points for $c = 20$. (i) Curves of constant Hamiltonian for $\bar{\delta} = -9.1646$ and $c = 20$.

equilibrium point (from Eq. (8.187)), and (iii) a selection of curves of constant Hamiltonian for the bifurcation value of $\bar{\delta}$, all for three different values of c. Note the general similarity to the plots shown in Figs. 8.8, 8.9, and 8.10. As the value of c increases the bifurcation value of $\bar{\delta}$ becomes more negative (Figs. 8.14a,d,g), the equilibrium points move further from the origin (Figs. 8.14b,e,h), and the area enclosed increases (Figs. 8.14c,f,i).

So far we have only considered positive values of c. For negative values of c an interesting phenomenon occurs. The presence of the $\sqrt{x^2 + y^2 + c}$ term in the Hamiltonian in Eq. (8.186) means that for negative values of c the condition $R \geq \sqrt{-c}$ must hold. This places restrictions on the location of the equilibrium points and trajectories. This is illustrated in Fig. 8.15 for the case when $c = -5$. The general form of the various curves are the same as those shown in Fig. 8.14 but equilibrium points and trajectories cannot occur within a distance $R \leq \sqrt{5}$ of the origin.

The foregoing analysis can be extended to deal with the ee'^k, $e^k e'$, II'^k, and $I^k I'$ resonances. Consider the case of the II'^k resonance. The angular variables are

$$\theta_1 = j\lambda' + (k + 1 - j)\lambda + kz' + z, \tag{8.188}$$

$$\theta_2 = j\lambda' + ((k + 1 - j)\lambda + (k + 1)z,' \tag{8.189}$$

$$\theta_3 = \lambda, \tag{8.190}$$

$$\theta_4 = \lambda'. \tag{8.191}$$

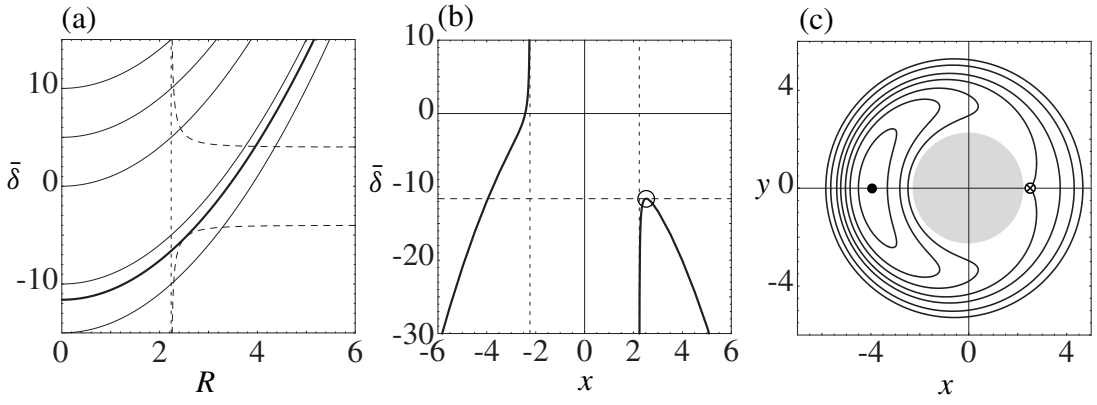

Fig. 8.15. The dynamics of the mixed resonance for $c = -5$. The conventions used in Fig. 8.14 apply. (a) Plots of $f(\bar{\delta}, R)$ (parabolas) and $g(R, c)$ (dashed curves). The thicker parabola denotes f for the bifurcation value $\bar{\delta} = -11.6098$. The vertical dashed line denotes the asymptote at $R = \sqrt{5}$. (b) The relationship between $\bar{\delta}$ and the value of x associated with the equilibrium points. The vertical dashed lines denote the asymptotes at $x = \pm\sqrt{5}$. (c) Curves of constant Hamiltonian in the x–y plane for $\bar{\delta} = -11.6098$. The shaded area denotes the excluded region defined by the circle $x^2 + y^2 = 5$.

The conjugate momenta, Θ_i, are

$$(k+1-j)(\Theta_1+\Theta_2)+\Theta_3=\Lambda, \tag{8.192}$$

$$j(\Theta_1+\Theta_2)+\Theta_4=\Lambda', \tag{8.193}$$

$$\Theta_1=Z, \tag{8.194}$$

$$\Theta_1+(k+1)\Theta_2=Z', \tag{8.195}$$

where the new constant of interest,

$$\Theta_2=\frac{1}{k+1}\left(Z'-Z\right), \tag{8.196}$$

again depends on the difference in the inclinations. The final Hamiltonian is

$$\mathcal{H}=\bar{\delta}\Phi+\Phi^2+2(-1)^k\left(2\Phi\right)^{1/2}\left(2\Phi+c\right)^{k/2}\cos\phi, \tag{8.197}$$

where $\phi=\theta_1$. It is clear that the analysis we have developed for the II' resonance can be easily extended to the case of the II'^k and other mixed resonances. However, in cases where k is odd and c is negative, there is always the possibility of excluded regions.

8.9 The 2:1 Resonance

We now consider some numerical examples that illustrate some of the concepts discussed in this chapter. We have carried out full numerical integrations of the equations of motion of the planar, circular, restricted, three-body problem for test particle orbits in the vicinity of the internal 2:1 resonance using a mass ratio of $m'/(m_c+m')=0.001$. The results are based on the work of Winter & Murray (1997). In the regime we have selected the effects of the additional equilibrium point found by Wisdom (1980) and discussed in Sect. 8.8.1 are not important (see Colombo et al. 1968).

The model can be considered analogous to an investigation of the motion of asteroids close to 3.29 AU, the location of the strong, first-order, 2:1 jovian resonance in the asteroid belt. We have chosen a system of units where the semi-major axis of Jupiter is unity. From Table 8.5 we have

$$\alpha=0.629961, \qquad \alpha f_{s,1}=0.244190, \qquad \alpha f_d=-0.749964, \tag{8.198}$$

where α is the nominal value of a/a' for the 2:1 resonance. We are dealing with a first-order, internal resonance and so Eq. (8.132) with $j=2$ gives the appropriate scaling of the eccentricity. We have

$$\sqrt{2\Phi}=R=15.874\,e, \tag{8.199}$$

where e is the eccentricity of the test particle (or asteroid), and the only resonant

Table 8.6. The initial values of semi-major axis (a_0), eccentricity (e_0), and longitude of perihelion (ϖ_0) for the numerical integrations shown in Fig. 8.16 and Fig. 8.17. The value of λ_0 was zero in each case. The initial orbital elements were calculated using the position and velocity with respect to an origin at the centre of mass of the system.

Plot	a_0	e_0	ϖ_0	Description
a	0.625277	0.128386	0°	exact resonance
b	0.633424	0.0725011	0°	medium-amplitude libration
c	0.637837	0.0122862	0°	large-amplitude libration
d	0.636705	0.060146	180°	apocentric libration
e	0.638222	0.0184545	180°	inner circulation
f	0.610592	0.1975	0°	outer circulation

angle is

$$\phi = 2\lambda' - \lambda - \varpi \, . \tag{8.200}$$

For each of the six starting conditions given in Table 8.6 we have integrated the full equations of motion for 100 Jupiter periods and calculated the semi-major axis, eccentricity, longitude of pericentre, and the resonant argument as a function of time. The results are displayed in Fig. 8.16 where the data are plotted six times per Jupiter period. Note that in Fig. 8.16 the dashed line in each of the semi-major axis plots denotes the location of the nominal resonance. The equivalent plots of $x = \sqrt{2\Phi}\cos\phi$ and $y = \sqrt{2\Phi}\sin\phi$ are shown in Fig. 8.17. Again a point is plotted six times per Jupiter period. Note that we have chosen the starting conditions such that all orbits have the same value of the Jacobi constant, $C_{\rm J} = 3.163$.

We now examine each of the plots in detail and comment on the various resonant and near-resonant phenomena that are illustrated.

8.9.1 Exact Resonance

Figures 8.16a and 8.17a show the trajectory of a test particle started close to the exact resonance. In the plot of a as a function of time it is clear that the particle is staying close to the resonant value, while its eccentricity also maintains a constant value. Although the pericentre is regressing at a near-uniform rate (due to the resonant effects), the resonant angle is fixed close to $\phi = 0$. This is more clearly seen in Fig. 8.17a where the amplitude of libration is small. Note that although the test particle is close to exact resonance, the value of the semi-major axis given in Table 8.6, 0.625277, differs from the resonant value of 0.629961 because the former is calculated in the centre of mass frame whereas the latter is in the heliocentric frame.

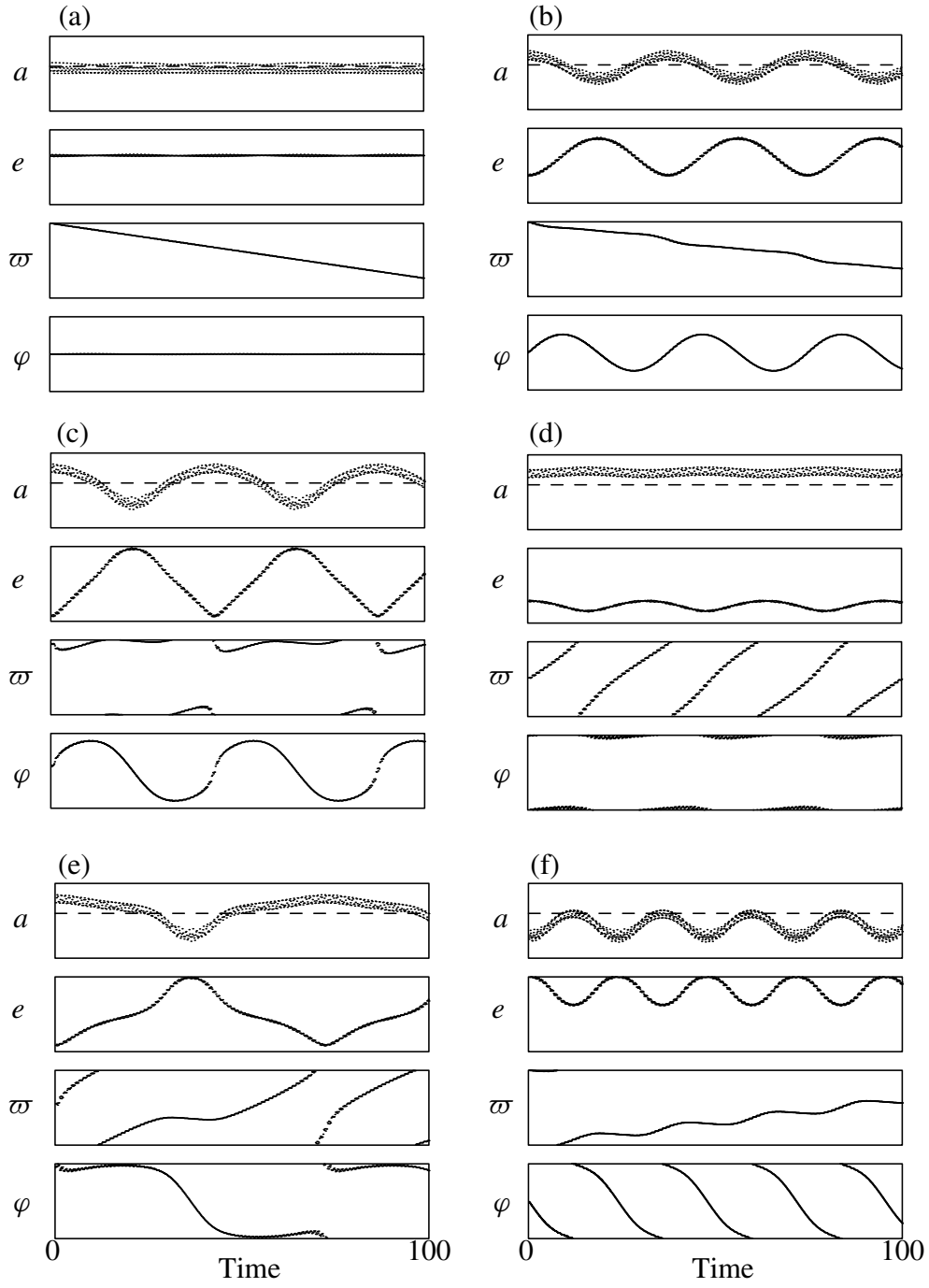

Fig. 8.16. The variation of the orbital elements of test particles started near the 2:1 jovian resonance and integrated for 100 Jupiter periods. In each plot a is the semi-major axis (on a scale from 0.6 to 0.65), e is the eccentricity (on a scale from 0 to 0.2), ϖ is the longitude of perihelion (on a scale from 0° to 360°), and $\varphi = 2\lambda' - \lambda - \varpi$ is the resonant argument (on a scale from -180° to 180°). The starting values are given in Table 8.6. The plots illustrate (a) exact resonance, (b) medium-amplitude libration, (c) large-amplitude libration, (d) apocentric libration, (e) inner circulation, and (f) outer circulation.

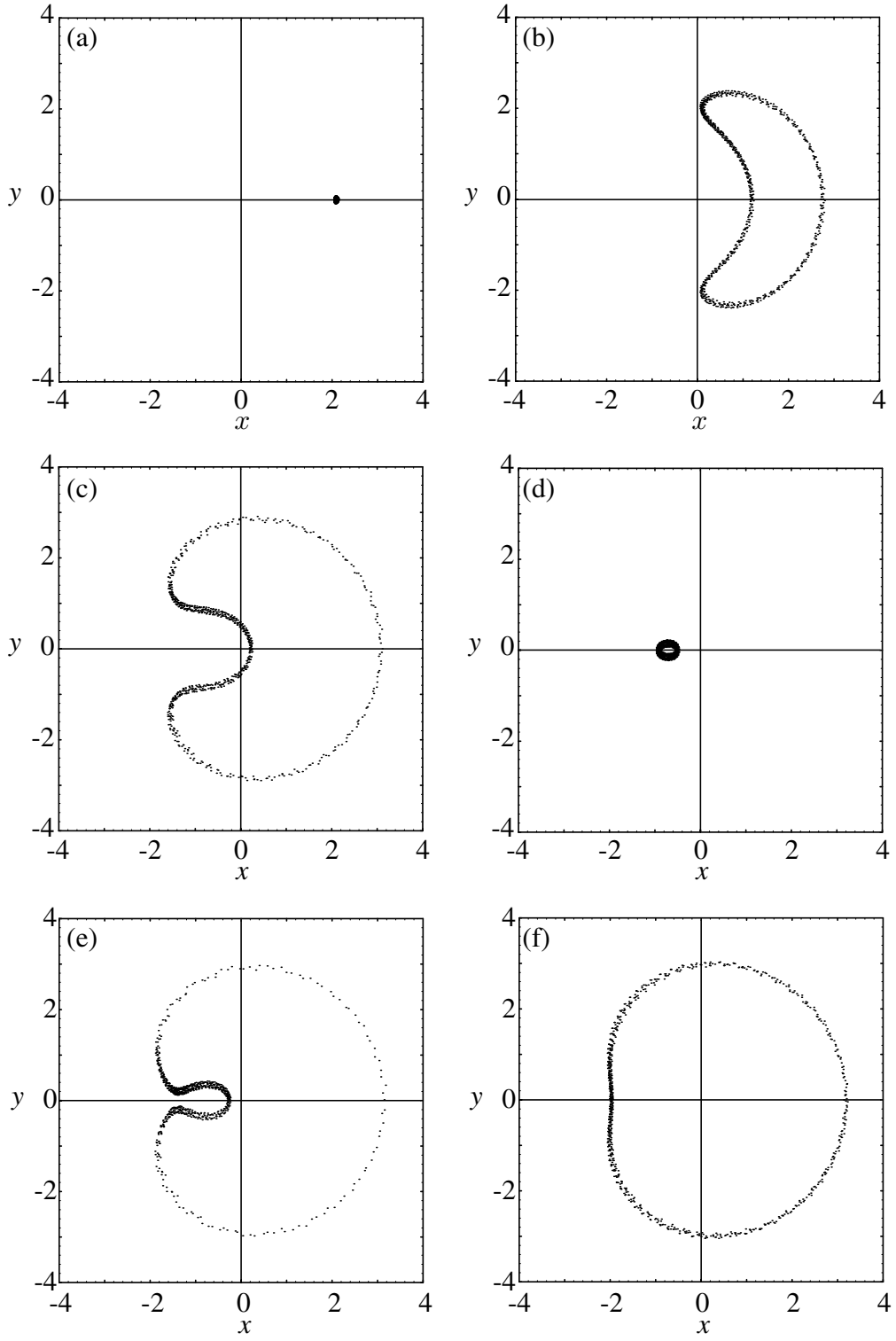

Fig. 8.17. The variation of $x = \sqrt{2\Phi}\cos\phi$ and $y = \sqrt{2\Phi}\sin\phi$ for the same trajectories that are shown in Fig. 8.16. The quantity $\sqrt{2\Phi}$ is defined in Eq. (8.199) and $\phi = 2\lambda' - \lambda - \varpi$ is the resonant angle. The plots illustrate (a) exact resonance, (b) medium-amplitude libration, (c) large-amplitude libration, (d) apocentric libration, (e) inner circulation, and (f) outer circulation.

8.9.2 Medium-Amplitude Libration

Figures 8.16b and 8.17b show the trajectory of a test particle undergoing a medium-amplitude libration about the exact resonance. The semi-major axis has an approximate amplitude of 0.0068 as it undergoes a long-period oscillation about the resonant value. The eccentricity also varies about a mean value close to that at the exact resonance shown in Fig. 8.16a. Note that the a and e variations are correlated as suggested by Eq. (8.92), such that when a is a maximum, e is a minimum, and vice versa. The pericentre regresses at a near-uniform rate, although the regression is largest when e is at a minimum, as expected. The overall rate is slower than that shown in Fig. 8.16a. The resonant angle undergoes sinusoidal oscillations, as predicted by the pendulum approximation.

8.9.3 Large-Amplitude Libration

Figures 8.16c and 8.17c show the trajectory of a test particle undergoing a large-amplitude libration about the exact resonance. The libration is close to the maximum value and so the excursions in a and e are at their largest. Despite the large excursions in e our numerical calculations show that the approximation $e^2 \approx 2\Gamma/\Lambda$ is valid to within 20%. Note that ϖ is itself librating about 0. The resonant angle ϕ takes values in the range of -146° to $+146^\circ$.

8.9.4 Apocentric Libration

Figures 8.16d and 8.17d show the trajectory of a test particle undergoing apocentric libration. In Figs. 8.9 and 8.10 we see that, provided $\bar{\delta} < -3$, there is a stable equilibrium point to the left of the origin in the x–y plots. Therefore it is possible for orbits started with $\phi = 180^\circ$ and sufficiently low values of e to have a trajectory that will not enclose the origin in the x–y diagram. Note that in our case the semi-major axis is always well outside the resonant value and that the variation of e is small. The pericentre was started at 180° and it is precessing quickly; this explains why the resonant angle ϕ always remains close to 180° – the $\dot{\varpi}$ contribution to $\dot{\phi}$ is large enough to compensate for the fact that $2n' - n \not\approx 0$. Because we define a resonance to be the libration rather than circulation of a particular resonant argument, a particle in apocentric libration is in a resonance. Note that a similar situation arises for small eccentricities at large positive values of $\bar{\delta}$ where there is always a stable equilibrium point to the right of the origin at low values of e. Both phenomena are illustrated in Fig. 8.11.

8.9.5 Inner Circulation

Figures 8.16e and 8.17e show the trajectory of a test particle undergoing inner circulation. It is clear from Fig. 8.17e that the trajectory encloses the origin and hence there is circulation of the resonant argument. However, the trajectory is still inside the critical curve that passes through the unstable equilibrium point

close to $(-1.5, 0)$. Note that although the motion is circulatory, there are still large variations in a and e, with magnitudes comparable to those at maximum libration of the resonant argument. The minimum a and maximum e occur when $\phi = 0$. When $\phi \approx 180^\circ$ the trajectory is close to apocentric libration and for a while aspects of the plots resemble those seen in Fig. 8.16d and Fig. 8.17d.

8.9.6 Outer Circulation

Figures 8.16f and 8.17f show the trajectory of a test particle undergoing outer circulation. From the semi-major axis plot we see that a is almost always less than the resonant value. Note that although the semi-major axis can take values on either side of the resonant value, it does not follow that the particle is in resonance; that must be determined from other considerations, the most important of which is the behaviour of the resonant angle. The variations in a and e are much smaller than those shown for inner circulation, primarily because the particle does not undergo a "detour" around the apocentric libration point. The pericentre is precessing and the resonant angle is clearly circulating.

8.9.7 Other Types of Motion

The orbits discussed above illustrate the basic types of motion to be found at the 2:1 and other first-order resonances. Other forms of motion include circulation about the single equilibrium point for large, negative values of $\bar{\delta}$ and circulation about the stable equilibrium point to the left of the origin for large, positive values of $\bar{\delta}$ (see Fig. 8.11) These and other types of orbits are not discussed here although their properties can easily be deduced from the information above.

8.9.8 Comparison with Analytical Theory

The validity of the Hamiltonian approach is illustrated in Fig. 8.18 where we compare the trajectories shown in Fig. 8.17 with those calculated analytically. One of the drawbacks of the Hamiltonian approach is that quantities such as $\bar{\delta}$, a measure of the proximity to exact resonance, have to be determined from observation. It is important to note that the analytical theory is an approximation to the motion, albeit a good one in certain circumstances. Numerical integration of the full equations of motion incorporates all the short-period effects and their influence is clearly seen in the numerical integrations; in contrast, the averaged Hamiltonian theory, by its very nature, ignores all short-period effects. This explains the basic differences between Fig. 8.18a and Fig. 8.18b. Each of the trajectories shown in Fig. 8.17 crosses the $y = 0$ line at two points, x_1 and x_2, which must have the same value of both $\bar{\delta}$ and $\mathcal{H}_1$. Setting $\mathcal{H}_1(x_1, 0) = \mathcal{H}_1(x_2, 0)$ in Eq. (8.131) gives

$$\bar{\delta} = \frac{1}{2}(x_2^2 + x_1^2) + 4(x_1 + x_2)^{-1} \tag{8.201}$$

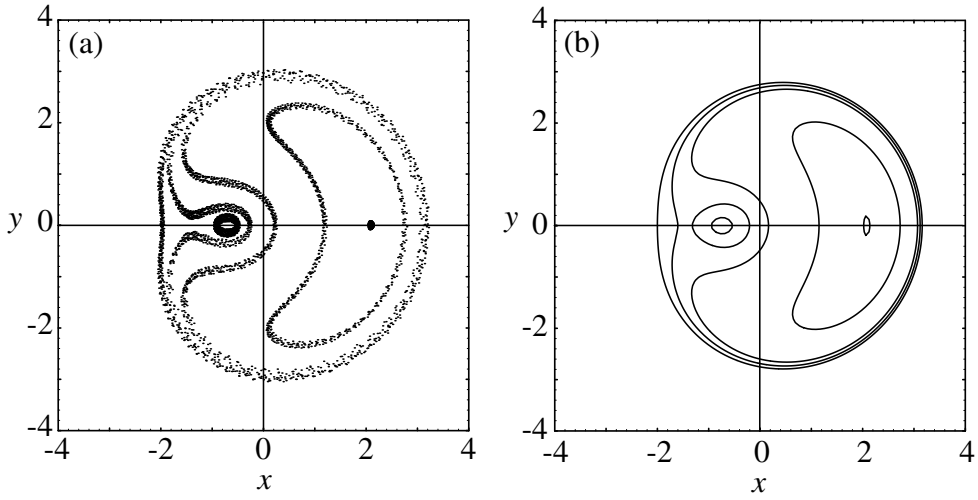

Fig. 8.18. A comparison of the results of the numerical integrations with analytical theory. (a) The accumulated trajectories in x–y space taken from Fig. 8.17. (b) The equivalent curves of constant Hamiltonian based on the analytical theory. The values of $\bar{\delta}$ and $\mathcal{H}_1$ for each curve are given in Table 8.7. In the case of the apocentric libration, the outer branch of the $\mathcal{H}_1$ curve has not been plotted. Note from Table 8.7 that all the trajectories have different values of $\bar{\delta}$ and $\mathcal{H}_1$.

for the approximate value of $\bar{\delta}$ for the trajectory. We can then find $\mathcal{H}_1$ by calculating $\mathcal{H}_1(x_1, 0)$ or $\mathcal{H}_1(x_2, 0)$. The resulting values of $\bar{\delta}$ and $\mathcal{H}_1$ are given in Table 8.7.

Note that the match between Figs. 8.18a and 8.18b is by no means perfect. There are two notable differences. The extent of the medium-amplitude libration has been underestimated by the analytical theory. The numerical results for the inner circulation show a single branch for the trajectory, whereas the analytical theory predicts motion on one of two branches, either a variation on apocentric libration or an outer circulation. Exact correspondence between the results from

Table 8.7. The values of $\bar{\delta}$ and $\mathcal{H}_1$ that were used to produce the theoretical trajectories shown in Fig. 8.18b. The plot identification refers to Fig. 8.17.

Plot	$\bar{\delta}$	$\mathcal{H}_1$	Description
a	−3.62568	−7.31775	exact resonance
b	−3.57917	−4.45861	medium-amplitude libration
c	−3.69155	−0.685164	large-amplitude libration
d	−3.44688	0.562329	apocentric libration
e	−2.38857	0.271609	inner circulation
f	−3.58826	0.692563	outer circulation

different methods should not be expected, especially when the motion is close to a critical curve.

8.10 The 3:1 and 7:4 Resonances

To illustrate motion at other resonances we have carried out numerical integrations of the planar, circular, restricted three-body problem close to two other resonances.

At the 3:1 resonance the expected resonant argument is $\theta = 3\lambda' - \lambda - 2\varpi$. In units in which the perturber has unit semi-major axis the nominal resonance location is at $a_{\rm res} = (1/3)^{2/3} = 0.48075$. Figure 8.19 shows the results of a single numerical integration of the equations of motion for starting conditions giving rise to librational motion in the resonance. The heliocentric starting values are $a_0 = 0.4809$, $e_0 = 0.13$, $\varpi_0 = 0$, and $\lambda_0 = 180^\circ$ with $\lambda_0' = 0$ and $\mu_2 = 0.001$. The value of a_0 is just greater than the nominal resonant value. Note from Fig. 8.19a that ϖ is always increasing. The positive pericentre rate compensates for the fact that $3n' - n$ is also positive, such that the combination $\dot{\theta} = 3n' - n - 2\dot{\varpi}$ is close to zero. As expected from theory, stable libration is seen to occur around $\theta = 180^\circ$. For these starting conditions the amplitude of libration is large ($\sim 130^\circ$).

According to the Hamiltonian approach, the scaling factor R for the e^2 resonance is given by Eq. (8.156) with $j = 3$. Using the value of $f_{\rm d} = 0.598756$ for the 3:1 resonance derived from Table 8.5 gives $R = 51.044e$. A plot of the values

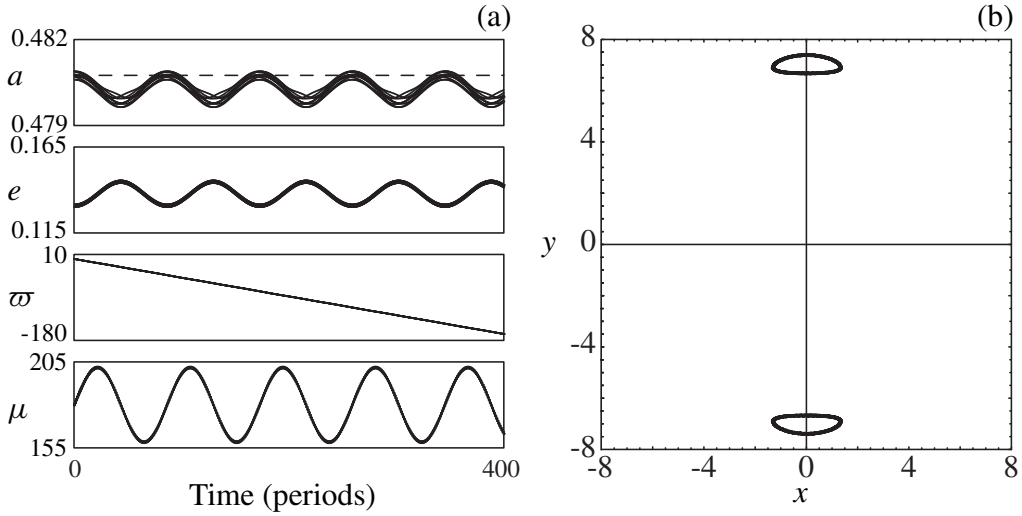

Fig. 8.19. Libration of a test particle in the 3:1 e^2 resonance in the planar circular restricted three-body problem. (a) Plots of the semi-major axis a, the eccentricity e, the longitude of pericentre ϖ, and the resonant angle $\theta = 3\lambda' - \lambda - 2\varpi$ as a function of time. (b) A plot of $x = \sqrt{2R}\cos\phi$ and $y = \sqrt{2R}\sin\phi$ (where $\phi = \theta/2$) for the same integration showing the two branches of the stable libration.

of $x = \sqrt{2R}\cos\phi$ and $y = \sqrt{2R}\sin\phi$ (where $\phi = \theta/2$) is shown in Fig. 8.19b. This shows the type of librational behaviour already seen in Fig. 8.12 for values of $\bar{\delta} < -4$

At the 7:4 resonance in the planar circular problem we expect the argument $\theta = 7\lambda' - 4\lambda - 3\varpi$ to be librating. The scaling relationship is given by the first part of Eq. (8.168) with $j = 5$ and, from Tables B.12 and B.14,

$$f_{\rm d} = \frac{1}{48}\left[-1456 - 408\alpha D - 36\alpha^2 D^2 - \alpha^3 D^3\right] b_{1/2}^{(7)} = -3.86673. \qquad (8.202)$$

Using $\alpha = (4/7)^{\frac{2}{3}} = 0.688612$ gives $R = 2003.0e$. Figure 8.20 shows the evolution of the test particle's orbital elements and (x, y) values for librational motion at the 7:4 resonance for a mass value of $\mu_2 = 0.001$. The heliocentric starting values are $a_0 = 0.691249$, $e_0 = 0.204339$, $\varpi_0 = 0.0$, $\lambda_0 = 0$, with $\lambda_0' = 0$. It is clear from Fig. 8.20 that there are a number of additional short-period terms present in the orbital elements. Furthermore, although there are three clear centres of libration in Fig. 8.20b, the presence of the short-period terms causes significant departures from the expected trajectories shown in Fig. 8.13. This is due to the fact that the resonance lies between the 2:1 and 3:2 resonances where perturbations from other resonances cannot be avoided.

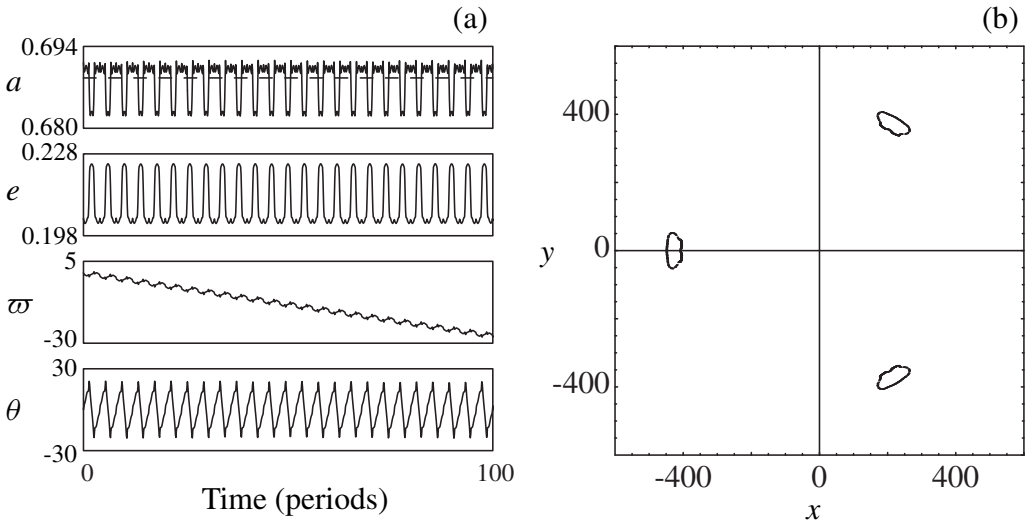

Fig. 8.20. Libration of a test particle in the 7:4 e^3 resonance in the planar circular restricted three-body problem. (a) Plots of the semi-major axis a, the eccentricity e, the longitude of pericentre ϖ, and the resonant angle $\theta = 7\lambda' - 4\lambda - 3\varpi$ as a function of time. (b) Plot of $x = \sqrt{2R}\cos\phi$ and $y = \sqrt{2R}\sin\phi$ (where $\phi = \theta/3 + \pi$) for the same integration showing the three branches of the stable libration.

8.11 Additional Resonances and Resonance Splitting

In all of the numerical integrations carried out in Sects. 8.9 and 8.10 there was good agreement with the theoretical models derived from a Hamiltonian approach based on a truncated form of the disturbing function. This is exemplified by Fig. 8.18 where a direct comparison was made. The unavoidable presence of short-period terms in the full integrations (Fig. 8.18a) gives rise to the "fuzziness" of the (x, y) curves when compared to those of constant Hamiltonian (Fig. 8.18b), but otherwise the comparison is good. However, there are circumstances where use of just a single resonant term from the disturbing function may not be appropriate.

So far we have considered resonances in isolation and yet at an arbitrary separation in semi-major axis from the perturber, basic number theory tells us that the mean motion can always be approximated by a rational number. Hence the perturbed object is always close to *some* resonance although, as we have seen, the strength depends on the order of the resonance. For example, if we restrict ourselves to first-order resonances then the separation in semi-major axis between the nominal locations of the consecutive p+1:p and p+2:p+1 resonances is

$$\Delta a = \left[\left(\frac{p+1}{p+2} \right)^{2/3} - \left(\frac{p}{p+1} \right)^{2/3} \right] a' \approx \frac{2}{3} \frac{1}{p^2} a', \tag{8.203}$$

where a' is the semi-major axis of the perturber. Therefore, Δa decreases as p increases and the orbit of the external perturber is approached. Therefore, where the perturbed mass lies close to the perturbing mass, it may no longer be valid to consider just a single resonance. Given that each resonance has a finite libration width there will come a point where adjacent first-order resonances overlap. The consequences of this phenomenon are discussed in the next chapter. Note that if there are additional perturbing masses then we may also have to consider additional resonances.

Now consider the case where the particle's eccentricity is moderate to large. In such cases we would have to use expansions to higher order in e. Because of the relationship between the order of an expansion and the order of the resonant argument, the inclusion of higher-order terms has implications for the number of arguments to be considered. For example, at the 2:1 resonance we have considered the single resonant argument $\theta_1 = 2\lambda' - \lambda - \varpi$ and its associated term of first order in e. Although there *are* higher order terms in e associated with this argument (see the entry for 4D1.1 in Table B.4) if we include them then for consistency we would need to include second- and higher-order arguments such as $\theta_2 = 4\lambda' - 2\lambda - 2\varpi$, $\theta_3 = 6\lambda' - 3\lambda - 3\varpi$, and $\theta_4 = 8\lambda' - 4\lambda - 4\varpi$ and their associated terms of order 2, 3, and 4 respectively. The exact locations of these resonances are determined by values of the semi-major axes for which the time derivative of the resonant argument is exactly zero. Because θ_2, θ_3,

and θ_4 are all simple multiples of θ_1, exact resonance occurs at the same semi-major axis. The effect on the curves of constant Hamiltonian is to introduce additional equilibrium points as we change from first- to second- and higher-order resonances.

Further complications arise if we allow the perturber to move in an elliptical orbit in a different plane to the perturbed object. Many additional resonant arguments are now possible, with the location of each exact resonance depending on the particular combination of angles. For example, if our analysis is to second order in the orbital elements then at the 2:1 resonance we must consider the additional first-order argument $2\lambda' - \lambda - \varpi'$ as well as the additional second-order arguments $4\lambda' - 2\lambda - \varpi' - \varpi$, $4\lambda' - 2\lambda - 2\varpi'$, $4\lambda' - 2\lambda - 2\Omega$, $4\lambda' - 2\lambda - \Omega' - \Omega$, and $4\lambda' - 2\lambda - 2\Omega'$. Given that the exact locations of these resonances depend on the values of the quantities $\dot{\varpi}$, $\dot{\varpi}'$, $\dot{\Omega}$, and $\dot{\Omega}'$ it is clear that the resonances can be widely separated where these values are large. This is the phenomenon of *resonance splitting* and it is particularly important in satellite systems. Although it increases the number of resonances to be considered, if the resonances are sufficiently well separated then each can be treated individually, irrespective of the perturbing effects of the others.

Saturn's oblateness guarantees that the rates of pericentre precession and nodal regression are large for objects orbiting close to the planet. Figure 8.21 shows the location of the Mimas 6:4 and Tethys 3:1 resonances in the saturnian system, with e and I denoting the eccentricity and inclination of the object in resonance, with single and double primes denoting the equivalent values for Mimas and Tethys respectively. The resonant locations were calculated using the formulae

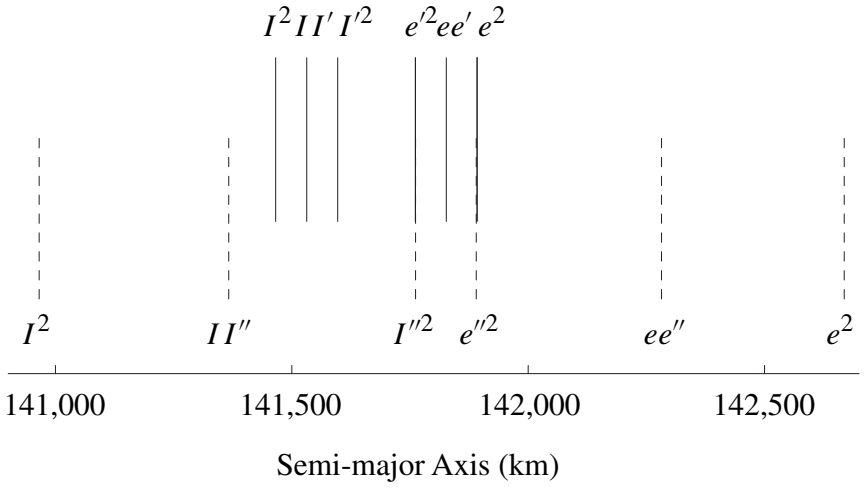

Fig. 8.21. Resonance splitting in the saturnian system illustrated by the locations in semi-major axis of the Mimas 6:4 (solid lines) and Tethys 3:1 (dashed lines) exact resonances. The symbols above and below each set of lines denote the appropriate terms in eccentricity and inclination associated with each argument.

in Sect. 6.11 and the values of $\dot{\varpi}$, $\dot{\Omega}$, $\dot{\varpi}'$, and $\dot{\Omega}'$ given by Harper & Taylor (1993). The Mimas 3:2 e and e' resonances are coincident with the e^2 and e'^2 resonances for the reasons explained above. Note that the resonances associated with each satellite are arranged in groups of three because of the resonance splitting. The rates of change of the longitudes of pericentre and node are always of opposite sign under the effect of the planet's J_2, resulting in the inclination resonances always lying interior to the eccentricity ones. The fact that Tethys is more distant than Mimas results in rates that are a factor five smaller ($\sim \pm 0.19^\circ \mathrm{d}^{-1}$ versus $\sim \pm 1^\circ \mathrm{d}^{-1}$). Note the near coincidence of the Tethys I''^2 and the Mimas e'^2 resonances, as well as the Tethys e''^2 and Mimas e^2 resonances. The reason for the general proximity of the resonances of these satellites is the fact that Mimas and Tethys are involved in a 4:2 resonance with each other (see Sect. 8.14.2 below). Some of the resonances shown in Fig. 8.21 may also have played a role in the orbital evolution of the satellite Pandora (see Sect. 10.11).

8.12 Resonant Encounters

In Chapter 4 we saw how the effect of tides raised on a planet by a satellite leads to an increase in the satellite's semi-major axis, provided that it is in a prograde orbit outside the synchronous location. We also showed that there is some evidence that the satellite systems of Saturn and Uranus have undergone significant tidal evolution over the age of the solar system. Indeed, such evolution is thought to be the reason why there are so many mean motion resonances between the satellites of Saturn (Goldreich 1965), although a primordial origin is more likely in some cases. The fact that there are no known resonances between the satellites of Uranus does not imply that there was no tidal evolution, since this absence can be explained by fundamental differences between the nature of resonances at Saturn and Uranus (see Chapter 9). Other uncertainties exist. For example, we do not know the rate of tidal evolution, because it depends on the tidal dissipation function of the planet, a poorly determined quantity for most solar system objects.

If significant tidal evolution has occurred in satellite systems, then we expect that there would have been occasions in the past when a resonant encounter occurred between a pair of satellites. Indeed, such encounters may have led to the observed preference for commensurabilities in some systems. Not all encounters would have resulted in resonant capture, although, as we shall see, the outcome would always have led to some change in the characteristics of the orbit. In Chapter 4 we saw how the major satellites of Saturn and Uranus are thought to have encountered a number of first- and second-order resonances during their dynamical evolution. It is important to note that although all these satellites are evolving outwards (i.e., their semi-major axes are increasing), relatively speaking some pairs are approaching one another and some are retreating. As we shall

see it is the relative direction of motion that determines whether or not capture is possible in the classical problem.

One of the major advantages of the Hamiltonian approach to resonance introduced in Sect. 8.8 is that it improves our knowledge of the dynamics of resonance encounter and provides a unified approach to the problem. It also demonstrates that the *action* of an orbit can be used to predict the outcome of a resonant encounter. For a given value of $\bar{\delta}$ the action of the orbit is defined as

$$J = \oint \Phi \, \mathrm{d}\phi = \oint x \, \mathrm{d}y \tag{8.204}$$

and this is just the area enclosed by the trajectory in the (Φ, ϕ) or (x, y) plots. Provided the orbit is expanding or contracting sufficiently slowly (i.e., the change in $\bar{\delta}$ over one cycle is negligible) the action is an *adiabatic invariant* of the system and its value is a conserved quantity. Note that the curves of constant Hamiltonian (i.e., the trajectories) far from the librational region for the first- and second-order resonances can be closely approximated to circles centred on the origin (see Figs. 8.10 and 8.11). Therefore the initial action, J_0, is simply the area of that circle and hence

$$J_{\mathrm{init}} = \pi (x_{\mathrm{init}}^2 + y_{\mathrm{init}}^2) = 2\pi \Phi_{\mathrm{init}}, \tag{8.205}$$

where x_{init}, y_{init}, and Φ_{init} are the initial values of x, y, and Φ, which are related by Eqs. (8.130).

However, the adiabatic condition is not satisfied when the orbit evolves to a position close to the resonant separatrix (see, for example, Lichtenberg & Lieberman 1983). This is because the period of the librational or circulatory motion goes to infinity as the separatrix is approached. After the separatrix has been crossed the final action can once again become an approximate adiabatic invariant of the motion. For example, if the object was captured into resonance then the final action will be the area enclosed by the separatrix when it was encountered. We can make use of these properties to predict the outcome of resonant encounters and hence understand some of the orbital histories of natural satellites and other solar system objects that have undergone significant orbital evolution over the past 4.6×10^9 y.

Using this approach it is convenient to view the phenomenon as that of the resonance encountering the orbit rather than the other way around. The orbit and the area enclosed by it remain fixed as the curves of constant Hamiltonian change around it following the increase or decrease in $\bar{\delta}$. Eventually a separatrix encounters the orbit with the outcome depending on a number of factors; the end result is a change in the nature of the orbit, in terms of its eccentricity and/or its librational or circulatory character.

8.12.1 Encounters with First-Order Resonances

In order to understand the possible outcomes of resonant encounters we consider the evolution of several orbits as they evolve towards resonance. Following Peale (1986) we concentrate on encounters with first-order resonances. Here we change from the use of $\bar{\delta}$ (where $\bar{\delta} = 0$ denotes exact resonance) to δ, where, for first-order resonances, the two quantities are related by

$$\delta = -\frac{1}{3}\bar{\delta} - 1 \tag{8.206}$$

and $\delta = 0$ now denotes the bifurcation value. This is in keeping with the notation of Peale (1986). If we consider the orbit of the external body to be fixed then the relationship between $\bar{\delta}$ and $\bar{\alpha}$ given in Eq. (8.117) implies that for $\delta < 0$ the inner body has a semi-major axis less than the resonant value. Similarly $\delta > 0$ implies a semi-major axis greater than the resonant value. Whether δ increases or decreases with time depends on how fast each mass is evolving in semi-major axis. As we shall see below, the key quantities are the initial value of δ and the sign of $\dot{\delta}$, that is, whether the two masses are approaching exact resonance at $\delta = 0$ from above ($\delta > 0$ and $\dot{\delta} < 0$) or below ($\delta < 0$ and $\dot{\delta} > 0$).

Figure 8.22 shows the evolution of an orbit that starts with a large negative value of δ (a large positive value of $\bar{\delta}$) and a relatively small value of the eccentricity, which, we recall, is proportional to the radial distance from the origin. The area enclosed by the trajectory is constant and equal to the initial action of the orbit (Figs. 8.22a,b). We see that when $\delta = 0$ (Fig. 8.22c, when the critical curve first exists) this area is less than the area of the critical curve (drawn for comparison); this is the condition for certain, but smooth, capture into resonant libration and it obviously depends on the initial area and hence on the initial eccentricity of the orbit. As δ increases beyond 0 (Figs. 8.22d,e) the orbit continues to evolve but now it is captured within the resonance region. In this case the action is still approximately equal to the initial value. However, as the stable equilibrium point moves further to the right with increasing δ (cf. Fig. 8.9), so the eccentricity of the captured orbit increases. From the properties of the curves

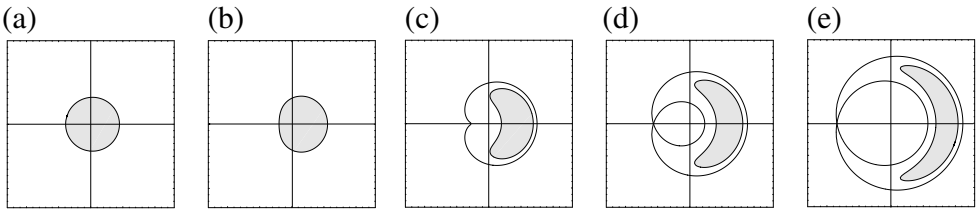

Fig. 8.22. Resonance encounter for increasing δ for a trajectory with an initial eccentricity smaller than the critical value. (a) $\delta = -6$, (b) $\delta = -1$, (c) $\delta = 0$, (d) $\delta = 1$, and (e) $\delta = 3$. The separatrix is shown for all values of $\delta \geq 0$.

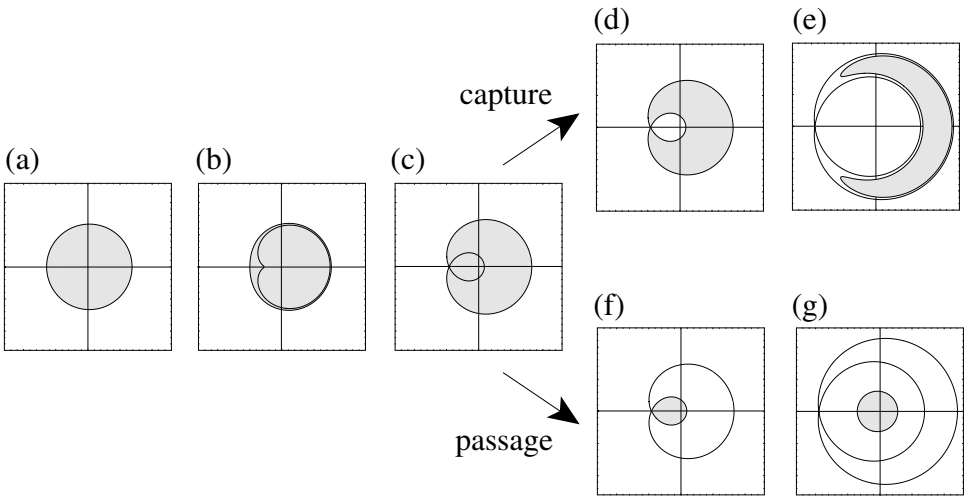

Fig. 8.23. Resonance encounter for increasing δ for a trajectory with an initial eccentricity larger than the critical value. In (a) $\delta = -6$ and in (b) $\delta = 0$. In (c), (d), and (f) $\delta = 0.485584$, the critical value, associated with the initial area enclosed by the trajectory. In (e) and (g) $\delta = 4$. The separatrix is shown for all values of $\delta \geq 0$.

shown in Fig. 8.10d we see that this evolution coincides with a decrease in the libration amplitude.

In Fig. 8.23 we show the evolution of an orbit with increasing δ for an initial enclosed area (see Fig. 8.23a) that is larger than that associated with the critical curve at $\delta = 0$. This orbit has an initial eccentricity that is larger than that shown in Fig. 8.22. Again the action is conserved but in this case when the resonant separatrix is finally encountered beyond the $\delta = 0$ value at $\delta = 0.485584$, there is a discontinuous change in the action. There are two possible outcomes, each depending critically on the exact conditions at separatrix crossing, and there is only a finite probability of capture. In the first case (Figs. 8.23d,e) capture into resonance occurs and the action changes to the area enclosed between the two branches of the encountered separatrix (Fig. 8.23d); there is no change in the eccentricity associated with the capture process. As δ increases further the resonance continues and a process similar to that shown in Fig. 8.22d,e occurs; conservation of the new action implies a gradual increase in eccentricity and a corresponding decrease in libration amplitude.

If resonant capture had not occurred during the stage of evolution shown in Fig. 8.23c, then the new action would have been the area enclosed by the inner defining curve of the separatrix. Since this always encloses the origin there would always be circulation. However, since the enclosed area is now less than the initial area, the instantaneous encounter with the separatrix has reduced the eccentricity of the orbit. Therefore, failure to be captured into resonance with increasing δ always implies an outcome that leads to a reduction in the eccentricity of the orbit as the separatrix is encountered (see Fig. 8.23f). As

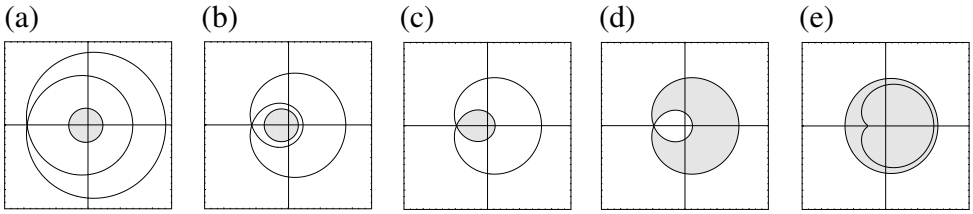

Fig. 8.24. Resonance encounter for decreasing δ. In (a) $\delta = 4$ and in (b) $\delta = 1$. In (c) and (d) $\delta = 0.581777$, the critical value, associated with the initial area enclosed by the trajectory. In (e) $\delta = 0$. The separatrix is shown for all values of $\delta \geq 0$.

δ increases further the trajectory continues to circulate in a near-circular path about the origin (see Fig. 8.23g).

Figure 8.24 shows the outcome of a resonant encounter in the case of decreasing δ. The initial orbit has a relatively small eccentricity enclosing the origin (see Fig. 8.24a). As δ decreases, circulation can continue (Fig. 8.24b) until the resonant separatrix is encountered (Fig. 8.24c) and the area enclosed by the orbit must expand to fill the area enclosed by the outer branch of the separatrix (Fig. 8.24d). In these circumstances capture into resonance cannot occur. However, since the resulting action is larger than the initial value, the encounter will always lead to an increase in the eccentricity. Subsequent evolution still conserves the action and the new eccentricity maintains its value. Note that in the case of decreasing δ it is also possible for the orbit to exhibit apocentric libration (cf. Fig. 8.17d).

To provide a quantitative understanding of these evolutionary histories we have to study the properties of the various curves. In particular we must examine the separatrices as functions of δ and the critical curve at $\delta = 0$.

In our discussion of the Hamiltonian approach above we showed that the locations of the equilibrium points (in terms of Φ) for first-order resonances are given by Eqs. (8.136)–(8.137). Because the unstable equilibrium point at Φ_3 (or x_3) lies on the critical curve that encloses the resonant region around the stable equilibrium point at Φ_1, we can use information about the location of Φ_3 to obtain the area of the critical curve associated with the formation of the resonant separatrix at $\delta = 0$ (see Fig. 8.10c). From Eq. (8.128) and transforming to δ, the equation describing the critical curve at $\delta = 0$ is given by

$$-3\Phi + \Phi^2 - 2\sqrt{2\Phi}\cos\phi = \frac{3}{4}. \tag{8.207}$$

Following Peale (1986) and Malhotra (1988), the area enclosed by this curve can be calculated by deriving an expression for $\mathrm{d}\phi$ in terms of Φ and $\mathrm{d}\Phi$, thereby changing the integration variable from ϕ to Φ. By deriving expressions for $\mathrm{d}\phi$ from $\mathrm{d}\phi/\mathrm{d}\tau = \partial\mathcal{H}_1/\partial\Phi$ and $\mathrm{d}\Phi/\mathrm{d}\tau = -\partial\mathcal{H}_1/\partial\phi$, where τ is the scaled time, the

action associated with the critical curve can be calculated. This gives

$$J_{\rm crit} = 2\int_{1/2}^{9/2} \frac{\Phi\dot{\phi}}{\dot{\Phi}}\,{\rm d}\Phi = 6\pi = 2\pi\,\Phi_{\rm crit}, \tag{8.208}$$

where it is understood that we are integrating along the upper part of the curve and we have made use of the symmetry of the curve about the x axis. The lower and upper limits on the integral are derived from the values of Φ on the critical curve at $\phi = 180^\circ$ and $\phi = 0^\circ$ respectively.

Therefore, provided $J_{\rm init} \le J_{\rm crit}$ (i.e., $\Phi_{\rm init} \le \Phi_{\rm crit} = 3$), the orbit will be captured into resonance as δ increases. Using Eqs. (8.132) this reduces to the condition $e_{\rm init} \le e_{\rm crit}$, where $e_{\rm init}$ is the initial eccentricity of the interior object (assumed to have negligible mass) and

$$e_{\rm crit} = \sqrt{6}\left[\frac{3}{f_{\rm d}}(1-j)^{\frac{4}{3}} j^{\frac{2}{3}} \frac{m_{\rm c}}{m'}\right]^{-1/3}. \tag{8.209}$$

In the case of an exterior object of negligible mass we use Eq. (8.134) and the condition is $e'_{\rm init} \le e'_{\rm crit}$, where

$$e'_{\rm crit} = \sqrt{6}\left[\frac{3}{f_{\rm d}} j^2 \frac{m_{\rm c}}{m}\right]^{-1/3}. \tag{8.210}$$

Note that we can also modify the values of $e_{\rm crit}$ and $e'_{\rm crit}$ by using Eqs. (8.125) and (8.126) with $k = 1$ if we wish to consider situations where neither mass is negligible.

To calculate the changes in the eccentricity when a resonance is encountered we need to calculate the corresponding change in the action, which is related to the area enclosed by the outer and inner branches of the separatrix that starts at the unstable equilibrium point at Φ_3. Above we outlined the procedure to be adopted for the critical curve at $\delta = 0$; now we need to generalise this for arbitrary, positive values of δ.

To do the integral we need to make use of the equation for the value of Φ_3 as a function of δ derived from Eq. (8.137) and then calculate the other two values of Φ where the separatrix crosses at $\phi = 0$. Malhotra (1988) gives the following exact formulae for these two crossing points, $\Phi_{\rm min}$ and $\Phi_{\rm max}$, as well as expressions for the areas $|A_{\rm inner}|$ and $|A_{\rm outer}|$ enclosed by the inner and outer branches of the separatrix respectively. Using our notation these expressions are

$$\Phi_{\rm min} = 3(\delta+1) - \Phi_3 - 2\left(2\Phi_3\right)^{1/4}, \tag{8.211}$$

$$\Phi_{\rm max} = 3(\delta+1) - \Phi_3 + 2\left(2\Phi_3\right)^{1/4}, \tag{8.212}$$

$$A_{\rm inner} = 3\left[\frac{1}{2}\left[\Phi_{\rm max} + \Phi_{\rm min} + 2\Phi_3 - 2(\delta+1)\right]\left(\frac{\pi}{2} - \gamma\right) - \sqrt{(\Phi_{\rm max} - \Phi_3)(\Phi_3 - \Phi_{\rm min})}\right], \tag{8.213}$$

$$A_{\text{outer}} = -3\left[\frac{1}{2}\left[\Phi_{\max} + \Phi_{\min} + 2\Phi_3 - 2(\delta+1)\right]\left(\frac{\pi}{2} + \gamma\right)\right.$$
$$\left. + \sqrt{(\Phi_{\max} - \Phi_3)(\Phi_3 - \Phi_{\min})}\right], \tag{8.214}$$

where

$$\gamma = \sin^{-1}\left(\frac{\Phi_{\max} + \Phi_{\min} - 2\Phi_3}{\Phi_{\max} - \Phi_{\min}}\right). \tag{8.215}$$

Although the expressions for A_{inner} and A_{outer} are complicated, it can be shown (see, for example, Peale 1986) that their sum is given by the simpler expression

$$A_{\text{inner}} + A_{\text{outer}} = 6\pi(\delta_{\text{t}} + 1), \tag{8.216}$$

where δ_{t} is the value of $\delta \geq 0$ when transition occurs.

Provided that (i) we know δ_{t} and (ii) we can approximate the initial and final trajectories as circles centred on the origin in the x–y plane, we have the following relationship between the initial and final values of Φ:

$$\Phi_{\text{init}} + \Phi_{\text{final}} = 3(\delta_{\text{t}} + 1). \tag{8.217}$$

Hence the initial and final values of the eccentricity are related by

$$e_{\text{init}}^2 + e_{\text{final}}^2 = 6(\delta_{\text{t}} + 1)\left[\frac{3}{f_{\text{d}}}(1-j)^{\frac{4}{3}} j^{\frac{2}{3}} \frac{m_{\text{c}}}{m'}\right]^{-\frac{2}{3}} \tag{8.218}$$

for internal resonances and by

$$e_{\text{init}}'^2 + e_{\text{final}}'^2 = 6(\delta_{\text{t}} + 1)\left[\frac{3}{f_{\text{d}}} j^2 \frac{m_{\text{c}}}{m}\right]^{-\frac{2}{3}} \tag{8.219}$$

for external resonances.

These formulae cover the case when capture does not occur either because δ is always decreasing (and so capture is impossible) or δ is always increasing but the initial eccentricity is greater than the critical value and resonant capture (a probabilistic event in such circumstances) does not occur.

We can quantify the expected changes in Φ when capture does not occur by plotting values of $|A_{\text{inner}}|/2\pi$ and $|A_{\text{outer}}|/2\pi$ as a function of δ_{t}. This is shown in Fig. 8.25. If we know Φ_{init}, we can use the plot to calculate Φ_{final} in the case when capture into resonance has not occurred. This can happen in two ways. The first case occurs when δ is increasing and $\Phi_{\text{init}} > \Phi_{\text{crit}}$ (see Fig. 8.23). We find the value of $|A_{\text{outer}}|/2\pi = \Phi_{\text{init}}$ and read off the corresponding value of $|A_{\text{inner}}|/2\pi = \Phi_{\text{final}}$. In the second case δ is decreasing (see Fig. 8.24). We find the value of $|A_{\text{inner}}|/2\pi = \Phi_{\text{init}}$ and read off the corresponding value of $|A_{\text{outer}}|/2\pi = \Phi_{\text{final}}$. In each case we can calculate the changes in the eccentricity from the scaling relations given in Eqs. (8.132) and (8.134).

We have already noted that in the case of decreasing δ (i.e., orbits that are receding from one another) the probability of capture into resonance is zero. In

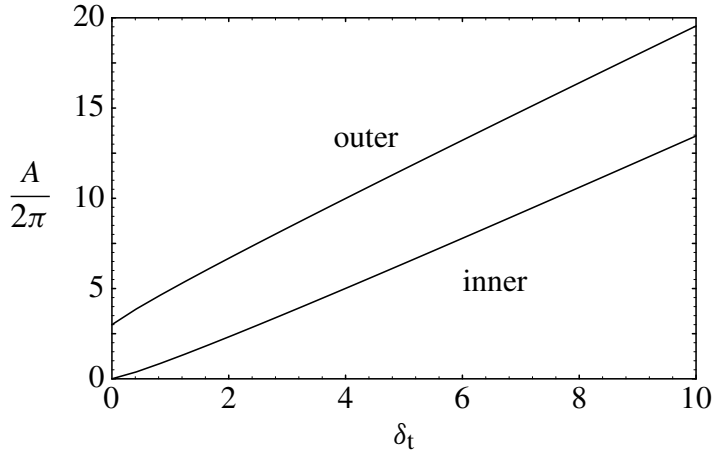

Fig. 8.25. Plots of the scaled action, $A/2\pi$, for the inner and outer branches of the separatrix as a function of δ_t, the value of δ at transition, for the case of first-order resonances.

the case of increasing δ (i.e., orbits that are approaching one another) capture into resonance is certain if $\Phi_{\rm init} \leq \Phi_{\rm crit} = 3$. In situations where $\Phi_{\rm init} > \Phi_{\rm crit}$, the probability, $P_{\rm cap}$, of capture into resonance can be quantified by means of formulae devised by Henrard (1982) and then greatly simplified by Borderies & Goldreich (1984). By introducing the concept of "balance of energy integrals" these authors have shown that

$$P_{\rm cap} = \frac{4\gamma}{\pi + 2\gamma}, \tag{8.220}$$

where γ, as defined in Eq. (8.215), is evaluated using the value of $\delta = \delta_t$. Figure 8.26 shows the value of $P_{\rm cap}$ as a function of δ_t.

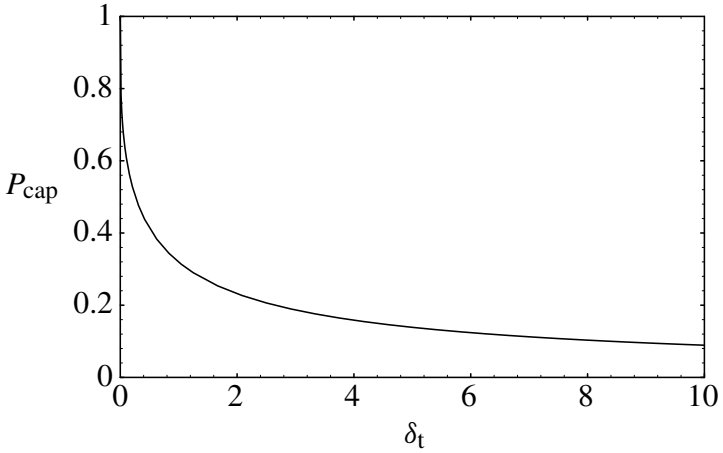

Fig. 8.26. The probability of resonance capture as a function of δ_t, the value of δ at transition, for the case of first-order resonances.

8.12.2 Encounters with Second-Order Resonances

In the case of second-order resonances the approach is similar to that used above for first-order resonances. Again there is a critical separatrix at $\delta = 0$ and it is easy to show that for this value of δ there are five equilibrium points at $\Phi_1 = 1/2$ (with $x = \pm 1$, $y = 0$) and $\Phi_2 = \Phi_3 = 0$ (three points coincident at the origin). Therefore the critical curve passes through the origin; in common with all curves in the x–y plane for second-order resonances, the critical curve will be symmetric about the x axis and y axis. It is described by

$$2\Phi^2 - \Phi(1 + \cos 2\phi) = 0. \tag{8.221}$$

The area enclosed by this curve, the critical action, is given by

$$J_{\rm crit} = 4\int_{1/2}^{0} \frac{\Phi\dot{\phi}}{\dot{\Phi}}\,{\rm d}\Phi = \pi = 2\pi\,\Phi_{\rm crit}, \tag{8.222}$$

where the lower and upper limits on the integral are derived from the values of Φ on the critical curve when $\phi = 0$ and $\phi = \pi/2$.

As before, we are primarily interested in the case when δ is always increasing, since this can lead to capture if $\Phi_{\rm init}$ is less than a critical value. Therefore, in the case of second-order resonance, provided $J_{\rm init} < J_{\rm crit}$ (i.e., $\Phi_{\rm init} < \Phi_{\rm crit} = 1/2$), the orbit will be captured into resonance as δ increases. Using Eqs. (8.156) and (8.158) the condition for certain capture reduces to $e_{\rm init} < e_{\rm crit}$, where

$$e_{\rm crit} = \left[\frac{3}{16 f_{\rm d}}(2 - j)^{\frac{4}{3}} j^{\frac{2}{3}} \frac{m_{\rm c}}{m'}\right]^{-1/2} \tag{8.223}$$

in the case of an internal resonance and

$$e'_{\rm crit} = \left[\frac{3j^2}{16 f_{\rm d}} \frac{m_{\rm c}}{m}\right]^{-1/2} \tag{8.224}$$

in the case of external resonances. Using Eqs. (8.125) and (8.126) we can also make use of more accurate scaling relationships in cases where the two masses are comparable.

In order to calculate the outcome of the resonant encounters we need to calculate the areas enclosed by the inner and outer branches of the separatrix that has an unstable equilibrium point at Φ_3 corresponding to the $x = 0$, $y = \pm\sqrt{\delta_{\rm t}}$, where $\delta_{\rm t} \geq 0$ is the value of δ when the transition occurs. Malhotra (1988) gives the formulae for the minimum and maximum values of Φ along the separatrix and the area enclosed by their inner and outer boundaries of the separatrix. These are

$$\Phi_{\rm min} = \frac{1}{2}(1 + \delta) - \frac{1}{2}\sqrt{1 + 2\delta}, \tag{8.225}$$

$$\Phi_{\rm max} = \frac{1}{2}(1 + \delta) + \frac{1}{2}\sqrt{1 + 2\delta}, \tag{8.226}$$

$$A_{\rm inner} = 2\Bigg[\frac{1}{2}\left[\Phi_{\rm max} + \Phi_{\rm min} + 2\Phi_3\right]\left(\frac{\pi}{2} - \gamma\right) - \sqrt{(\Phi_{\rm max} - \Phi_3)(\Phi_3 - \Phi_{\rm min})}\Bigg], \tag{8.227}$$

$$A_{\rm outer} = -2\Bigg[\frac{1}{2}\left[\Phi_{\rm max} + \Phi_{\rm min} + 2\Phi_3\right]\left(\frac{\pi}{2} + \gamma\right) + \sqrt{(\Phi_{\rm max} - \Phi_3)(\Phi_3 - \Phi_{\rm min})}\Bigg], \tag{8.228}$$

where, as before,

$$\gamma = \sin^{-1}\left(\frac{\Phi_{\rm max} + \Phi_{\rm min} - 2\Phi_3}{\Phi_{\rm max} - \Phi_{\rm min}}\right). \tag{8.229}$$

In this case,

$$A_{\rm inner} + A_{\rm outer} = \pi(1 + 2\delta_{\rm t}). \tag{8.230}$$

Provided we can approximate the initial and final trajectories far from resonance as circles in the x–y plane, we can write

$$\Phi_{\rm init} + \Phi_{\rm final} = \frac{\pi}{2}, \tag{8.231}$$

and hence the initial and final values of the eccentricity are related by

$$e_{\rm init}^2 + e_{\rm final}^2 = (1 + 2\delta_{\rm t})\left[\frac{3}{16 f_{\rm d}}(2 - j)^{\frac{4}{3}} j^{\frac{2}{3}} \frac{m_{\rm c}}{m'}\right]^{-1} \tag{8.232}$$

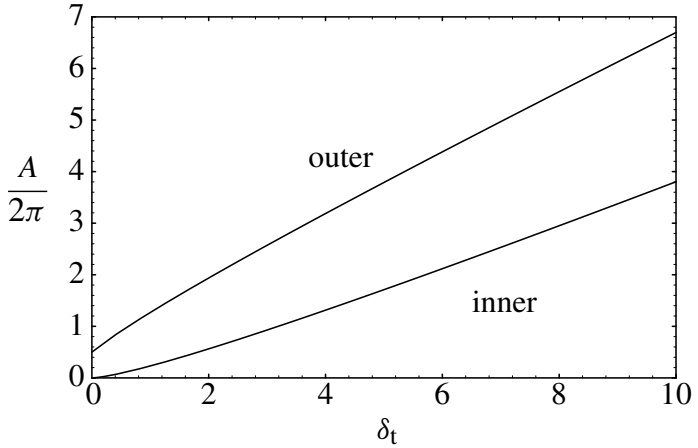

Fig. 8.27. Plots of the scaled action, $A/2\pi$, for the inner and outer branches of the separatrix as a function of $\delta_{\rm t}$, the value of δ at transition, for the case of second-order resonances.

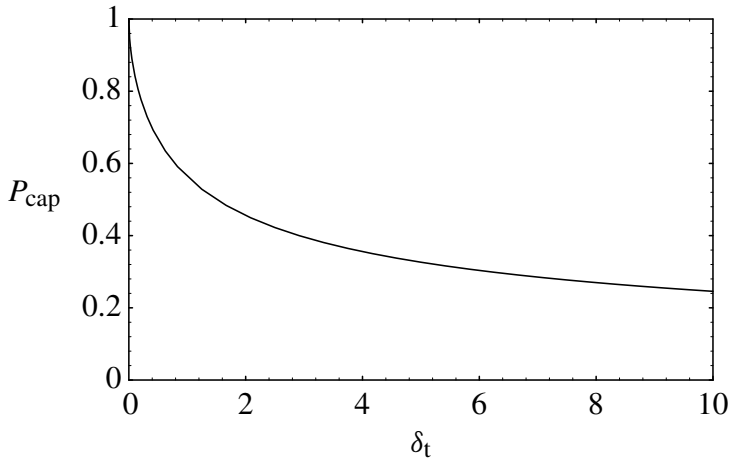

Fig. 8.28. The probability of resonance capture as a function of $\delta_{\rm t}$, the value of δ at transition, for the case of second-order resonances.

for internal resonances and by

$$e'^2_{\rm init} + e'^2_{\rm final} = (1 + 2\delta_{\rm t}) \left[\frac{3j^2}{16 f_{\rm d}} \frac{m_{\rm c}}{m} \right]^{-1} \tag{8.233}$$

for external resonances.

Following the example shown above for the case of first-order resonances, we can plot $A/2\pi$ for the inner and outer branches of the separatrix as a function of $\delta_{\rm t}$, the value of δ at the transition. These are shown in Fig. 8.27. The formula for the probability, $P_{\rm cap}$, of capture into a second-order resonance in the case of increasing δ is identical to that given in Eq. (8.220), where the values of $\Phi_3 = \delta/2$, $\Phi_{\rm min}$, and $\Phi_{\rm max}$ are given by Eqs. (8.225) and (8.226). Figure 8.28 shows the resulting probability as a function of $\delta_{\rm t}$.

8.13 The Dynamics of Capture and Evolution in Resonance

We have already discussed the dynamics of capture in the context of spin–orbit resonance (see Sect. 5.5) and there are a number of similarities when we consider the orbit–orbit case. In order for resonance capture to occur there must be dissipation in the system. In Sect. 8.12 above we used the conservation of the action to analyse the effect of resonant encounters. We noted that capture is impossible in the classical system if the resonance is approached from above with decreasing δ. When approached from below, capture is certain for an initial eccentricity below a critical value, while it is a probabilistic event for larger initial values.

To illustrate the dynamics of capture and the subsequent evolution, consider the case of two satellites of masses m and m' evolving due to tides. The satellites are assumed to be in prograde orbits outside the synchronous orbit. Using Kepler's

third law and Eq. (4.160) we can write the rate of change of the mean motion due to tides as

$$\dot{n}_{\rm t} = -\frac{9}{2}\frac{n^2}{Q_{\rm p}} k_2 \frac{m}{m_{\rm p}} \left(\frac{R_{\rm p}}{a}\right)^5, \tag{8.234}$$

where a is the semi-major axis of the satellite; n is its mean motion, and k_2, $m_{\rm p}$, and $Q_{\rm p}$ denote the Love number, mass, and the tidal dissipation function, respectively, of the planet. There is a similar equation for $\dot{n}'_{\rm t}$ with m, n, and a replaced by m', n', and a'. Here unprimed and primed quantities refer to the inner and outer satellites respectively.

Now consider the effect of a resonance. Let the resonant variable have the general form

$$\varphi = j_1\lambda' + j_2\lambda + j_3\varpi' + j_4\varpi + j_5\Omega' + j_6\Omega, \tag{8.235}$$

and let the averaged disturbing functions experienced by the inner and outer satellites be

$$\mathcal{R} = \mu' S\cos\varphi, \qquad \mathcal{R}' = \mu S\cos\varphi, \tag{8.236}$$

where $\mu = \mathcal{G}m$, $\mu' = \mathcal{G}m'$ and, from the d'Alembert properties,

$$S = e'^{|j_3|} e^{|j_4|} s'^{|j_5|} s^{|j_6|} \frac{f_{\rm d}(\alpha)}{a'}. \tag{8.237}$$

Here $s = \sin\frac{1}{2}I$ and $s' = \sin\frac{1}{2}I'$, where I denotes inclination, and $f_{\rm d}(\alpha)$ denotes the contribution of the direct part of the disturbing function as a combination of Laplace coefficients in $\alpha = a/a'$ (see Sect. 6.7).

From the lowest-order form of Lagrange's equation for $\dot{n}$ (see Eq. (8.12)) we can write the second time derivative of φ as

$$\ddot{\varphi} = 3gS\sin\varphi + F, \tag{8.238}$$

where

$$g = \frac{j_1^2\mu}{a'^2} + \frac{j_2^2\mu'}{a^2} \qquad \text{and} \qquad F = j_1\dot{n}'_{\rm t} + j_2\dot{n}_{\rm t}. \tag{8.239}$$

Here we have ignored any contributions to $\ddot{\varphi}$ from the second time derivatives of the pericentres and longitudes at epoch. Note that j_1 and j_2 have opposite signs for a standard resonant argument. Treating a, a', e, e', s, and s' in S as constants, we can integrate Eq. (8.238) to obtain the energy equation

$$\frac{1}{2}\dot{\varphi}^2 + 3gS\cos\varphi = E + F\varphi. \tag{8.240}$$

As pointed out by Allan (1969), the dynamics of this system correspond to those of a particle moving with velocity $\dot{\varphi}$ in a one-dimensional potential that is a function only of φ. As with the case of spin–orbit resonance, (i) the variation of $\frac{1}{2}\dot{\varphi}^2$ with φ can be thought of as comprising a sinusoidal part and a linear part

(cf. Fig. 5.14) and (ii) capture into the resonance depends on the magnitude and sign of the change in energy over one cycle (cf. Fig. 5.15).

Once the two satellites are trapped in resonance the mean value of the second derivative of φ, $\langle\ddot{\varphi}\rangle$, is zero and hence

$$\langle S \sin\varphi\rangle = -\frac{F}{3g}. \tag{8.241}$$

Allan (1969) shows that once capture occurs the two satellites will remain in resonance even though each continues to evolve away from the planet. We can make use of Eq. (8.241) and our lowest-order form of Lagrange's equations given in Eqs. (8.12)–(8.17) to derive expressions for the time-averaged variation in the orbital elements of the satellites in resonance. For the eccentricities these are

$$\frac{\langle\dot{e}\rangle}{e} = -\frac{j_4}{e^2}\frac{m'}{m_\mathrm{p}} na \frac{F}{3g}, \qquad \frac{\langle\dot{e}'\rangle}{e'} = -\frac{j_3}{e'^2}\frac{m}{m_\mathrm{p}} n'a' \frac{F}{3g}, \tag{8.242}$$

with similar equations for the inclinations.

Dermott et al. (1988) point out that the tidal torque on the inner satellite is usually larger than that on the outer satellite because of the extreme dependence on semi-major axis. However, as it is the perturbation of the outer satellite on the inner that dominates their gravitational interaction, we can often neglect the first terms in g and F. Using Kepler's third law the variation in e can be written as

$$\frac{\langle\dot{e}\rangle}{e} = +\frac{1}{e^2}\frac{j_4}{2j_2}\left(\frac{\dot{a}}{a}\right)_\mathrm{t}. \tag{8.243}$$

Because j_2 and j_4 have the same sign this implies that the eccentricity will always grow as the satellite evolves outwards. There is a similar result for the inclination, although, provided there is significant resonance splitting, the satellite should enter the inclination resonance at a different time. These phenomena were described analytically and investigated numerically by Dermott et al. (1988). They point out that in cases where the individual resonances at a given commensurability are not well separated, the evolution within a given resonance can cause the effects of a neighbouring resonance to become important (see Sect. 9.6).

8.14 Two-Body Resonance in the Solar System

The solar system has many examples of two objects orbiting a central mass where both objects are involved in a mean motion resonance. We refer to these as *two-body resonances* and in each case one (or more) arguments in the expansion of the disturbing function is librating. In Chapter 3 examples of the special case of objects librating in a 1:1 resonances (e.g., the Trojan asteroids and the coorbital satellites of Saturn) were discussed. Table 8.8 gives examples of the known first- and second-order two-body resonances involving planets and satellites in the solar system. In addition to these resonances listed in Table 8.8 several asteroids

Table 8.8. Known first- and second-order mean motion resonances involving planets or satellites in the solar system. In each case the unprimed and primed quantities refer to the inner and outer bodies respectively. All known planetary and satellite resonances are included.

System	Resonant Argument	Amplitude	Period (y)
Planets			
Neptune–Pluto	$3\lambda' - 2\lambda - \varpi'$	76°	19,670
Jupiter			
Io–Europa	$2\lambda' - \lambda - \varpi$	1°	—
Io–Europa	$2\lambda' - \lambda - \varpi'$	3°	—
Europa–Ganymede	$2\lambda' - \lambda - \varpi$	3°	—
Saturn			
Mimas–Tethys	$4\lambda' - 2\lambda - \Omega' - \Omega$	43.6°	71.8
Enceladus–Dione	$2\lambda' - \lambda - \varpi$	0.297°	11.1
Titan–Hyperion	$4\lambda' - 3\lambda - \varpi'$	36.0°	1.75

are known to be involved in mean motion resonances with Jupiter. These include (279) Thule, (153) Hilda, (1362) Griqua, and (887) Alinda, which are in 4:3, 3:2, 2:1, and 3:1 resonances respectively (see Yoshikawa (1989) for a study of the dynamics of a number of these resonances). The ring systems of Saturn, Uranus, and Neptune contain many resonant features due to perturbing satellites; these will be discussed in Chapter 10. Resonances involving three gravitationally interacting objects orbiting a central mass will be discussed in Sect. 8.15.

To gain some insight into resonance mechanisms, we provide a study of two of the satellite resonances listed in Table 8.8. The Neptune–Pluto resonance is discussed in Sect. 9.9.

8.14.1 The Titan–Hyperion Resonance

Titan ($e = 0.0292$, $I = 0.33^\circ$) and Hyperion ($e' = 0.1042$, $I' = 0.43^\circ$) are trapped in a 4:3 resonance. The mass of Hyperion is negligible compared to that of Titan and the resonance can be considered in the context of the planar, circular, restricted problem of three bodies where Hyperion is in an external 3:4 resonance with Titan. From observations the argument

$$\varphi = 4\lambda' - 3\lambda - \varpi' \tag{8.244}$$

librates about 180° so that conjunction of the two satellites librates about the apocentre of Hyperion. From the orbital periods given in Table A1.8 in Appendix A, we have

$$4n' - 3n = -18.679\,^\circ\mathrm{y}^{-1}. \tag{8.245}$$

The observed motion of Hyperion's pericentre is

$$\dot{\varpi}' = -18.663\,^{\circ}\mathrm{y}^{-1}. \tag{8.246}$$

Recall that the effect of Saturn's J_2 should cause a prograde motion of Hyperion's pericentre (see Sect. 6.11), and therefore the observed regression must be due to Titan. With these values

$$4n' - 3n - \dot{\varpi}' \approx 0 \tag{8.247}$$

to within observational error, where we have used averaged rates throughout.

The dynamics of the resonance are difficult to study because Hyperion's large eccentricity causes convergence problems if standard expansions of the disturbing function are used. An alternative method developed by Woltjer (1928) and used by Message (1989, 1993) is to determine the location of the periodic orbit associated with exact resonance and investigate the perturbed motion in its vicinity.

It is unlikely that the Titan–Hyperion resonance resulted from tidal evolution, even though both satellites would have been approaching each other as they receded from Saturn. Sinclair (1972) showed that the critical eccentricity below which Hyperion's capture was guaranteed is $e' = 0.068$, implying significant evolution of e' within the resonance to reach its present value. However, to be captured into the 4:3 resonance Hyperion likely would have come close to Titan's orbit without the resonance mechanism allowing it to avoid dangerous conjunctions (Sinclair 1972). Hyperion may well be the last example of a number of objects that once orbited in the region close to Titan. Without the protection of a resonance the other moons would have been scattered by Titan. If Hyperion is the sole survivor of such a group then this would imply that the resonance is primordial.

8.14.2 The Mimas–Tethys Resonance

Mimas ($e = 0.02$, $I = 1.53^{\circ}$) and Tethys ($e' = 0.0$, $I' = 1.09^{\circ}$) are trapped in 4:2 resonance, which, since it is of second order, can involve the inclinations of the satellites as well as their eccentricities. Of the six known resonances between pairs of planets or satellites this is the only example of a second-order resonance. From observations the particular librating argument is

$$\varphi = 4\lambda' - 2\lambda - \Omega' - \Omega. \tag{8.248}$$

This implies that conjunction of the two satellites librates about the midpoint of the nodes. The observed amplitude of libration is 43.6°. Our knowledge of the disturbing function tells us that the term associated with φ will involve a factor II' as well as the usual combination of Laplace coefficients. Yet this is one of three possible arguments at the 4:2 commensurability that involve inclinations, the others having factors I^2 and I'^2. There will also be eccentricity

terms associated with the same commensurability. Hence, at the 4:2 Mimas–Tethys commensurability there are six possible resonant terms:

$$\begin{aligned}
\langle\mathcal{R}\rangle_1 &= f_1 e^2 \cos(4\lambda' - 2\lambda - 2\varpi), & \langle\mathcal{R}\rangle_2 &= f_2 ee' \cos(4\lambda' - 2\lambda - \varpi' - \varpi),\\
\langle\mathcal{R}\rangle_3 &= f_3 e'^2 \cos(4\lambda' - 2\lambda - 2\varpi'), & \langle\mathcal{R}\rangle_4 &= f_4 I^2 \cos(4\lambda' - 2\lambda - 2\Omega),\\
\langle\mathcal{R}\rangle_5 &= f_5 II' \cos(4\lambda' - 2\lambda - \Omega' - \Omega), & \langle\mathcal{R}\rangle_6 &= f_6 I'^2 \cos(4\lambda' - 2\lambda - 2\Omega'),
\end{aligned} \tag{8.249}$$

where the $f_i = f_i(\alpha)$ are different combinations of Laplace coefficients that can be derived from our expansion of the disturbing function. Each resonance has a different location in semi-major axis determined by knowledge of the mean motions, pericentre, and node rates (cf. Fig. 8.21).

The question of why the Mimas–Tethys system is actually librating in the II' resonance rather than any other can only be answered by considering the origin of such resonances and their link with the tidal evolution of satellite systems. Allan (1969), Sinclair (1972), and Greenberg (1973) have investigated this question in detail. Our analysis of the mechanism of resonance capture shows that the satellites have to be approaching each other as both recede from the planet under the effects of tides. Therefore it is likely that the I^2 resonance was encountered first and then the II' resonance (see Fig. 8.21). However, Sinclair (1972) showed that the probability of capture into each of these resonances was as low as 0.07 and 0.04 respectively.

At this stage it is worthwhile making a comparison with resonance in the asteroid belt. In the case of the asteroid belt resonances, where tidal effects are unimportant, if an asteroid is trapped in a resonance it is usually the argument with the largest associated coefficient that is seen to be librating. In a sense the asteroid will be found to be librating in the strongest resonance. For example, if we consider a simple 3:2 first-order resonance (such as found in the Hilda group of asteroids), then a resonant asteroid could be in either the e resonance with argument $3\lambda' - 2\lambda - \varpi$ or the e' resonance with argument $3\lambda' - 2\lambda - \varpi'$. However, Jupiter's eccentricity of 0.048 is smaller than the average asteroid eccentricity of 0.15. Therefore, because usually $e' \ll e$ and the Laplace coefficient terms are comparable, the e resonance will be stronger, although the relative masses of the objects are also important.

8.15 Resonant Encounters in Satellite Systems

Tidal evolution provides a mechanism for pairs of satellites to encounter a resonance. Consider a satellite of mass m and semi-major axis a moving in a prograde orbit about a planet. In Sect. 4.9 we showed that the tides raised on the planet by the satellite cause a to change at a rate given by

$$\dot{a}_{\rm t} = \frac{3k_2}{Q_{\rm p}} \left(\frac{\mathcal{G}}{m_{\rm p}}\right)^{1/2} R_{\rm p}^5 \frac{m}{a^{11/2}} \tag{8.250}$$

(cf. Eq. (4.160)), where m_p, R_p, Q_p, and k_2 denote the mass, radius, tidal dissipation function, and Love number of the planet, respectively. If the physical properties of the planet remain constant over time, then $\dot{a}_\mathrm{t}$ is purely a function of a and m. Therefore, if we consider another satellite with semi-major axis a' and mass m' on an exterior orbit, the two satellites will be approaching one another if at a given time the ratio

$$\left(\dot{a}/\dot{a}'\right) = \left(m/m'\right)\left(a'/a\right)^{11/2} \tag{8.251}$$

is greater than one. In terms of the mean motions, using the ratio $\mathcal{N} = n'/n$, the condition for capture can be written as $\dot{\mathcal{N}} = \mathrm{d}\left(n'/n\right)/\mathrm{d}t > 1$.

The equation for $\dot{a}_\mathrm{t}$ can be solved to give

$$a(t) = \left[a_0^{13/2} - \frac{13}{2} K m \left(t - t_0\right)\right]^{2/13}, \tag{8.252}$$

where $a_0 = a(t_0)$ (the current value of a) and K (assumed to be constant) is a function of m_p, R_p, Q_p, and k_2. Although m_p and R_p are well known (see Table A.4), it is more difficult to estimate Q_p and k_2, let alone their primordial values (see Sect. 4.13). Nevertheless, Kepler's third law and the fact that the semi-major axes of satellites vary with time means that resonances can be encountered.

For capture to take place between satellites above the synchronous orbit, it is required that the orbit of the inner satellite must be expanding faster than the orbit of the outer satellite and thus that the satellites are on converging orbits (Dermott et al. 1988). On capture into a stable orbit–orbit resonance, $\dot{\mathcal{N}} \approx 0$ and the orbits of the satellites expand at the same rate. Angular momentum is lost from the spin of the planet at the same rate as before the resonance encounter, but now gravitational forces between the satellites due to the resonance act to transfer angular momentum from the inner to the outer satellite allowing their orbits to expand together, thus maintaining the resonance and keeping $\dot{\mathcal{N}} \approx 0$. But these same resonant forces also act to increase the eccentricities or inclinations of the satellites involved in the resonance at rates determined by the resonant argument (see Sect. 8.13), and it is these increases that provide the evidence for orbital evolution.

For example, as we have seen, the satellites Mimas and Tethys are trapped in an inclination-type resonance for which

$$4n' - 2n - \dot{\Omega}' - \dot{\Omega} = 0, \tag{8.253}$$

where the primed and unprimed quantities refer, respectively, to Tethys and Mimas. To a good approximation, we have

$$\frac{\langle \dot{I} \rangle}{I} \approx \frac{1}{4I^2}\left(\frac{\dot{a}}{a}\right)_\mathrm{tides} \tag{8.254}$$

and

$$\frac{\langle \dot{I}' \rangle}{I'} \approx \frac{1}{4I'^2} \left(\frac{\dot{a}'}{a'} \right)_{\text{tides}} . \tag{8.255}$$

Thus, the timescales for the increase of the orbital inclinations are considerably less than those for the increase of the semi-major axes. The present orbital inclinations of Mimas and Tethys are 1.53° and 1.09°, respectively, and are significantly greater than their near neighbours. Allan (1969) argued that these anomalously high values are evidence for significant orbital evolution. Furthermore, if Q_{p} is independent of amplitude and frequency, then, for this resonance, the condition for stability, $\dot{\mathcal{N}} > 1$, is only marginally satisfied. For Mimas $m/a^{13/2} = 2.19 \times 10^{-38}$ while for Tethys $m'/a'^{13/2} = 1.75 \times 10^{-38}$ in cgs units. It follows that we might expect the resonance to be young and the amplitude of libration to be still high. This is indeed the case. The observed amplitude of libration of the resonant argument is 97.040° and Allan (1969) calculated that the resonance was formed 2.4×10^8 years ago, an age that is only 5% of the age of the solar system. An interesting extension of the work of Allan (1969) has recently been given by Champenois & Vienne (1999a,b)

The orbital inclinations of the major uranian satellites (see Table A.11) are particularly interesting. The anomalously high inclination of Miranda (4.22°) clearly suggests the action of resonance. However, unlike the satellite systems of Jupiter and Saturn, which are nearly saturated with orbit–orbit resonances, the uranian system does not contain a single resonance involving any of the five major satellites, Miranda, Ariel, Umbriel, Titania, and Oberon. Dermott (1984) suggested that this difference arises from the fact that the dynamical oblateness, J_2, of Uranus is small and consequently that any orbit–orbit resonances in the uranian system would be chaotic and unstable. Therefore, although the uranian satellite system is devoid of resonances now, the satellites may have been trapped in resonances at some time in the past and these resonances may have been responsible for significant changes in both the orbital inclinations and eccentricities. This problem has been considered by Dermott et al. (1988) for the uranian and saturnian satellites, by Peale (1988) for the uranian satellites, and in more detail by Tittemore & Wisdom (1988, 1989, 1990) also for the uranian satellites.

We can provide examples of possible evolutionary paths by using Eq. (8.252) (with suitable values of K) to describe the semi-major axis of each satellite as a function of time over the same fixed interval. This follows the example of Dermott et al. (1988) who carried out a study of tidal evolution in the saturnian and uranian satellite systems, both of which are thought to be tidally evolved. Figure 8.29 shows possible relative changes in semi-major axis over time for each system. In these plots the time is to be regarded as an integral involving

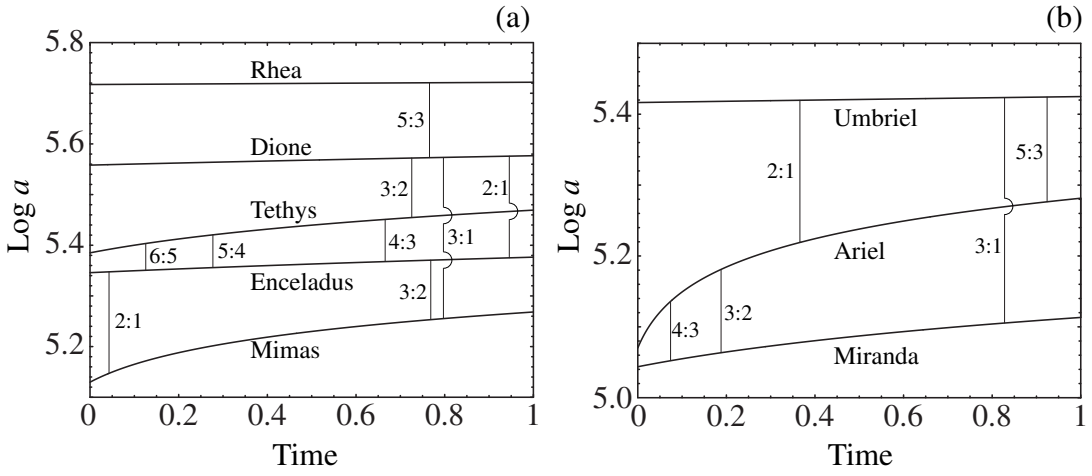

Fig. 8.29. Sample changes in the semi-major axes (measured in km) of satellites in (a) the saturnian and (b) the uranian system. A selection of first- and second-order resonances between pairs of satellites is indicated on each plot.

averaging of $Q_{\rm p}$ (see Dermott et al. 1988). Consequently, the zero point on the time axis should not be considered to be fixed.

Recall that in the saturnian system (Fig. 8.29a) we know that there are currently two resonances: the Mimas–Tethys 4:2 and the Enceladus–Dione 2:1. The plots show that currently each pair of satellites is evolving outwards at almost the same rate although they approached one another at a higher rate in the past. Consequently, the necessary condition for capture occurs in each case. In contrast Enceladus and Tethys have always evolved on diverging paths and could have passed through a number of first-order resonances without capture. Curiously Mimas and Enceladus are on clearly converging paths and yet have managed to escape capture into a resonance.

There are no known resonances between pairs of satellites in the uranian system and yet the paths shown in Fig. 8.29b suggest that the pairs Miranda–Ariel and Ariel–Umbriel are on converging paths. In particular, for reasonable values of $Q_{\rm p}$, it is likely that Miranda and Umbriel once encountered the 3:1 resonance in a direction that could permit capture. In light of this it is reasonable to ask the question: Why did resonances arise in the saturnian system and not in the uranian one? One possible explanation may be related to the fact that because the J_2 of Uranus is a factor ten smaller than that of Saturn, the resonances in the uranian system are less well separated than those in the saturnian system. Therefore, for resonances of similar strengths (i.e., similar widths in semi-major axis) overlap of adjacent resonances will occur for lower values of eccentricity and inclination. Furthermore, the individual resonances cannot be treated in isolation. Because resonance overlap leads to chaotic motion (see Sect. 9.6) we would expect satellites at Uranus entering resonances to be more likely to exhibit

chaotic motion and less likely to conform to the classical model of capture than those at Jupiter or Saturn.

8.16 Three-Body Resonance

We have already investigated the dynamics of a two-body resonance where there is a simple numerical relationship between the mean motions of two orbiting bodies (see Eq. (8.1)). A *three-body resonance* occurs when there is a simple relationship involving three orbiting bodies.

Let n_1, n_2, and n_3 denote the mean motions of three objects of mass m_1, m_2, and m_3 that lie on near-circular, near-coplanar orbits at increasing distances from a central object of mass m_c. We assume that $n_1 > n_2 > n_3$ and hence that the first mass has the smallest semi-major axis of the three, and the third mass the largest semi-major axis. A *Laplace relation* is said to exist between the three orbiting masses if there is a numerical relationship among the masses of the form

$$qn_1 - (p+q)n_2 + pn_3 \approx 0, \tag{8.256}$$

where p and q are positive integers. The existence of a Laplace relation is a special example of a three-body resonance. If $T_{\rm rep}$ is the time between successive repetitions of the initial configuration, we can write

$$\frac{p}{n_1 - n_2} \approx \frac{q}{n_2 - n_3} \approx \frac{p+q}{n_1 - n_3} \approx \frac{T_{\rm rep}}{2\pi}, \tag{8.257}$$

where the mean motions are measured in radians per time unit. It is important to note that the existence of a Laplace relation does not necessarily imply that there is a resonant relationship between any pair of satellites, such as that given in Eq. (8.1).

To study the dynamics of three-body resonances we have to isolate from the disturbing function all those arguments that give rise to the resonant combination of mean longitudes given by

$$\varphi = q\lambda_1 - (p+q)\lambda_2 + p\lambda_3. \tag{8.258}$$

Note that this angle is independent of the longitudes of pericentre of any of the bodies. Having isolated the relevant terms we must then find expressions for the three components on the right-hand side of

$$\ddot{\varphi} = q\frac{\mathrm{d}^2\lambda_1}{\mathrm{d}t^2} - (p+q)\frac{\mathrm{d}^2\lambda_2}{\mathrm{d}t^2} + p\frac{\mathrm{d}^2\lambda_3}{\mathrm{d}t^2} \tag{8.259}$$

and show that $\ddot{\varphi}$ has the form of a pendulum equation,

$$\ddot{\varphi} = c\sin\varphi, \tag{8.260}$$

where c is a function of p, q, and the masses, semi-major axes, and mean motions of the three bodies involved in the resonance.